Impact of Very Short-Lived Substances on Stratospheric Bromine Loading

Dissertation zur Erlangung des akademischen Grades
Dr. rer. nat.
der Universität Bremen, Fachbereich Physik/Elektrotechnik

Vorgelegt von

Dipl.-Inf. Jan Aschmann

Gutachter:

Prof. Dr. J. P. Burrows
Prof. Dr. J. Notholt

Abgabe: 17. Juni 2011
Kolloquium: 14. Oktober 2011

Abstract

Recent studies have shown the importance of very short-lived substances (VSLS) for the abundance of stratospheric bromine. In this work, the transport of bromine VSLS into the stratosphere is investigated with a three-dimensional chemistry transport model. The novelty of this approach is the explicit treatment of convective transport in a purely isentropic model, a key prerequisite for the realistic reproduction of the complex interplay of horizontal advection, local deep convection and large-scale diabatic heating in the tropical tropopause layer (TTL).

Comparisons with observations show that the model is generally able to produce realistic distributions of the two major bromine VSLS, bromoform ($CHBr_3$) and dibromomethane (CH_2Br_2). In addition, an analysis of the regional transport efficiency suggests that the Western Pacific is the most important source area for VSLS into the stratosphere; approximately 50% of the total amount of bromine VSLS in the TTL is contributed by this region.

Another important question is how dehydration in the tropical tropopause impacts on stratospheric bromine loading. An idealized modeling approach assuming total solubility for inorganic bromine predicts that about 60% of bromine originated from VSLS is able to reach the stratosphere, which is consistent with earlier modeling approaches that use a comparable simple dehydration mechanism. However, when applying a more complete chemistry scheme the model results show that virtually the entire amount of bromine contributed by VSLS enters the stratosphere, rendering the impact of dehydration and scavenging on inorganic bromine insignificant in the TTL. This discrepancy is mainly caused by the low fraction of actually soluble inorganic bromine, the small available particle surface area density that restricts adsorption and finally heterogeneous reactions which are able to release adsorbed species into gas phase.

Long-term calculations of VSLS injection into the stratosphere reveal a robust correlation between sea surface temperature, convective activity and the amount of short-lived source gases in the TTL, which becomes especially clear during the perturbations induced by El Niño seasons.

Finally, the impact of additional bromine originated from VSLS on stratospheric ozone depletion is analyzed. The model predicts that for 5 parts per trillion by volume (pptv) of bromine contributed by VSLS on average about 1.3% of global total column ozone is destroyed.

Contents

Part I.

Introduction and Fundamentals

1. Introduction

Bromine is considered to be one of the most important species in atmospheric chemistry. Although its average concentration in the atmosphere is extremely small (about 20 molecules of bromine in 10^{12} molecules of air, World Meteorological Organization, 2010), it contributes significantly to the depletion of Earth's vital ozone layer and is to this day subject to intensive research. This thesis focuses on a current key question in the research of atmospheric bromine: the impact of very short-lived substances, abbreviated as VSLS, on the abundance of bromine in the stratosphere. This introductory chapter provides a concise overview of the historical background of atmospheric bromine (Section 1.1) and the main scientific questions regarding bromine VSLS (Section 1.2). The outline of the thesis is presented in Section 1.3.

1.1. Historical Background

Bromine was discovered about 200 years ago by Balard (1826) and Löwig (1828) in sea weed and mineral salts, respectively. Compared to typical atmospheric values the mixing ratio of bromine in sea water is relatively high (about 65 ppmv, e.g., Tallmadge et al., 1964). In fact, the major part of natural bromine emission can be attributed to the ocean, either by photochemical and heterogeneous release from sea salt or as metabolic byproduct of marine microorganisms (e.g., Montzka and Reimann, 2010). In the 20^{th} century, bromine compounds became used in industrial scale as gasoline additive, flame retardant and fumigation agent.

About 30 years ago, it was confirmed that catalytic cycles involving chlorine and bromine significantly contribute to ozone depletion (e.g., Stolarski and Cicerone, 1974; Molina and Rowland, 1974; Wofsy et al., 1975; Yung et al., 1980). Actually, bromine was found to be about 40–60 times more efficient in destroying ozone than the more abundant chlorine (e.g., Daniel et al., 1999; Sinnhuber et al., 2009), whose mixing ratio is roughly 150 times larger (e.g., Montzka and Reimann, 2010). Subsequent studies showed that stratospheric ozone is very sensitive to even small changes in bromine abundance (e.g., Salawitch et al., 2005; Feng et al., 2007; Sinnhuber et al., 2009; Pisso et al., 2010). Alarmed by the discovery of the catastrophic ozone destruction over the Antarctic by Farman et al. (1985), the international community agreed to widely restrict production and industrial application of ozone depleting substances (ODS) including anthropogenic bromine compounds by signing the "Montreal Protocol on Substances That Deplete the Ozone Layer" in 1987.

Until the end of the 20^{th} century, the primary source of atmospheric bromine was assumed to be long-lived source gases such as methyl bromide (CH_3Br), being predominantly of natural origin, and the anthropogenic halons (mainly Halon-1211, Halon-1301; e.g., Wamsley et al., 1998). It was generally believed that only these source gases, whose average lifetime in the lower atmosphere generally exceeds one year, are able to remain intact long enough to contribute to stratospheric bromine. However, several studies indicated a discrepancy between the observed amount of stratospheric bromine and the relatively well quantified sources of long-lived trace gases (e.g., Ko et al., 1997; Dvortsov et al., 1999; Sturges et al., 2000). They suggested that the apparent gap could be filled when taking into account

a previously neglected source – very short-lived bromine substances. These species had been already known but were thought to be unimportant for the stratosphere due to their short lifetime which restricts their atmospheric distribution (e.g., World Meteorological Organization, 1991). The aforementioned studies demonstrated that VSLS can contribute a significant amount to stratospheric bromine nonetheless, either by reaching the stratosphere directly by deep convection or by being transported into the upper troposphere where their degradation products may ascend further.

Today, after more than a decade of research, the importance of VSLS for stratospheric bromine is generally accepted. The most important bromine VSLS are assumed to be $CHBr_3$ and CH_2Br_2, both of natural origin, which contribute about 4.5 ± 3.5 pptv to stratospheric bromine loading, compared to approximately 15.5 pptv originated from long-lived source gases (e.g., World Meteorological Organization, 2010). However, this estimate along with other important details of VSLS sources and transport remains uncertain to this day.

1.2. Current Scientific Key Questions

Thanks to the extensive scientific activity in the past years our understanding of the role of VSLS has significantly improved. However, important pieces are still missing in the overall picture. The most pressing questions regarding VSLS can be condensed to the following three points:

- **Sources.** Our knowledge about strength and location of VSLS emissions is rather limited to this day. In situ measurements of very short-lived species are sparse and localized. In addition, the few available observations show large spatial and temporal variations and are difficult to compare due to significant inter-instrumental biases (Butler et al., 2010), rendering the quantification of source gas emissions a challenging task. Recently, some progress was made in measuring the concentration of major phytoplankton groups from space (Vountas et al., 2007; Bracher et al., 2009). As cyanobacteria and diatoms are assumed to be the major biological source for bromine VSLS (e.g., Montzka and Reimann, 2010), space-borne observations of these microorganisms could possibly reveal vital information regarding the emission of biogenic bromocarbons. However, existing parametrizations that relate the population of marine microorganisms or other observational data to bromine VSLS emissions still contain large uncertainties (Quack et al., 2007b; Palmer and Reason, 2009; Hense and Quack, 2009). On the other hand, top-down estimates relying on the observation of bromine product gases also lead to wide range of possible emission values and reveal little information about the location of VSLS sources (e.g, Montzka and Reimann, 2010, see also Table 3.2).

- **Transport.** A crucial point is how and to what extent VSLS are transported into the upper troposphere/lower stratosphere (UTLS). In order to contribute to stratospheric bromine, short-lived source gases must be lifted from the planetary boundary layer into the upper troposphere before they decay. From there, it is possible that either the VSLS themselves or their products are able to ascend further into the stratosphere. The most likely pathway for these species is thought to be tropical deep convection that penetrates well into the tropopause region (e.g., Sinnhuber and Folkins, 2006; Gettelman et al., 2009; Aschmann et al., 2009). An important process to consider in this context is the efficient dehydration of moist tropospheric air to typical dry stratospheric values, which takes place in a relatively small and confined altitude

range at the tropical tropopause layer or TTL (e.g., Fueglistaler et al., 2009a). The formation of ice particles (cirrus clouds) in the course of the dehydration process could affect the abundance of inorganic bromine product gases in the TTL significantly. Most studies that investigate the impact of VSLS utilize a fixed washout lifetime of about 10 days for inorganic bromine, which is assumed to be highly soluble and thus easily adsorbed on sedimenting ice particles (e.g., Dvortsov et al., 1999; Nielsen and Douglass, 2001; Warwick et al., 2006; Hossaini et al., 2010). However, the dehydration process itself is still not fully understood and its possible impact on bromine species has not been investigated so far with a more refined model.

- **Trend.** An important question is how the contribution of VSLS to stratospheric bromine will respond to possible changes under future atmospheric conditions. Numerous modeling studies predict an increase of average sea surface temperature due to intensified radiative forcing by a growing amount of greenhouse gases (e.g. Rayner et al., 2003; Kumar et al., 2004; Dong et al., 2009). This warming is assumed to cause increased upwelling in the tropics and an overall acceleration of the Brewer-Dobson circulation (e.g., Butchart et al., 2006; Li et al., 2008; Oman et al., 2009; Bönisch et al., 2011). Unlike the long-lived anthropogenic ODS, whose emissions are restricted by international treaties and whose local abundance is not very sensitive to changes in atmospheric transport since they are generally well-mixed anyway, the situation for natural short-lived species is more complex. On the one hand, little is currently known about how the biological production of VSLS will respond to climate changes. A recent study by Butler et al. (2007) found a positive correlation of VSLS emission and sea surface temperature, though it is not entirely clear which processes cause this effect. On the other hand, intensified tropical upwelling will likely lead to an increased transport of short-lived species into the tropopause region. However, several studies indicate that increased upwelling is accompanied by higher mixing ratios of water vapor in the TTL (e.g., Austin et al., 2007; Shu et al., 2011), which in turn could possibly make the loss of soluble (bromine) species due to dehydration more efficient. The complex interplay of variable sources, transport and chemistry poses a major challenge for predicting the future contribution of bromine VSLS.

1.3. Outline of the Thesis

The main objective of this thesis is to contribute to the investigation of the primary scientific questions regarding bromine VSLS as described in the previous section. To study the relevant processes on a theoretical basis, a simulation framework has been developed that offers an adequate representation of VSLS transport in the TTL.

The necessary foundation is established in Chapters 2 and 3, presenting a brief overview of fundamental aspects of Earth's atmosphere and selected processes that are most relevant for this study, the current state of research regarding atmospheric bromine involving abundance and lifetime of source gases, partitioning of inorganic product gases and the most important catalytic cycles contributing to depletion of stratospheric ozone.

The utilized simulation framework, based on the three-dimensional (3-D) chemistry transport model (CTM) originally developed by Sinnhuber et al. (2003a), is described in Chapter 4. For this study, the existing CTM was extensively modified and forms the basis for different model experiments that investigate the transport of VSLS into the stratosphere.

An initial validation of the applied modeling approach is given in Chapter 5. Comparisons

with observations of bromine source and product gases along with other proxies are used to evaluate whether the model is able to adequately reproduce transport and related processes in the TTL.

Chapter 6 analyzes how and to what extent VSLS are able to contribute to stratospheric bromine loading. First, the possible impact of dehydration on inorganic bromine is investigated using different implementations of the related processes. In addition, sensitivity calculations are applied to assess the relative importance of the VSLS source distribution for the abundance of these species in the TTL.

A long-term analysis of the injection of VSLS into the stratosphere is provided in Chapter 7. This part focuses on the connection between sea surface temperature, convective activity and bromine in the TTL with special emphasis on the impact of the El Niño Southern Oscillation (ENSO). Since this periodical perturbation influences the whole TTL, the extreme conditions during these seasons offer the opportunity to study the response of VSLS transport to sea surface temperature changes. This is particularly relevant considering the expected increase of temperature in a future climate.

Finally, Chapter 8 evaluates the representation of stratospheric ozone in the model. In a second step, the contribution of additional bromine originated from VSLS to stratospheric ozone depletion is investigated.

2. The Earth's Atmosphere

This chapter provides a brief introduction to fundamental characteristics and processes of the terrestrial atmosphere that are relevant for this work. Section 2.1 discusses the vertical structure and Section 2.2 presents an overview of the general atmospheric circulation. The tropical upper troposphere/lower stratosphere and the associated transport processes are of particular importance for this study and are introduced in Section 2.3. Finally, the most relevant aspects of stratospheric ozone chemistry are outlined in Section 2.4.

2.1. Vertical Structure

The terrestrial atmosphere is commonly divided into different layers according to its typical temperature profile (e.g., Wallace and Hobbs, 2006, see also Figure 2.1). The lowermost compartment is the troposphere ranging from the planetary boundary layer (BL) near the surface to the tropopause at about 7 to 17 km, depending on the season and latitude. The troposphere is characterized by a negative temperature gradient with increasing altitude reaching a minimum at the tropopause. This temperature inversion frequently disturbs the tropospheric stratification causing turbulence and convection; phenomena we generally experience as "weather". As a consequence of perpetual convective overturning, the troposphere is well-mixed and relatively humid compared to higher altitudes. The next layer is the stratosphere limited by the stratopause at about 50 km. Radiative heating

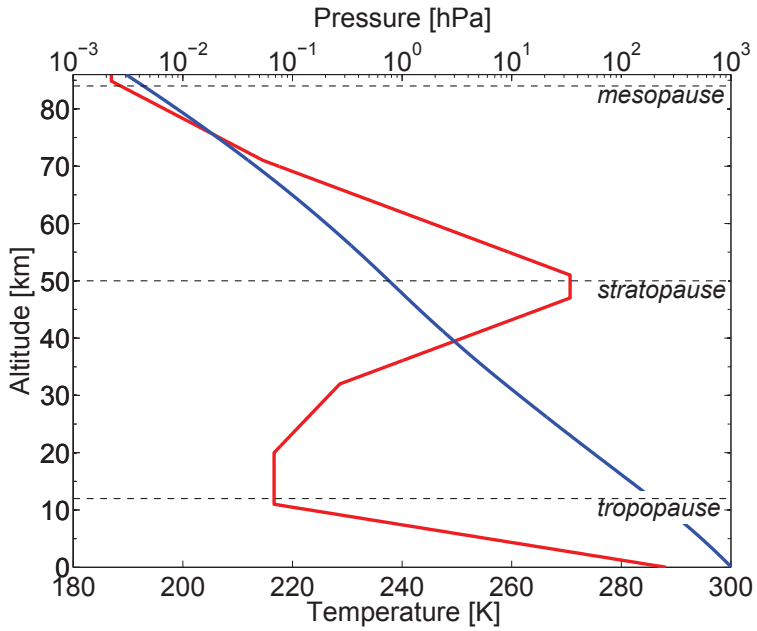

Figure 2.1.: Average profile of temperature (red) and pressure (blue, logarithmic scale) derived from the U.S. Standard Atmosphere (NOAA, 1976).

caused by the absorption of ultra-violet (UV) insolation by ozone molecules leads to increasing temperatures with altitude. The stable thermal layering inhibits vertical mixing and transport in contrast to the turbulent troposphere. Further above the mesosphere extends to about 80 to 90 km with the temperature constantly decreasing again until the minimum is reached at the mesopause, the coldest part of the atmosphere. Beyond this altitude the temperature rises again in the thermosphere, however, the density of air is so low that the usual conception of temperature is no longer valid.

Throughout the atmosphere the pressure of air is falling nearly exponentially (Figure 2.1) and can be approximated by using the barometric formula

$$p(z) \approx p(z_0) \exp\left(-\frac{(z - z_0)\, g}{RT}\right) \tag{2.1}$$

with altitude z, reference altitude z_0, mean temperature T, specific gas constant of dry air R and the gravitational acceleration g. Consequently, roughly 90% of the total atmospheric mass is concentrated below 17 km.

Beside altitude and pressure another important vertical coordinate in atmospheric sciences is the potential temperature θ. It is defined as the temperature an air parcel would have if it were expanded or compressed adiabatically (i.e. without the exchange of heat) from its existing temperature and pressure to a reference pressure p_0, typically 1000 hPa:

$$\theta = T \left(\frac{p_0}{p}\right)^{R/c_p} \tag{2.2}$$

Here, c_p denotes the specific heat capacity of dry air. Since atmospheric processes are often close to adiabatic on a timescale of 10 to 15 days (e.g., Wallace and Hobbs, 2006), the potential temperature offers a significant conceptual advantage being a conserved quantity for air parcels in good approximation. For example, horizontal advection of air masses generally occurs on surfaces of constant potential temperature, not altitude or pressure, which makes related calculations in a θ-coordinate system much easier.

2.2. Atmospheric Circulation

Obviously, the distribution of trace gases in the atmosphere is dependent on atmospheric transport processes, which especially applies for short-lived species. This section provides an overview of the fundamental circulation patterns in the atmosphere.

2.2.1. Geostrophic Equilibrium

Two key processes drive the atmospheric motion: the differential heating provided by the sun and the rotation of the planet (e.g., Andrews et al., 1987). The differential heating leads to a non-uniform temperature distribution across the surface and the atmosphere of Earth. Since temperature is directly related to air pressure as stated in Equation 2.1, the differing temperature induces the formation of low or high pressure areas. The pressure gradient causes a balancing flow of air from high to low pressure regions. However, the eastward spinning of the Earth provides angular momentum to all objects on the surface, including the atmosphere itself. Consequently, air flows are deflected by the Coriolis force, a pseudo force apparent in non-inertial systems such as the rotating Earth. The magnitude of the deflection can be described by the Coriolis parameter f:

$$f = 2\Omega \sin(\phi) \tag{2.3}$$

Here, Ω is the Earth's rotation rate and ϕ the latitude. For an air parcel moving with both zonal and meridional velocity components (commonly denoted by u and v), the deflective acceleration in zonal direction would be $-f \cdot v$ and in meridional direction $f \cdot u$. For example, an air parcel moving strictly northward on the Northern Hemisphere would be deflected to the right, i.e. eastward. The balance between the (horizontal) pressure gradient and the Coriolis force is called geostrophic equilibrium. Therefore, geostrophic winds do not flow directly in the direction of pressure gradient force but rather tend to spiral around regions of high and low pressure regions.

2.2.2. Tropospheric Circulation

As seen in Figure 2.1, the temperature gradient or lapse rate is negative with height in the troposphere. That means colder air masses with higher density generally lie above warmer, less dense layers heated by the surface. This causes static instability resulting in an upward flux of warm buoyant air which is referred to as convection. As a consequence, the troposphere is generally well mixed by convective overturning. The general flow patterns in the troposphere are typically separated into three primary circulation cells (e.g., Andrews et al., 1987; Wallace and Hobbs, 2006) which are illustrated in Figure 2.2:

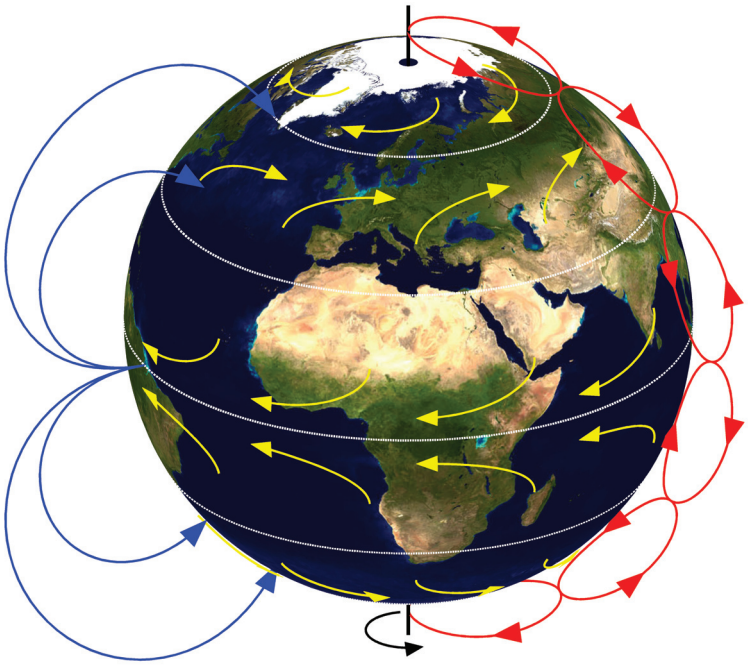

Figure 2.2.: Idealized depiction of the Earth's atmospheric circulation. The red and blue arrows denote the tropospheric circulation cells and the stratospheric Brewer-Dobson circulation, respectively. The yellow arrows illustrate the prevailing surface winds at different latitudes. The white lines mark the circles of latitude in a 30°-spacing.

- The **Hadley cell** is the largest and most distinctive circulation cell spanning poleward from the equator to about 30°N/S. Warm and moist air rises above the intertropical convergence zone (ITCZ) in a band of thunderstorm cloud towers into the upper

tropical troposphere where it is transported poleward. Eventually the cooled air descends at a latitude of about 30°N/S and flows back to the equatorial low pressure area. The Coriolis force deflects this flow westward (Section 2.2.1), a wind system which is also referred to as the trade winds.

- The mechanism that drives the **Polar cell** is similar to the one present in the tropics. Relatively warm and moist air rises at 60°N/S, is transported poleward, sinks and flows back near the surface, forming the polar easterlies. Like its counterpart in the tropics this circulation system is generally stable and predictable under normal circumstances.

- Between 30-60°N/S lies the **Ferrel cell**. It acts like a "gear-wheel" between the Polar and the Hadley cell with an opposite circulation direction compared to its neighbors. Warm air from the subpolar low pressure region at 60°N/S rises and turns equatorward, diverting from the polar circulation. At 30°N/S, the descending air masses mix with air from the tropical Hadley cell and flow back poleward, forming the westerlies. However, this circulation pattern is relatively unstable compared to the neighboring cells since around 60°N/S the westerlies have to compete against the polar easterlies. This so called polar front is constantly moving and may disturb the circulation in the Ferrel cell.

2.2.3. Stratospheric Circulation

In contrast to the troposphere which is dominated by static instability, convective overturning and turbulence the stratosphere is, as its name suggests, stably stratified. Radiative heating leads to a positive lapse rate (Section 2.1) that largely inhibits vertical transport. However, Brewer (1949) and Dobson (1956) postulated a poleward circulation in the stratosphere to explain the observed tracer distributions: air parcels in the tropical stratosphere are lifted up slowly and are transported poleward to higher latitudes, where they sink again (Figure 2.2). Unlike the convectively driven circulation in the troposphere, the Brewer-Dobson circulation is forced by atmospheric waves. There are several wave-like phenomena in the atmosphere that are important for the general circulation, but especially relevant for the stratosphere are the so called Rossby waves whose restoring mechanism is the meridional gradient of potential vorticity. Rossby waves propagating up from the tropical and mid latitude troposphere transfer energy and angular momentum to stratospheric air masses and drive the poleward circulation (e.g., Shepherd, 2000, 2007).

2.3. The Tropical Upper Troposphere/Lower Stratosphere

The tropical UTLS is especially important for this study being the interface between two very different dynamical regimes and acting as "gateway" for atmospheric trace gases traveling into the stratosphere (e.g., Holton et al., 1995; Fueglistaler et al., 2009a). In the tropics, the transition from the troposphere to the stratosphere extends over several kilometers and is also often referred to as tropical tropopause layer. Note that in the following "tropical" is defined as the meridional range between 20°N to 20°S.

Figure 2.3 shows a schematic of the vertical transport processes in the TTL. The lower part of the TTL is dominated by deep convection (denoted by convective flux ω_c), which extends typically from 10 to 15 km in the tropics, rarely reaching higher above 17 km. The altitude at which convection detrains is mainly constrained by three factors (Fueglistaler et al., 2009a): 1. The equivalent potential temperature θ_e of air parcels near the surface,

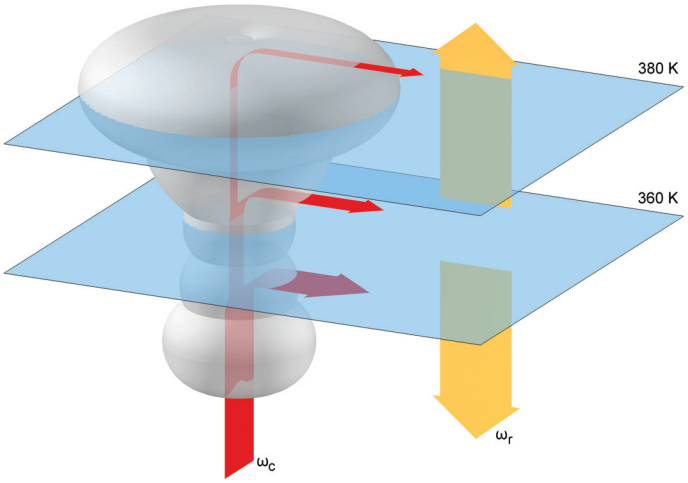

Figure 2.3.: Schematic of the vertical transport in the UTLS. The convective flux ω_c is denoted by the red arrows whereas the large-scale heating-rate-driven flux ω_r is represented by the orange arrows. The two layers at 360 K (∼15.5 km) and 380 K (∼17 km) depict the LZRH and the cold point, respectively.

i.e. the potential temperature that is reached when all latent heat is released. 2. The convectively available potential energy (CAPE) that corresponds to the vertically integrated buoyancy. 3. In-mixing of ambient air masses into the convective updraft (entrainment). Theoretically, a convective updraft detrains at its level of neutral buoyancy (LNB), which is located approximately where θ_e is equal to the ambient potential temperature if there is no entrainment. In reality, entrainment of ambient air with lower θ_e is assumed to significantly decrease the effective LNB of convective updrafts, however, quantitative evaluation of entrainment is difficult and remains uncertain. A recent study of Romps and Kuang (2010) suggests that convectively lifted air is highly diluted by entrainment, i.e. only about 10–30% of detrained air in the upper troposphere is actually originated from the boundary layer. Another process to consider here is "overshooting" convection: air parcels in a convective updraft generally arrive at their LNB with a non-zero velocity, i.e. the available kinetic energy will lift the air parcels above their LNB against the downward buoyant force. The main convective outflow in the tropics occurs approximately at 14 km or 355 K, which is defined as the lower boundary of the TTL by Fueglistaler et al. (2009a), however, especially strong overshooting convection is able to penetrate the tropopause and directly reach the stratosphere (e.g., Jorgensen and LeMone, 1989; Liu and Zipser, 2005).

Up to 15.5 km or 360 K air masses are cooling radiatively and generally subside outside of convective cells (denoted by ω_r). Above this level, referred to as level of zero clear sky radiative heating (LZRH, lower plane in Figure 2.3), this process reverses sign and air is predominantly ascending (e.g., Corti et al., 2005; Sinnhuber and Folkins, 2006). At 17 km or 380 K the temperature in the TTL reaches its minimum (cold point, upper plane). Here, ascending moist tropospheric air gets "freeze dryed" to stratospheric values. Though important aspects of TTL dehydration are not yet fully understood, it is confirmed that this phenomenon is caused by a combination of low temperatures and transport effects (e.g., Sherwood and Dessler, 2001; Holton and Gettelman, 2001; Gettelman et al., 2002a;

Fueglistaler et al., 2005, 2009a; Schoeberl and Dessler, 2011). During the relatively slow ascent through the TTL it is highly probable that air masses are transported horizontally into the coldest areas of the tropical tropopause typically residing over the Maritime Continent and Western Pacific regions. The so called "cold trap" hypothesis (Holton and Gettelman, 2001) states that a major part of the whole TTL air gets dehydrated in these particular areas. This process is not only important for the water content of the UTLS itself but also for soluble species which may be adsorbed to the surface of falling ice particles thus being unable to reach the stratosphere (see Section 6.1).

Above 425 K or 18.5 km, the direct influence of the troposphere on temperature and horizontal circulation diminishes, thus this altitude is defined as upper bound of the TTL by Fueglistaler et al. (2009a).

2.4. Stratospheric Ozone Chemistry

Ozone (O_3) is one of the most important constituents of Earth's atmosphere despite its very small concentration, which is typically in the range of a few molecules of O_3 per million molecules of air. As it efficiently absorbs incoming solar radiation in the spectral range between 230 and 320 nm, the intensity of biologically harmful UV radiation is greatly reduced at the Earth's surface (e.g., Wallace and Hobbs, 2006). On the other hand, the absorption of UV radiation by O_3 determines the vertical profile of temperature in the stratosphere (Section 2.1).

The understanding of atmospheric ozone has significantly improved since Chapman (1930) formulated a first photochemical theory of the formation and destruction of ozone that solely relies on oxygen (see, e.g., review by Solomon, 1999):

$$O_2 + h\nu \longrightarrow 2\,O \tag{2.4}$$
$$O + O_2 + M \longrightarrow O_3 + M \tag{2.5}$$
$$O_3 + h\nu \longrightarrow O_2 + O \tag{2.6}$$
$$O + O + M \longrightarrow O_2 + M \tag{2.7}$$
$$O + O_3 \longrightarrow 2\,O_2 \tag{2.8}$$

In the stratosphere, almost all of the atomic oxygen produced by ozone photolysis (Reaction 2.6) immediately reforms ozone by Reaction 2.5, thus both species are rapidly interchange with each other within seconds or less. Since the reaction with other species occurs on a much slower timescale, atomic oxygen and ozone are commonly considered together as odd oxygen (O_x). Chapman's assumptions regarding the production and transformation of ozone were correct, however, he overestimated the amount of stratospheric ozone by about a factor of two. The Reactions 2.7 and 2.8 that may lead to a net loss of O_x have a very small yield and could not explain the observed perturbations in O_x abundance.

In the following years it became clear that other species are involved in the destruction of stratospheric ozone, such as odd hydrogen (HO_x, e.g., Bates and Nicolet, 1950) and odd nitrogen (NO_x, e.g., Crutzen, 1970). The reactive members of these tracer families are able to trigger catalytic cycles that remove O_x:

$$O + OH \longrightarrow O_2 + H \tag{2.9}$$
$$H + O_2 + M \longrightarrow HO_2 + M \tag{2.10}$$
$$O + HO_2 \longrightarrow O_2 + OH \tag{2.11}$$
$$\text{Net: } 2\,O \longrightarrow O_2$$

$$\mathrm{OH} + \mathrm{O_3} \longrightarrow \mathrm{HO_2} + \mathrm{O_2} \tag{2.12}$$
$$\mathrm{HO_2} + \mathrm{O_3} \longrightarrow \mathrm{OH} + 2\,\mathrm{O_2} \tag{2.13}$$
$$\text{Net: } 2\,\mathrm{O_3} \longrightarrow 3\,\mathrm{O_2}$$
$$\tag{2.14}$$
$$\mathrm{NO} + \mathrm{O_3} \longrightarrow \mathrm{NO_2} + \mathrm{O_2} \tag{2.15}$$
$$\mathrm{O} + \mathrm{NO_2} \longrightarrow \mathrm{NO} + \mathrm{O_2} \tag{2.16}$$
$$\text{Net: } \mathrm{O} + \mathrm{O_3} \longrightarrow 2\,\mathrm{O_2}$$

However, one of the most important milestones of ozone research was the discovery of the catalytic destruction of O_3 by chlorine (Stolarski and Cicerone, 1974; Molina and Molina, 1987), for example:

$$\mathrm{Cl} + \mathrm{O_3} \longrightarrow \mathrm{ClO} + \mathrm{O_2} \tag{2.17}$$
$$\mathrm{ClO} + \mathrm{O} \longrightarrow \mathrm{Cl} + \mathrm{O_2} \tag{2.18}$$
$$\text{Net: } \mathrm{O} + \mathrm{O_3} \longrightarrow 2\,\mathrm{O_2}$$
$$\tag{2.19}$$
$$\mathrm{Cl} + \mathrm{O_3} \longrightarrow \mathrm{ClO} + \mathrm{O_2} \tag{2.20}$$
$$\mathrm{ClO} + \mathrm{ClO} + \mathrm{M} \longrightarrow \mathrm{Cl_2O_2} + \mathrm{M} \tag{2.21}$$
$$\mathrm{Cl_2O_2} + \mathrm{h}\nu \longrightarrow \mathrm{Cl} + \mathrm{ClO_2} \tag{2.22}$$
$$\mathrm{ClO_2} + \mathrm{M} \longrightarrow \mathrm{Cl} + \mathrm{O_2} + \mathrm{M} \tag{2.23}$$
$$\text{Net: } 2\,\mathrm{O_3} \longrightarrow 3\,\mathrm{O_2}$$

This discovery was especially delicate as man-made chlorofluorocarbons (CFCs) were identified to be a major source of atmospheric chlorine (Molina and Rowland, 1974; Crutzen et al., 1978). Shortly afterwards, similar catalytic cycles were identified also for bromine (e.g., Wofsy et al., 1975; Yung et al., 1980; McElroy et al., 1986, see also Section 3.2.3). The dangerous potential of the halogen species became fully clear in 1985 when Farman et al. (1985) discovered a drastic decrease of total column ozone at the British Antarctic Survey station at Halley in austral spring. Further measurements confirmed that the depletion of ozone occurs roughly above the entire Antarctic continent, a phenomenon that became known as Antarctic ozone "hole". The extensive scientific activity sparked by this discovery soon identified two major processes that cause this seasonal depletion of polar stratospheric ozone. The first one is a dynamical phenomenon called polar vortex that develops over the poles in the absence of light during winter which effectively isolates polar air masses from the surrounding mid latitudes (e.g., Holton et al., 1995). The second important cause is the presence of polar stratospheric clouds (PSCs) in the polar vortex, consisting mostly of ice and and solid nitric acid trihydrate (NAT) particles (McCormick et al., 1982; Steele et al., 1983; Crutzen and Arnold, 1986; Toon et al., 1986). Heterogeneous reactions on these particle surfaces are able to shift the halogen balance from inactive reservoir species towards highly reactive compounds (e.g., Solomon et al., 1986; McElroy et al., 1986, see also Table 4.5). When sunlight returns in spring time, the reactive halogens are able to quickly destroy large amounts of ozone in the isolated environment of the vortex (e.g., Solomon, 1999). Facing the overwhelming evidence of the dangerous potential of man-made halogens, almost all countries agreed to ban CFCs and other ozone depleting substances by signing the Montreal Protocol in 1987.

3. Atmospheric Bromine

An introduction to the current state-of-the-art regarding atmospheric bromine is presented in this chapter. The major sources of bromine are discussed in Section 3.1, covering long- and short-lived bromocarbons and possible inorganic emissions. Section 3.2 presents the relevant atmospheric bromine chemistry: degradation of source gases, chemical partitioning of product gases and the impact on stratospheric ozone.

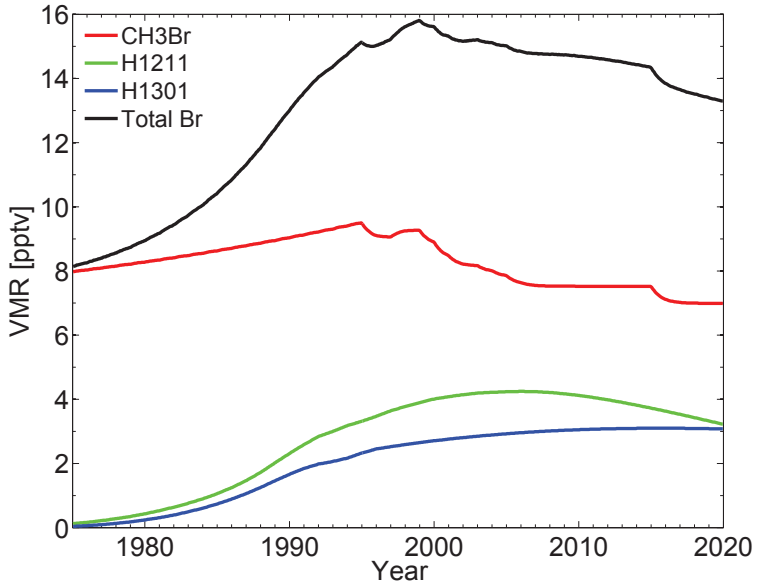

Figure 3.1.: Average tropospheric mixing ratios of bromine long-lived source gases derived from WMO 2010 scenario A1 calculations (Daniel and Velders, 2010).

3.1. Sources

The major sources of atmospheric bromine are assumed to be either natural or anthropogenic bromocarbons, with long-lived source gases contribute about 70% to stratospheric bromine loading. It is confirmed that also short-lived substances are important for the stratosphere, however, the extent of their contribution is still subject to research. Another possible source is thought to be emissions of inorganic species from sea salt aerosols, which can be important for the tropospheric bromine abundance. This section provides an overview of the most relevant species and their sources.

3.1.1. Long-Lived Compounds

According to the recent World Meteorological Organization (WMO) report (Montzka and Reimann, 2010), approximately 15–16 pptv out of 19–24 pptv of stratospheric inorganic

bromine (Br_y) is originated from long-lived source gases (60–80%; Table 3.1). The major constituent is CH_3Br, accounting for about 7.4 pptv in 2008. Approximately 34% can be attributed to anthropogenic emissions, caused for example by quarantine or pre-shipment use. However, the major part of CH_3Br emissions is of natural origin, mainly from the ocean, but also from wetlands and coastal salt marshes. The two other important long-lived source gases are the anthropogenic Halon-1211 ($CClBrF_2$) and Halon-1301 ($CBrF_3$) that were commonly used in fire extinguisher systems, accounting for about 4.3 pptv and 3.2 pptv in 2008, respectively. The average tropospheric photochemical lifetime of the halons is in the order of decades (Table 3.1), thus these species are relatively well-mixed throughout the atmosphere. The average lifetime of CH_3Br is shorter (about 1 year), which introduces an inter-hemispherical bias in its atmospheric distribution. On the Northern Hemisphere, where the anthropogenic emissions are higher, the mixing ratio of CH_3Br is increased by approximately 1.2 pptv (in 2008, Montzka and Reimann, 2010).

Figure 3.1 shows the development of long-lived bromocarbon abundance as projected by the WMO scenario A1 (Daniel and Velders, 2010). The combined amount of these species peaks in 1999 and is currently decreasing since the constituents are regulated by the Montreal Protocol (entered into force in 1989) which widely restricts their industrial application.

Table 3.1.: Estimated abundance of bromine source gases in the boundary layer and the average atmospheric lifetime (World Meteorological Organization, 2010). All mixing ratio values are in pptv.

Chemical Formula	Common or Industrial Name	Average BL Mixing Ratio	Lifetime
Long-lived species			
$CHBr_3$	Methyl bromide	8.5 ± 0.6[a]	0.7 y
$CClBrF_2$	Halon-1211	4.4 ± 0.3[a]	16 y
$CBrF_3$	Halon-1301	3.2 ± 0.8[a]	65 y
Short-lived species			
$CHBr_3$	Bromoform	1.6 ± 0.9	24 d[b]
CH_2Br_2	Dibromomethane	1.1 ± 0.4	123 d[b]
CH_2BrCl	Bromochloromethane	0.5 ± 0.1	137 d[b]
$CHBrCl_2$	Bromodichloromethane	0.3 ± 0.3	78 d[b]
$CHBr_2Cl$	Dibromochloromethane	0.3 ± 0.3	59 d[b]

[a] Values for 2004.
[b] Local tropospheric lifetime.

3.1.2. Very Short-Lived Substances

VSLS are defined by the World Meteorological Organization (2010) as trace gases whose local tropospheric lifetimes are comparable to, or shorter than, tropospheric transport time scales, such that their tropospheric distributions are non-uniform. In practice, trace gases with lifetimes of up to six months are considered to be “very short-lived”.

In contrast to their long-lived counterparts, where anthropogenic emissions play a significant role, the bromine VSLS are almost completely of natural origin. The most notable anthropogenic VSLS is n-propyl bromide (C_3H_7Br), but its emission is small compared to the major biogenic short-lived species (e.g., Montzka and Reimann, 2010;

Wuebbles et al., 2011). Estimated boundary layer mixing ratios and tropospheric lifetimes of the most important bromine VSLS currently known are listed in Table 3.1. $CHBr_3$ and CH_2Br_2 are assumed to be the most abundant short-lived species, with average BL mixing ratios of 1.6 pptv and 1.1 pptv, respectively.

The main source of bromine VSLS is considered to be marine microorganisms such as macroalgae and phytoplankton groups. In fact, the highest emissions of these species are measured near coastal and upwelling areas especially in the tropics (e.g., Carpenter and Liss, 2000; Quack and Wallace, 2003; Yokouchi et al., 2005; Butler et al., 2007; Quack et al., 2007a; Carpenter et al., 2009, see also Table 3.2). However, as indicated in the introduction (Section 1.2), it is difficult to give accurate large-scale VSLS flux estimates, as there are only few measurements available which in addition show very large spatial and temporal variability; for example, Quack and Wallace (2003) measure $CHBr_3$ in a range from 0.2 to 100 pptv in the marine boundary layer (MBL). To this day, our knowledge about the processes that control the biological production of VSLS is rather limited (e.g., Butler et al., 2007; Palmer and Reason, 2009; Hense and Quack, 2009). Furthermore, Butler et al. (2010) indicated that the variability of observed VSLS emissions can be partly attributed to inter-instrumental biases. Thus, the current global BL mixing ratios and flux estimates of VSLS presented in Table 3.1 and 3.2 contain large uncertainties, especially for the less abundant species.

Table 3.2.: Estimated bromine VSLS flux (unit: Gg Br/yr) from recent studies. Adapted from Montzka and Reimann (2010).

Reference	$CHBr_3$ flux			CH_2Br_2 flux		
	Global	Open Ocean	Coastal	Global	Open Ocean	Coastal
Yokouchi et al. (2005)	820					
Butler et al. (2007)	800	150	650	280	50	230
Carpenter et al. (2009)			200			
Warwick et al. (2006)	560	280	280	100		
Liang et al. (2010)	430	260	170	57	34	23

VSLS are not well-mixed in the lower atmosphere. This can be partly attributed to the spatial source distribution (see Section 6.2), but the more important factor is the short lifetime of these species. Strongly dependent on the efficiency of vertical transport, concentrations of VSLS in the TTL tend to be high in areas which show vigorous convective activity, such as the West Pacific or the Maritime Continent, forming localized "hot spots" (e.g., Berthet et al., 2007, see also Sections 5.1, 5.2, 6.3).

Another key process which is subject to current research is the impact of TTL dehydration on bromine originated from VSLS (Br_y^{VSLS}; e.g., Sinnhuber and Folkins, 2006; Gettelman et al., 2009; Aschmann et al., 2009; Hossaini et al., 2010; Schofield et al., 2011; Aschmann et al., 2011). The organic source gases are generally insoluble and thus not affected by dehydration. Inorganic bromine originated from long-lived species (Br_y^{Long}) is not significantly affected as well since the long-lived species are generally able to reach the stratosphere before they decay due to their chemical longevity. This process is also often referred to as "source gas injection" (SGI), i.e. the bromine source gases themselves are able to reach the stratosphere. However, in the case of VSLS, the lifetimes are generally assumed to be too short to reach the stratosphere intact which means that a major part of the source gases already decays in the TTL into Br_y^{VSLS}. This inorganic product gas

may reach the stratosphere eventually which is termed "product gas injection" (PGI). A significant part of inorganic bromine in the troposphere and at the base of the TTL is actually highly soluble (e.g., HBr, HOBr) and may be dissolved in water droplets or adsorbed on ice particles (e.g., Lary, 1996; Sinnhuber et al., 2002; Yang et al., 2005). As these droplets or particles sediment, the dissolved/adsorbed bromine is effectively removed from the TTL.

3.1.3. Inorganic Sources

In addition to organic long- and short-lived trace gases another possible source of atmospheric bromine are inorganic species. Several studies found elevated concentrations of bromine monoxide (BrO), especially in the polar troposphere, that cannot be explained solely by organic sources (e.g., Hausmann and Platt, 1994; Kreher et al., 1997; Richter et al., 1998; Fitzenberger et al., 2000; Platt and Hönninger, 2003; Sinnhuber et al., 2005; Salawitch et al., 2010). The exact mechanism is still not fully understood, but it is generally assumed that multiphase chemistry (Reaction 3.1) is able to release bromine from sea salt aerosols, or, at higher latitudes, from snow/sea ice surfaces, brine or frost flowers, triggering an autocatalytic cycle (e.g. McElroy et al., 1999; Simpson et al., 2007) such as:

$$\mathrm{HOBr} + \mathrm{Br}^- + \mathrm{H}^+ \longrightarrow \mathrm{H_2O} + \mathrm{Br_2} \tag{3.1}$$

$$\mathrm{Br_2} + \mathrm{h}\nu \longrightarrow 2\,\mathrm{Br} \tag{3.2}$$

$$\mathrm{Br} + \mathrm{O_3} \longrightarrow \mathrm{BrO} + \mathrm{O_2} \tag{3.3}$$

$$\mathrm{BrO} + \mathrm{HO_2} \longrightarrow \mathrm{HOBr} + \mathrm{O_2} \tag{3.4}$$

$$\text{Net: } \mathrm{Br}^- + \mathrm{H}^+ + \mathrm{HO_2} + \mathrm{O_3} \longrightarrow \mathrm{Br} + \mathrm{H_2O} + 2\,\mathrm{O_2}$$

At polar latitudes, this cycle is particular effective when sunlight returns in spring, sparking rapid growth of BrO concentration in large areas. This phenomenon is known as "bromine explosion" (e.g., Wennberg, 1999) and the resulting BrO plumes may even contribute to tropospheric bromine abundance at lower latitudes (e.g., Platt and Hönninger, 2003; Hollwedel et al., 2004). However, it is difficult to accurately quantify the contribution of inorganic sources to stratospheric bromine since important details of the associated tropospheric chemistry are still uncertain (Simpson et al., 2007; Pyle et al., 2007). A modeling study by Yang et al. (2005) suggests that about 0.1–1 pptv of tropospheric bromine is originated from sea salt aerosols, contributing about 70–90% to the amount of bromine in the lower and middle troposphere at high latitudes. This fraction decreases rapidly towards lower latitudes and with increasing altitude; near the tropopause it is generally below 10%. Currently, it is assumed that the release of bromine from sea salt aerosols does not play an important role for the stratosphere (likely contribution <1 pptv, Montzka and Reimann, 2010).

Another possible source of atmospheric bromine which is currently discussed are volcanic emissions. Several studies found drastically increased mixing ratios of BrO in volcanic plumes (>1 ppbv; e.g., Bobrowski et al., 2003; Aiuppa et al., 2005; Theys et al., 2009; Heue et al., 2011). Actually, the degassing flux contains HBr, which is assumed to be effectively converted to BrO by a similar heterogeneous process as the one causing the polar "bromine explosions" described above (e.g., Oppenheimer et al., 2006; von Glasow et al., 2009). According to recent estimates, the global volcanic flux of HBr is approximately 5–15 Gg/yr (e.g., Pyle and Mather, 2009). Compared to the annual flux of biogenic bromocarbons (about 650–1200 Gg/yr, Montzka and Reimann, 2010), the relative impact is very small,

however, volcanic bromine might be still important as strong explosive eruptions are able to inject reactive species directly into the UTLS (e.g., von Glasow et al., 2009).

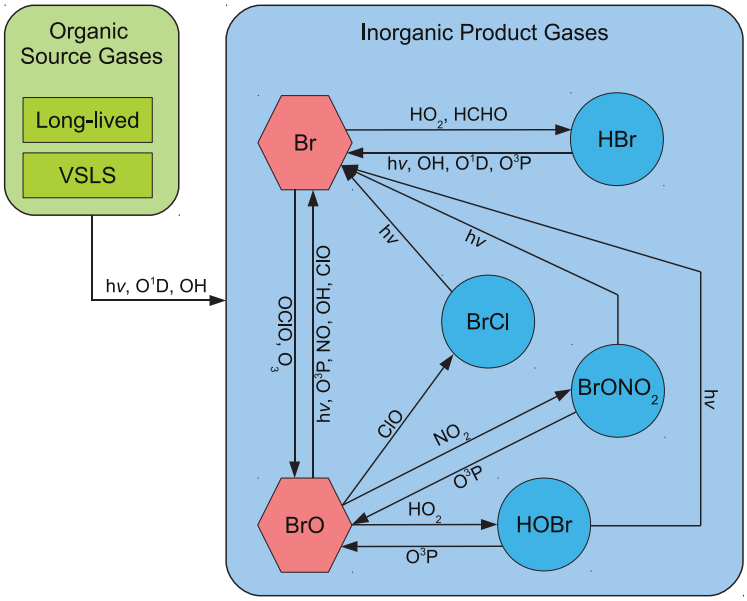

Figure 3.2.: Schematic of atmospheric bromine chemistry. The involved reactions are listed in Table 4.2–4.6.

3.2. Chemistry

A schematic of the relevant bromine chemistry is given in Figure 3.2. The organic long and short-lived source gases degrade eventually to inorganic bromine. The Br_y group is divided into reactive (BrO_x, depicted as red hexagons) and non-reactive or reservoir species (blue circles) which constantly get transformed chemically among each other. Note that "reactivity" in this context refers to the ability of the species to directly interfere with the stratospheric ozone chemistry (see Section 3.2.3). The following sections give a general overview of the bromine chemistry in the TTL whereas its implementation in the model is described in detail in Section 4.3. The corresponding reactions are listed in the Tables 4.2 to 4.6.

3.2.1. Degradation of Bromine Source Gases

The degradation of organic bromine occurs mainly by photolysis and the reaction with the hydroxyl radical (OH); in case of the long-lived source gases exited O^1D also plays a minor role in the upper stratosphere (see reactions in Table 4.2). Figure 3.3 shows the annually averaged loss rates of the most important bromine source gases for a standard tropical atmosphere and the corresponding lifetimes. The reaction coefficients and absorption cross sections were obtained from the Jet Propulsion Laboratory (JPL) recommendation (Sander et al., 2006). With the exception of $CBrF_3$, the shape of the photochemical lifetime profile is similar for the other bromine source gases. In the lower and middle troposphere, the impact of the OH reaction is still relevant, especially for CH_3Br and CH_2Br_2, but diminishes rapidly with increasing altitude. Above 10–15 km, photolysis becomes the dominant loss

process for all source gases. The resulting profiles of photochemical lifetime exhibit a large increase in the troposphere up to a maximum at approximately 12–16 km, where the local lifetimes are significantly longer than the average values given in Table 3.1, followed by a rapid decrease further above. At 30 km, the lifetime even of the most long-lived species is dropped to a few days due to efficient photodissociation. Note that also CH_2Br_2, although commonly regarded as "very short-lived", has a peak lifetime of about 1.5 years at 15 km thus one can safely assume that source gas injection is a major pathway into the stratosphere for this species.

3.2.2. Chemical Partitioning of Br_y

The average atmospheric mixing ratio of inorganic bromine is roughly 150 times lower than of inorganic chlorine (Cl_y); typical stratospheric values are around 20 pptv (e.g., Montzka and Reimann, 2010). The low mixing ratios of Br_y and its constituents present a challenge for experimental detection. To this date, only the most abundant Br_y constituent BrO can be measured from satellite instruments with sufficient accuracy, providing global coverage (Burrows et al., 1999; Richter et al., 2002; Sinnhuber et al., 2005; Sioris et al., 2006; McLinden et al., 2010; Rozanov et al., 2010a). Recently, Höpfner et al. (2009) presented satellite observations also of bromine nitrate ($BrONO_2$), however, these measurements are still subject to higher uncertainties. Furthermore, there are several local balloon or aircraft measurements available for BrO (e.g., Fitzenberger et al., 2000; Pfeilsticker et al., 2000; Pundt et al., 2002; Dorf et al., 2008; Laube et al., 2008) and also for HBr (e.g., Johnson et al., 1995; Carlotti et al., 1995; Nolt et al., 1997), although especially the latter observations show also large uncertainties. Models that calculate the partitioning of Br_y are generally consistent with these observations (e.g., Lary, 1996; Salawitch et al., 2005; Feng et al., 2007; Aschmann et al., 2011).

Figure 3.4 shows the average partitioning of tropical Br_y as a function of altitude for day and nighttime, derived from the chemistry and transport model used in this work (see Chapter 4; relevant reactions are listed in Table 4.3 and 4.4). In the troposphere, the mixing ratio of Br_y is relatively constant with altitude at about 1 pptv up to the TTL region. Here, the mixing ratio of Br_y rapidly increases with height, reaching its final value of about 20 pptv at approximately 30 km. One reason for the shape of the Br_y profile is linked to the average lifetime of the long-lived source gases which is dropping fast from high tropospheric values in the altitude region between 20 and 30 km (Figure 3.3). Furthermore, the low concentration of Br_y in the troposphere can be explained by the partitioning among the Br_y constituents. At lower altitudes, the reactions of Br with HO_2 and HCHO dominate the partitioning, shifting the chemical equilibrium towards HBr (fraction up to 80%, Lary, 1996; Sinnhuber et al., 2002). Since HBr is very soluble it is efficiently removed by wet deposition and therefore lost for the atmosphere (e.g., Liang et al., 2010).

In the sunlit stratosphere, the major constituents of Br_y are BrO and, at the stratopause, Br (Figure 3.4). This means that generally more than 50–70% of Br_y is in chemically reactive form, in contrast to the chlorinated species, where the fraction of active chlorine in the stratosphere is generally in the range of 10-30% (Brasseur et al., 1999). The reason for this difference is that the bromine non-reactive reservoir species such as HBr, HOBr or $BrONO_2$ are significantly shorter-lived with regard to photolysis than their chlorine counterparts and consequently less abundant. During nighttime in the absence of dissociating radiation, most inorganic bromine in the lower stratosphere is in the form of $BrONO_2$.

Other processes that can strongly influence the partitioning of Br_y are heterogeneous reactions on ice particles particles or sulfate aerosols (see reactions listed in Table 4.5).

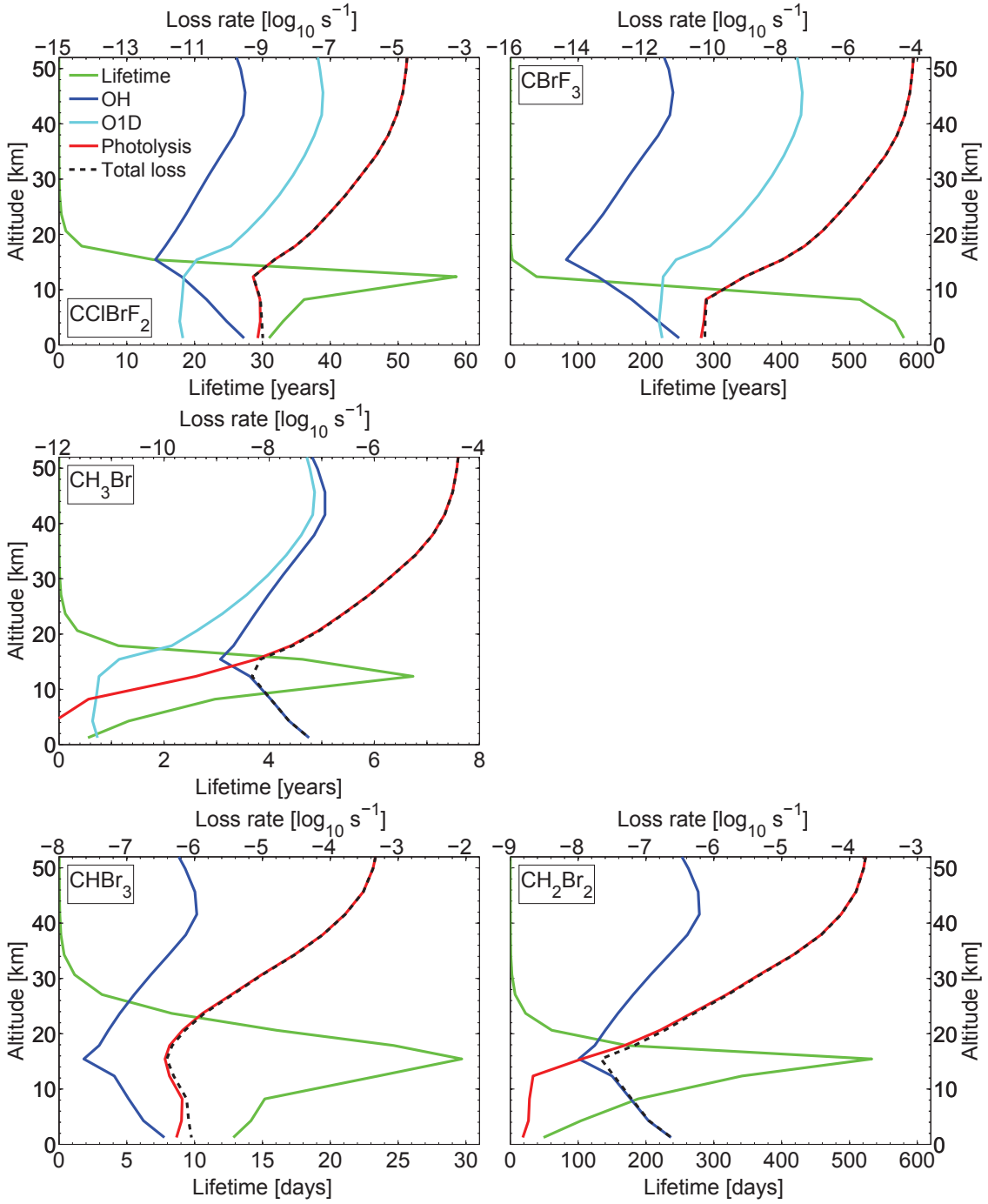

Figure 3.3.: Annually average loss rate of long and short-lived bromine source gases due to OH- and O^1D-reaction and photolysis for a standard tropical atmosphere. Reaction constants and absorption cross sections taken from Sander et al. (2006). The local lifetime is given by the green line.

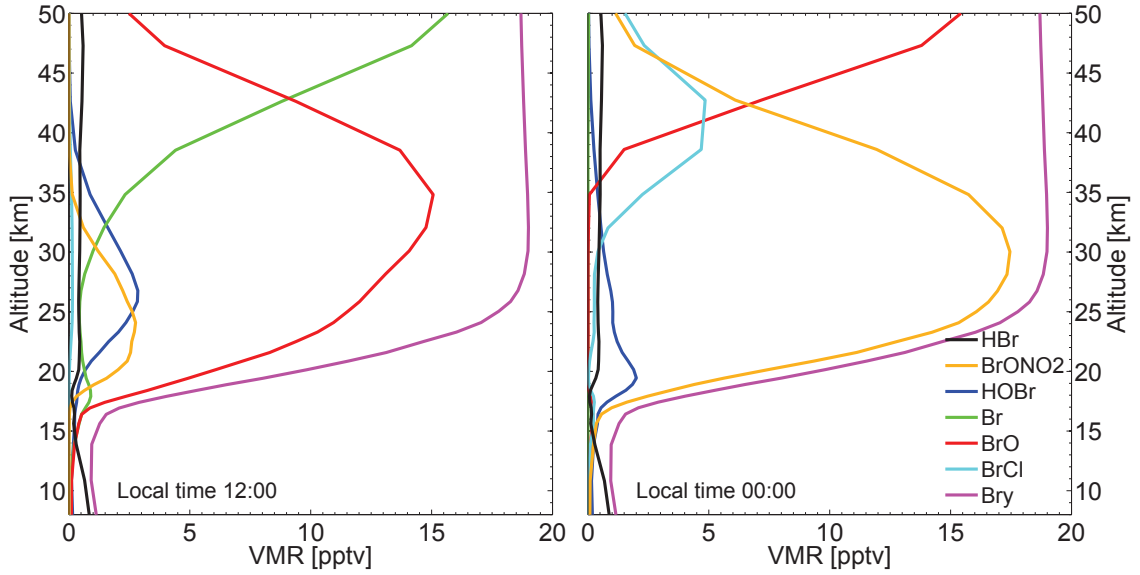

Figure 3.4.: Modeled annually averaged partitioning of tropical inorganic bromine for local noon (left) and midnight (right). Reactions and model description are provided in Section 4.3.

These surfaces offer further pathways for adsorbed non-reactive species to re-enter the gas phase in reactive form. Especially in an isolated environment such as the polar vortex these reactions play a key role in recycling ozone-destroying halogens (e.g., Solomon, 1999, see also Section 2.4), however, also the ubiquitous BrO background concentration in the troposphere is thought to be caused by continuous heterogeneous activation (e.g., Fitzenberger et al., 2000; Platt and Hönninger, 2003; von Glasow et al., 2004; Sinnhuber et al., 2005). In this work, the impact of heterogeneous reactions on bromine in the TTL will be discussed in detail in Section 6.1.

3.2.3. Impact on Stratospheric Ozone

Several studies have shown the importance of bromine for stratospheric ozone chemistry (e.g., Wofsy et al., 1975; Yung et al., 1980; McElroy et al., 1986; Tung et al., 1986; Poulet et al., 1992). Though of lower abundance compared to chlorine, bromine is considered to be far more effective in ozone depletion (e.g., Sinnhuber et al., 2009). The main reason for this difference is the weaker bonding and therefore shorter lifetime of inactive bromine reservoir species such as HBr, HOBr or $BrONO_2$ in contrast to their chlorine counterparts (e.g. Brasseur et al., 1999). Consequently, the partitioning of stratospheric inorganic bromine is shifted towards the radical species, especially BrO (Section 3.2.2). In the following, the most important ozone depleting catalytic cycles involving bromine are presented.

Especially at the upper stratosphere (above 30 km) the BrO_x-O_x cycle is effective (Wofsy et al., 1975), as the major part of Br_y is actually Br and BrO during daytime (Figure 3.4):

$$\mathrm{BrO} + \mathrm{O} \longrightarrow \mathrm{Br} + \mathrm{O_2} \tag{3.5}$$

$$\mathrm{Br} + \mathrm{O_3} \longrightarrow \mathrm{BrO} + \mathrm{O_2} \tag{3.6}$$

$$\text{Net: } \mathrm{O} + \mathrm{O_3} \longrightarrow 2\,\mathrm{O_2}$$

At the lower stratosphere, the interaction of bromine with odd hydrogen and odd nitrogen becomes important (e.g., Yung et al., 1980; Poulet et al., 1992):

$$\begin{aligned} \mathrm{BrO} + \mathrm{HO_2} &\longrightarrow \mathrm{HOBr} + \mathrm{O_2} && (3.7)\\ \mathrm{HOBr} + \mathrm{h}\nu &\longrightarrow \mathrm{OH} + \mathrm{Br} && (3.8)\\ \mathrm{OH} + \mathrm{O_3} &\longrightarrow \mathrm{HO_2} + \mathrm{O_2} && (3.9)\\ \mathrm{Br} + \mathrm{O_3} &\longrightarrow \mathrm{BrO} + \mathrm{O_2} && (3.10)\\ \hline \text{Net: } 2\,\mathrm{O_3} &\longrightarrow 3\,\mathrm{O_2} \end{aligned}$$

$$\begin{aligned} \mathrm{BrO} + \mathrm{NO_2} + \mathrm{M} &\longrightarrow \mathrm{BrONO_2} + \mathrm{M} && (3.11)\\ \mathrm{BrONO_2} + \mathrm{h}\nu &\longrightarrow \mathrm{Br} + \mathrm{NO_3} && (3.12)\\ \mathrm{NO_3} + \mathrm{h}\nu &\longrightarrow \mathrm{NO} + \mathrm{O_2} && (3.13)\\ \mathrm{NO} + \mathrm{O_3} &\longrightarrow \mathrm{NO_2} + \mathrm{O_2} && (3.14)\\ \mathrm{Br} + \mathrm{O_3} &\longrightarrow \mathrm{BrO} + \mathrm{O_2} && (3.15)\\ \hline \text{Net: } 2\,\mathrm{O_3} &\longrightarrow 3\,\mathrm{O_2} \end{aligned}$$

Together with the ClO dimer cycle discovered by Molina and Molina (1987, see also Reactions 2.20–2.23), the coupling of the bromine and chlorine families as pointed out by McElroy et al. (1986); Tung et al. (1986) is mainly responsible for the repeated depletion of polar stratospheric ozone in springtime:

$$\begin{aligned} \mathrm{BrO} + \mathrm{ClO} &\longrightarrow \mathrm{Br} + \mathrm{Cl} + \mathrm{O_2} && (3.16)\\ \mathrm{Br} + \mathrm{O_3} &\longrightarrow \mathrm{BrO} + \mathrm{O_2} && (3.17)\\ \mathrm{Cl} + \mathrm{O_3} &\longrightarrow \mathrm{ClO} + \mathrm{O_2} && (3.18)\\ \hline \text{Net: } 2\,\mathrm{O_3} &\longrightarrow 3\,\mathrm{O_2} \end{aligned}$$

As stated above, the catalytic cycles involving bromine are generally more effective in depleting ozone compared to their chlorine equivalents. Consequently, stratospheric ozone is highly sensitive to even small changes of the bromine abundance, as indicated by several modeling studies (e.g., Salawitch et al., 2005; Feng et al., 2007; Sinnhuber et al., 2009; Dessens et al., 2009; Pisso et al., 2010). In this work, the impact of bromine on stratospheric ozone is discussed in Chapter 8.

Part II.

Methodology

4. Model

Computer-based modeling of the Earth system, e.g. atmosphere, ocean, land surface, biosphere, etc., has become an integral and ubiquitous element in geosciences. The origins of this technique can traced back to the beginnings of numerical weather prediction in the 20th century (for an historical overview, see, e.g., Lynch, 2008). Interestingly, the first attempt to use a numerical model for weather forecasting was undertaken even before the development of electronic computers: Richardson (1922) formulated a basic set of differential equations to predict changes in wind and surface pressure at two points in Europe over a time span of six hours, conducting the necessary calculations manually. The results were grossly wrong, but his pioneering work laid the foundation for later forecast models. About 30 years later, Charney et al. (1950) implemented a single-layer barotropic model of atmospheric dynamics on the first digital general-purpose computer ENIAC[1], that was able to realistically reproduce the large-scale flow in the mid troposphere in general.

Since then, the dramatic increase of computational power within relatively short time enabled general circulation models (GCM) to resolve atmospheric dynamics in much more detail than thought possible in previous years. Today, the current state-of-the-art in (geo-) scientific modeling is to couple GCMs to detailed chemistry schemes and other important domains, for example the ocean or the biosphere, forming coupled chemistry-climate models (CCM) that simulate the whole Earth system. These models are found to be extremely successful in gaining insight in the complex interaction of environmental processes and predicting future climate conditions (e.g., Eyring et al., 2005).

However, this kind of model is not always the best tool for every scientific problem. On the one hand, the necessary calculations are extremely costly in terms of computational effort, easily requiring thousands of processing units to complete the computation in acceptable time. On the other hand, when future projections are not needed it is often better to rely on models that incorporate real world observations ("data assimilation"; see, e.g., Evensen, 2009) to "nudge" the simulation towards reality. In contrast, a chemistry transport model (CTM) represents an "offline" simulation framework, that means it relies on external input data (e.g., temperature, pressure, winds), for example provided by an GCM, to force the atmospheric transport. Since it does not contain a dynamical core it is far less computationally expensive.

For this study[2], a 3-D CTM is used which is described in detail in Section 4.1. This framework forms the basis for different experimental approaches regarding tracer treatment and chemistry that will be introduced in the Sections 4.2 and 4.3.

4.1. CTM framework

The "Bremen 3D CTM" (B3DCTM), originally developed by Sinnhuber et al. (2003a), was extensively updated and modified for this work (see also Aschmann et al., 2009, 2011). This section provides an overview of its fundamental structure, characteristics and setup.

[1] Electronic Numerical Integrator And Computer.

[2] This chapter is based mainly on the work presented in Aschmann et al. (2009, 2011).

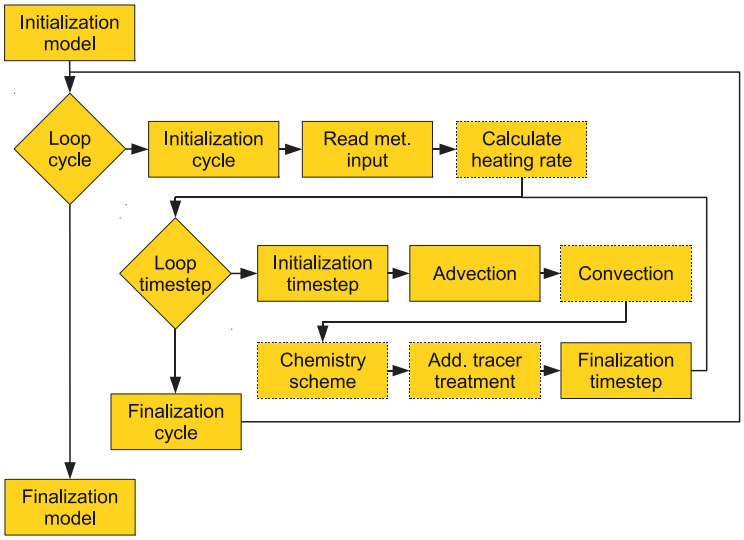

Figure 4.1.: Simplified flowchart of the B3DCTM. Each box represents a module which fulfills a specific task. The boxes with a dashed frame are optional modules that do not belong to the basic model framework.

4.1.1. Structure

The design of the B3DCTM is strictly modular and offers a basic framework which is versatile and easily extendable, written entirely in FORTRAN 77. An overview of the model structure is given in Figure 4.1. Most calculations take place in two main loops that form the base of the model. The outer loop iterates over the available meteorological input data, called "cycles" in this context. Typically, one cycle is 6, 12 or 24 hours long, i.e. meteorological data is read four, two or one time a day, respectively. Between the cycles the input data is linearly interpolated. The inner loop runs over the actual model timestep, usually in the range between 10 to 30 minutes. Here, most calculations take place, for example tracer advection or chemical reactions. Due to the flexible design of the model framework the inner loop can be easily reassembled to meet the requirements of the particular task, e.g. additional processes can be inserted or removed with little effort (see Section 4.2 and 4.3). Output can be generated at arbitrary intervals (with the model timestep as lower bound) and is stored in the common data format netCDF.

4.1.2. Resolution and Model Grid

The choice of spatial and temporal resolution in a model is always a compromise between speed and accuracy. On the one hand, a finer resolution is generally desired to improve accuracy and the representation of small-scale processes. On the other hand, increasing the spatial resolution requires significantly more model grid boxes, e.g., in a 3-D model, doubling the spatial resolution increases the number of grid boxes by a factor of eight. In addition, spatial and temporal resolution must match the Courant-Friedrichs-Lewy criterion (Courant et al., 1928), given here in the case of 1-D advection:

$$\frac{u \cdot \Delta t}{\Delta x} \leq C \tag{4.1}$$

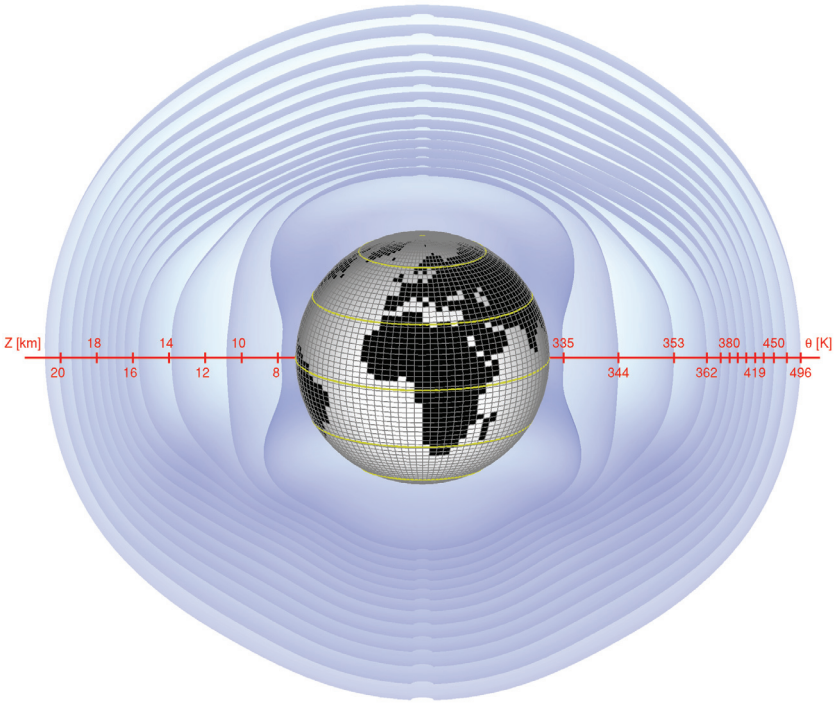

Figure 4.2.: Illustration of the spatial resolution of the model. The horizontal resolution is 2.5° latitude × 3.75° longitude. There are 29 levels of potential temperature θ ranging from 335 K to 2726 K (only the UTLS region up to 20 km is shown here). Note that globe and atmosphere are not drawn on the same scale.

Here, u denotes the velocity, Δt the timestep and Δx the length interval. C is a constant depending on the particular differential equation to be solved; in the presented example $C = 1$. If the relation is violated, explicit numerical methods to solve the equation become unstable. Consequently, an increase in spatial resolution requires an increase in temporal resolution, i.e. doubling the spatial resolution increases the number of boxes by a factor of eight and reduces the timestep by a factor of two. As a result, the total computational cost rises by a factor of 16.

For this study, a horizontal resolution of 2.5° latitude × 3.75° longitude with 29 vertical levels was chosen (Figure 4.2) which corresponds to $96 \times 72 \times 29 = 200448$ model grid boxes in total. Together with a timestep of 15 or 30 minutes the spatial and temporal resolution of the utilized model is on par with the current state-of-the-art in global atmospheric modeling (e.g., Warwick et al., 2006; Hossaini et al., 2010; Liang et al., 2010; Eyring et al., 2010) and offers a pragmatic trade-off between accuracy and computational expense considering the available hardware resources (see Section 4.1.6 for a brief analysis of computational performance).

A distinctive feature of the model is the usage of potential temperature (see Section 2.1) as vertical coordinate. In the absence of diabatic heat input or loss the potential temperature θ of an air parcel is a conserved quantity in good approximation. Therefore, the usage of isentropic levels offers significant conceptual and practical advantages for modeling the large-scale transport, especially in the UTLS and above. However, this approach is unsuitable in the troposphere where turbulent flow must be taken into account. Even more important are the meridional altitude differences on a level of equal potential temperature

(see Figure 4.2) that make the extension into the troposphere difficult: a θ-level of about 300 K would be at the Earth's surface in the warm tropics, though at higher latitudes, the same level could be kilometers above the ground. To solve this problem, some models use a hybrid coordinate where isentropic surfaces are blended with terrain following surfaces in the lower atmosphere (e.g., Rasch et al., 1997; Chipperfield, 2006). However, in the B3DCTM, originally designed as stratospheric model, most of the troposphere is not covered; its θ-levels range from 335 to 2726 K (about 8 to 55 km in the tropics). Therefore, to model injection of boundary layer air nonetheless a convective parametrization is used which is described in Section 4.1.5.

4.1.3. Meteorological Input Data

The CTM has a unified interface for external meteorological data which simplifies the development of appropriate input routines. Currently available are routines for the United Kingdom Met Office (UKMO) Unified Model and for different kinds of data from the European Centre for Medium-Range Weather Forecasts (ECMWF), i.e. operational data and the reanalyses ERA-40 (Uppala et al., 2005) and ERA-Interim (Dee et al., 2011). For this study, the ERA-Interim data set was used which is based on 4-D assimilation of multi-decadal series of observations into a GCM (technical details in ECMWF, 2009). Despite the inevitable errors and artifacts this data set represents a powerful tool for studying atmospheric processes under relatively realistic conditions and was extensively used and evaluated in past studies (e.g., Kobayashi et al., 2009; Fueglistaler et al., 2009b; Chuang et al., 2010; Dee et al., 2011).

The ERA-Interim data set currently spans the years from 1989 to 2010 and is frequently updated. Analyses are available four times a day, at 0, 6, 12 and 18 UTC on a reduced Gaussian grid with latitudinal spacing of about 0.7°. The longitudinal spacing is variable, about 0.7° in the tropics, increasing further towards higher latitudes. The data fields used for the CTM simulations are temperature, pressure, geopotential height, horizontal wind velocities, long and short-wave radiation under clear-sky conditions and the convective detrainment rate.

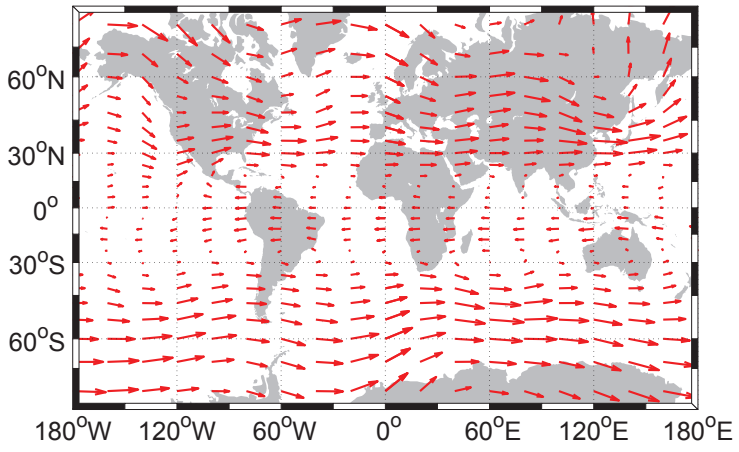

Figure 4.3.: Horizontal ECMWF ERA-Interim wind field at about 17.5 km altitude during March 2006.

4.1.4. Tracer Advection

The quasi-horizontal transport on isentropes is calculated using the meteorological wind field from ERA-Interim, with the east and northward component defined as u and v, respectively (Figure 4.3). However, for the vertical transport, the model does not use the vertical (w) component of the wind field. The w-wind combines the effects of different transport processes such as the large-scale diabatic tendency and fast localized convective updraft into a single vertical velocity which would make the vertical transport of the CTM unrealistically diffusive (e.g., Sinnhuber and Folkins, 2006). Therefore the large-scale vertical advection is derived from diabatic heating rates. The original B3DCTM relies on the MIDRAD radiation scheme (Shine, 1987) to calculate the heating rates interactively, however, the current version was modified to use the ERA-Interim data for tendency of clear sky long and short-wave radiation (Figure 4.4). They are found to be more accurate in the tropopause region and are (at least in principle) consistent with the large-scale wind fields and convective mass fluxes (Aschmann et al., 2009), although they lack a feedback to interactive ozone (Fueglistaler et al., 2009b). The fast and localized convective transport is treated separately and is described in detail in Section 4.1.5.

The utilized advection algorithm is an adaption of the original advection scheme by Prather (1986) which is based on the conservation of higher-order moments of the trace gas distribution. The idea behind this approach is that the distribution of a tracer in a model is not only described alone by the amount of this tracer in every model box (0^{th}-order), but also by its spatial gradient (1^{st}-order) and curvature (2^{nd}-order). This approach requires significantly more memory than comparable advection schemes (for every grid box and tracer 10 variables have to be stored), but it was also shown that it generally offers a better compromise in terms of absolute accuracy and numerical diffusion compared to other algorithms (Prather, 1986).

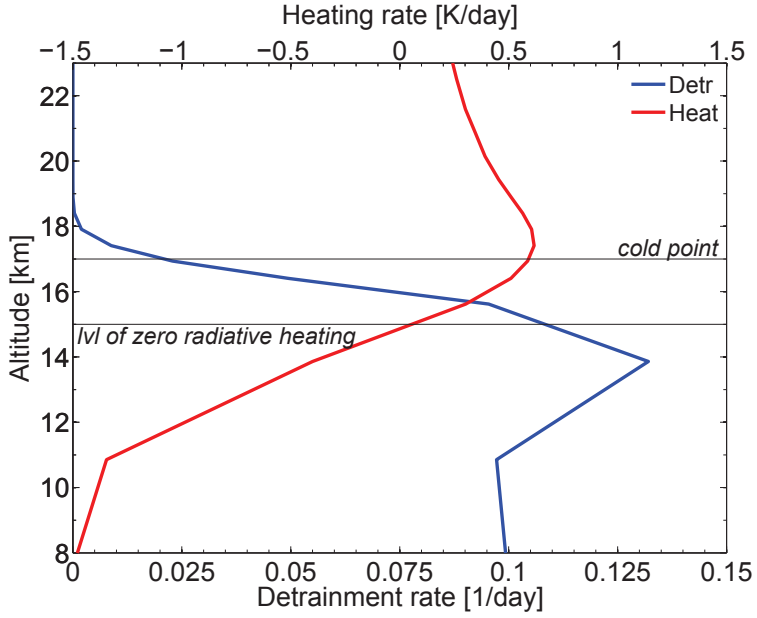

Figure 4.4.: Annually averaged profiles of ECMWF ERA-Interim detrainment rate (blue, bottom abscissa) and diabatic heating rate (red, top abscissa) in the TTL for 2006. Adapted from Aschmann et al. (2009).

4.1.5. Convection

To study the impact of VSLS on stratospheric bromine an adequate representation of convective transport in the model is an indispensable prerequisite. As it is difficult to extend a purely isentropic model into the lower troposphere and down to Earth's surface, so far isentropic models either did not include any parametrization of convection at all, or have used some kind of hybrid coordinate (see Section 4.1.2). Therefore, the inclusion of convective transport into the B3DCTM in the course of this work is a novelty (Aschmann et al., 2009). Instead of using an interactive convective parametrization, the model relies on archived convective updraft mass fluxes from the ERA-Interim reanalysis. This approach has the additional advantage that the convective mass fluxes are calculated during the assimilation process in a consistent way. In contrast, when using a convective parametrization inside a CTM, there is always the potential problem that the driving large-scale temperature and pressure fields from the meteorological analysis have already been stabilized by a convective parametrization within the assimilation. The representation of convection in the ERA-Interim reanalysis is based on the original Tiedtke (1989) scheme that considers deep, shallow and mid-level convective mass fluxes in cumulus clouds (ECMWF, 2009).

Here, the 6-hourly updraft convective mass fluxes from ERA-Interim are used, or more specifically the updraft detrainment rates, which are the vertical divergence of the updraft convective mass fluxes. An example is shown in Figure 4.4. The detrainment rate d_c gives the convective flux of mass into a grid box per time. It is derived from the original ECMWF updraft detrainment rate by integration over the model grid box divided by the air density inside the box and has therefore the unit $1/s$[3]. Convective injection of tracers is then modeled by specifying a tracer detrainment mixing ratio $[X]_c$ that multiplied with the detrainment mass flux d_c and the total grid box mass m gives the convective tracer flux $f_{X,c}$ into the grid box:

$$f_{X,c} = d_c \cdot m \cdot [X]_c \tag{4.2}$$

Since the model does not cover the boundary layer and the free troposphere, entrainment in convective plumes cannot be explicitly calculated. Instead the detrainment mixing ratio $[X]_c$ is a free parameter in the model that can be set individually for each tracer, representing the tracer's mixing ratio in the range between boundary layer and free troposphere, dependent on location and time if required.

With this approach the model is able to simulate the slow large-scale transport constrained by diabatic heating rates with fast updrafts taking place quasi instantaneously as a sub-grid scale process. However, this approach is not strictly mass conserving, which is the case also in other isentropic CTMs even without convective transport. To force mass conservation the total mass inside a grid box after advection and convection steps is set to the calculated mass from the large-scale meteorological analysis. Tracer masses are scaled proportionally to keep the calculated tracer mixing ratios constant.

4.1.6. Computational Performance

In order to be able to conduct multi-decadal simulations with complex chemistry in reasonable time the original B3DCTM was heavily modified to speed up its execution time. The most important optimization was the redesign of the code to support multi-processor architectures. Input/Output functions are now completely separated from the main model

[3] d_c is expressed relative to the individual grid box mass. For example, $d_c = 1/s$ means that the convective mass flux per second into a particular grid box is equal to the total mass of this box.

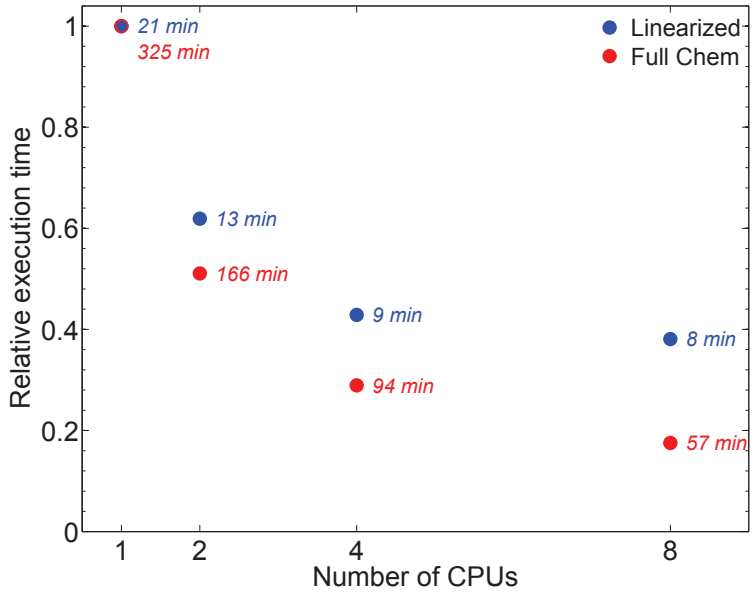

Figure 4.5.: Absolute and relative execution time of the CTM with linearized (blue, 6 tracers) and full chemistry (red, 59 tracers) for a 31-day simulation run on multiple CPUs.

structure and are executed in parallel threads, for example the input of meteorological data or the output generation. Furthermore, all computational expensive parts such as the advection or the chemistry scheme are parallelized using the OpenMP[4] library. Figure 4.5 shows the computational performance of the CTM with respect to multiple processing units. The timings are averages measured on the Bremen Institute of Environmental Physics Nexus computing cluster using a single node (OpenMP-usage is restricted to a single node, only). Each node comprises two Intel Xeon X5570 quadcore processors, i.e. each node is able to handle up to eight threads or processes concurrently. As seen in Figure 4.5, the execution time of the updated B3DCTM scales well with the number of available processing units (PU). In the case of the simple setup using the linearized chemistry with six tracers (see Section 4.2) up to four PUs can be used efficiently. However, if applying the complex chemistry scheme with 59 tracers (see Section 4.3) the model benefits from the full eight PUs per node. Here, the execution time for one month of simulation drops from 325 to 57 minutes when using 8 PUs, i.e. by a factor of about 5.7.

4.2. Idealized Approach

The simplified approach relies solely on idealized tracers and processes. Its "light-weight" setup, i.e. the small number of tracers (< 10) and the lack of detailed chemistry, reduces significantly its computational cost (Figure 4.5) and complexity making this approach a capable tool for sensitivity calculations and model validation.

The idealized approach is used in different variants throughout this study but generally comprises several VSLS and Br_y tracers, in addition to water vapor, ozone and a passive age of air tracer whose treatment is detailed in the following sections.

[4]For details, refer to the OpenMP homepage `www.openmp.org`

4.2.1. Bromine Source and Product Gases

Naturally, the treatment of bromine species is the central part of the idealized approach. The short-lived source gases are represented by idealized tracers with a constant and uniform chemical lifetime typical for the particular compound, approximating the loss by photolysis and oxidation. For example, the average lifetime of the idealized bromoform tracer in the TTL is assumed to be 20 days, for dibromomethane it is 120 days. Note that in this context lifetime is defined as "e-folding time", i.e. the time when the initial tracer mixing ratio is dropped by a factor of $1/e$. The idealized bromine source tracers are named after their lifetime, e.g. TT20 ("test tracer with 20 days lifetime") for bromoform and TT120 for dibromomethane. In every timestep i the source gases degrade according to their assumed lifetime τ:

$$m_{i+1}^{\mathrm{T}} = m_i^{\mathrm{T}} \cdot \exp\left(-\frac{\Delta t}{\tau}\right) \tag{4.3}$$

with timestep length Δt and tracer mass m^{T}. The only source of VSLS in the model is convective detrainment usually assuming a constant and uniform detrainment mixing ratio (Equation 4.2).

The inorganic bromine product gases are combined into a single $\mathrm{Br_y}$ tracer, ignoring the partitioning between the individual species (as described in Section 3.2.2). It is produced solely by the degradation of the aforementioned VSLS according to the number of bromine atoms in the particular compound, that means the decay of one unit of TT20 ($\mathrm{CHBr_3}$) and TT120 ($\mathrm{CH_2Br_2}$) yields three and two units of $\mathrm{Br_y}$, respectively. Here, the intermediate degradation products are omitted, which is according to the recent study of Hossaini et al. (2010) a valid approximation. $[\mathrm{Br_y}]_c$, the detrainment mixing ratio of $\mathrm{Br_y}$, is generally set to zero, assuming that $\mathrm{Br_y}$ is efficiently removed by rainout in the boundary layer and lower troposphere, since a significant part of inorganic bromine at this altitude region is actually HBr which is highly soluble in liquid water (e.g., Lary, 1996; Yang et al., 2005; Liang et al., 2010). Note that a detrainment mixing ratio of zero effectively leads to a dilution of the corresponding species, i.e. the mixing ratio of $\mathrm{Br_y}$ drops if there is convective influx into the particular grid box.

To study the sensitivity of inorganic bromine to washout and dehydration in the TTL region the utilized experimental setup generally contains two variants of the $\mathrm{Br_y}$ tracer. The first variant is assumed to be completely insoluble, thus being not affected by dehydration at all. Therefore, the insoluble variant $\mathrm{Br_y^{ins}}$ acts like a inert tracer, its mixing ratio solely related to the amount of available source gases. In contrast, the second variant is assumed to be perfectly soluble, i.e. whenever dehydration occurs in a model grid box (see Section 4.2.2), the soluble variant $\mathrm{Br_y^{sol}}$ is removed completely and instantaneously. Although the approach is simple, it is more physically motivated than the application of a fixed washout lifetime used in most of the previous modeling studies dealing with bromine in the TTL. These two extremal cases allow an assessment of the impact of dehydration on $\mathrm{Br_y}$ by identifying the upper and lower limit of this effect.

4.2.2. Treatment of Water Vapor

Water vapor plays an important role in this study because an adequate representation of atmospheric humidity is needed to model the possible loss of soluble inorganic bromine due to dehydration (Section 4.2.1). Furthermore, its distribution in the atmosphere is another convenient means to validate the model assumptions since there are plenty of measurements of this quantity that can be considered. The treatment of the $\mathrm{H_2O}$ tracer is based on three simplistic assumptions. Firstly, for the convective transport, the detrainment mixing ratio

$[H_2O]_c$ is set to the saturation mixing ratio of water vapor over ice of the particular model box, following Dessler and Sherwood (2004). This corresponds to the assumption that air detraining from a convective cloud is fully saturated. The saturation mixing ratio W_s is obtained by relating the ice vapor pressure P_{vap} to the ambient pressure P:

$$W_s = \frac{P_{\text{vap}}}{P - P_{\text{vap}}} \tag{4.4}$$

P_{vap} is calculated using the parametrization of Marti and Mauersberger (1993):

$$\log P_{\text{vap}} = \frac{A}{T} + B \tag{4.5}$$

Here, the empirical coefficients A and B are -2663.5 and 12.537, respectively, while T denotes the temperature. Secondly, if the relative humidity of a box exceeds 100%, all surplus water is removed immediately thus modeling precipitation as instantaneous fallout of ice particles. Finally, there is a second water source in the stratosphere implemented by a simple methane oxidation scheme as described in the ECMWF Integrated Forecast System documentation (ECMWF, 2009). The basic supposition is that the sum of methane and water is constant in the stratosphere and can be approximated by:

$$2\,[CH_4] + [H_2O] = 6.8\,\text{ppm} \tag{4.6}$$

Therefore the production of water via methane oxidation can be expressed as:

$$\frac{d\,[H_2O]}{dt} = \frac{(6.8\,\text{ppm} - [H_2O])}{\tau} \tag{4.7}$$

Here τ denotes a pressure dependent chemical lifetime of methane which is set to 100 days at 0.5 hPa pressure and increases roughly linearly to $\approx$ 6000 days at 100 hPa. Above this mark the lifetime is set to infinity, i.e. the H_2O production due to methane oxidation is zero at lower altitudes.

4.2.3. Additional Diagnostic Tracers

Ozone and a passive age of air (AoA) tracer are included in the idealized setup as additional diagnostic tracers. Although not in the primary focus of this work, they represent a useful means for evaluation purposes.

The ozone tracer uses the linearized chemistry scheme LINOZ originally developed by McLinden et al. (2000) and further updated by Kiesewetter et al. (2010b). LINOZ relies on tabulated production rates of ozone dependent on the current ozone mixing ratio, temperature and ozone overhead column of the individual grid box. Although the underlying mechanism is simple, it was shown that the chemistry scheme is able to reproduce relatively realistic ozone distributions (e.g., McLinden et al., 2000; Aschmann et al., 2009; Kiesewetter et al., 2010a).

The artificial AoA tracer offers insight on the performance of the general circulation in the model (e.g., Hall et al., 1999; Waugh and Hall, 2002). At the begin of the simulation the mixing ratio of the AoA tracer is initialized on the whole grid to the date number (e.g., Julian date) of the start date. Since convection is the only way for tropospheric air to enter the model space the detrainment mixing ratio of the AoA tracer is always updated to the current date number, i.e. there is a constant influx of "young" air into the AoA tracer distribution. The tracer gets advected and mixed normally like the other species but is completely passive otherwise. After the model has reached its quasi-steady state and is therefore well mixed the difference of the AoA tracer mixing ratio in a grid box and the current model date number gives the mean age of the particular air parcel, i.e. the time elapsed since it was convectively detrained.

4.2.4. Simulation Setup

The main simulation run using the idealized approach is named ID1 (see also Appendix A, Table A.1 for an overview of all conducted model runs). The simulation starts at the begin of 1989 running to the end of 2009 (21 years), relying on ERA-Interim input. ID1 comprises six tracers (O_3, H_2O, TT20, TT120, Br_y^{ins}, Br_y^{sol}). In order to obtain a reasonable initial configuration and therefore reducing the necessary spin-up time the results of a previous run with the same approach was used: this run is set up identically but all tracers are initialized at "best guess" values. The tracer distribution after 21 years is then used as initial configuration for the bromine species in the actual production run. The detrainment mixing ratios $[TT20]_c$ and $[TT120]_c$ are set uniformly to 1 pptv, each. These values are lower than the recommended mixing ratios of the VSLS in the marine boundary layer (1.6 and 1.1 pptv for $CHBr_3$ and CH_2Br_2, respectively, Montzka and Reimann, 2010), taking into account dilution by entrainment of free tropospheric air, which may have significant impact on deep convective plumes (e.g., Romps and Kuang, 2010). Tropospheric profiles of these species obtained from a compilation of aircraft measurements (Liang et al., 2010) suggest that a detrainment mixing ratio of 1 pptv for bromoform and dibromomethane is a valid approximation.

Furthermore, two sensitivity calculations based on the ID1 run were conducted. The ID2 run uses the same setup as ID1 but restricts the removal of Br_y^{sol} to within 40°N–40°S in order to reflect the actual partitioning of inorganic bromine (see Section 6.1.1 for details). ID2 incorporates also an AoA tracer to assess the transport in the CTM. The ID3 run is identical to ID2 but uses a special emission scenario for the very short-lived source gases (TT20 and TT120). The detrainment mixing ratios of both species are set up similarly to the model studies of Warwick et al. (2006) and Liang et al. (2010): strong emissions near the coast, none over land (Section 6.2).

The last run, ID4, uses different emission areas for TT20/TT120 to identify the regional transport efficiency of VSLS (Section 6.3). Each region is associated with a group of four tracers ($TT20_i$, $TT120_i$, $Br_{y,i}^{ins}$, $Br_{y,i}^{sol}$). The detrainment mixing ratio $[TT20_i]_c/[TT120_i]_c$ for a particular region is 1 pptv inside and zero outside the corresponding area.

4.3. Full Chemistry Approach

The idealized approach is a suitable tool for sensitivity studies but to obtain a more realistic picture of the tracer distribution in the TTL a more complex and complete chemistry scheme is necessary. The one utilized in this work, SLIMCAT, was originally developed by Chipperfield et al. (1993) and has undergone several updates and modifications since then (e.g., Chipperfield, 1999; Sinnhuber et al., 2003b; Feng et al., 2005; Winkler et al., 2008).

The current version of the SLIMCAT chemistry scheme comprises 59 species (Table 4.1) and 181 gas phase, heterogeneous and photochemical reactions (Appendix B). The following sections give an overview of the integral parts of the chemistry scheme, especially regarding the treatment of bromine species which is most relevant for this study. For further details refer to SLIMCAT manual[5] and the references given above.

4.3.1. Gas Phase Chemistry

The bulk of included reactions are gas phase reactions. Most of these fall into the category of bimolecular second-order reactions whose rate constant k_g can be described by the

[5]The manual can be found at http://homepages.see.leeds.ac.uk/~lecmc/slimcat.html

Table 4.1.: Chemical species included in the SLIMCAT chemistry scheme.

Category	Advected species	Non-advected species
Source gases and long-lived species	CH_4, N_2O, H_2O, H_2SO_4, CO, CH_3Cl, CH_3CCl_3, CCl_4, CCl_3F, CCl_2F_2, $CHClF_2$, $CClF_2CClF_2$, $CHBr_3$, $CClBrF_2$, $CBrF_3$, CH_2Br_2, $CHBr_3$, HF, COF_2, COFCl	
Coupled short-lived species	O_x, H_2O_2, NO_x, N_2O_5, HNO_3, HO_2NO_2, ClO_x, $ClONO_2$, HCl, HOCl, BrO_x	O_3,[a] $O(^3P)$,[a] $O(^1D)$,[a] N,[b] NO,[b] NO_2,[b] NO_3, Cl,[c] ClO,[c] Cl_2O_2,[c] OClO, Br,[d] BrO,[d] $BrONO_2$, BrCl, HOBr, HBr
Steady state species	HCHO, CH_3OOH	HCO, CH_3, CH_3O_2, CH_3O, H, OH, HO_2,
Fixed species		N_2, O_2, H_2

[a] Part of O_x family.
[b] Part of NO_x family.
[c] Part of ClO_x family.
[d] Part of BrO_x family.

Arrhenius equation:

$$k_g = A \cdot \exp\left(-\frac{E/R}{T}\right) \tag{4.8}$$

Here, A is the Arrhenius A-factor (unit: $cm^3molec^{-1}s^{-1}$), the coefficient E/R describes the temperature dependence of the reaction ("activation temperature") and the temperature T. A-factor and E/R are generally obtained from the JPL 2006 recommendation (Sander et al., 2006) unless stated otherwise.

It is, however, impractical to integrate the individual species separately ignoring the different time scales of the involved reactions. Therefore, certain short-lived[6] species are grouped into families assuming they are in photochemical equilibrium (e.g., BrO_x which contains BrO and Br, Table 4.1). Furthermore, these species are not transported individually, only the corresponding families which are treated as additional tracers. To model the change of photochemical equilibrium during nighttime some species whose lifetime increases drastically in the absence of sunlight such as $BrONO_2$ or BrCl are integrated individually although they are associated to a family for transportation purposes (BrO_x in the given example). The reactive hydrogen species (HO_x) and most of the methane oxidation products (CH_yO_x) are assumed to be in steady state and therefore not affected directly by transport.

Especially relevant for this study are the included gas phase reactions of the bromine species which are separately listed here. Table 4.2 shows all reactions that lead to the destruction of bromine source gases including the VSLS bromoform and dibromomethane.

[6] Note that "short-lived" in this context means a photochemical lifetime in or below the magnitude of a typical chemistry integration timestep, i.e. 15 minutes.

Table 4.2.: Gas phase reactions of organic bromine source gases. The intermediate reaction steps are omitted. R denotes the organic rest. A-factor and E/R (see Equation 4.8) obtained from Sander et al. (2006).

Reactants		Products	A-factor	E/R
$CClBrF_2 + OH$	$\longrightarrow \cdots \longrightarrow$	$Br + Cl + COF_2 + R$	1.0×10^{-12}	>2600[a]
$CClBrF_2 + O^1D$	$\longrightarrow \cdots \longrightarrow$	$Br + Cl + COF_2 + R$	1.5×10^{-10}	0
$CBrF_3 + OH$	$\longrightarrow \cdots \longrightarrow$	$Br + COF_2 + HF + R$	1.0×10^{-12}	>3600[a]
$CBrF_3 + O^1D$	$\longrightarrow \cdots \longrightarrow$	$Br + COF_2 + F + R$	1.0×10^{-10}	0
$CH_3Br + OH$	$\longrightarrow \cdots \longrightarrow$	$Br + R$	2.35×10^{-12}	1300
$CH_3Br + O^1D$	$\longrightarrow \cdots \longrightarrow$	$Br + R$	1.8×10^{-10}	0
$CH_3Br + Cl$	$\longrightarrow \cdots \longrightarrow$	$Br + HCl + R$	1.4×10^{-11}	1030[a]
$CH_2Br_2 + O^1D$	$\longrightarrow \cdots \longrightarrow$	$2Br + R$	2.7×10^{-10}	0
$CH_2Br_2 + OH$	$\longrightarrow \cdots \longrightarrow$	$2Br + R$	2.0×10^{-12}	840
$CH_2Br_2 + Cl$	$\longrightarrow \cdots \longrightarrow$	$2Br + HCl + R$	6.3×10^{-12}	800[a]
$CHBr_3 + O^1D$	$\longrightarrow \cdots \longrightarrow$	$3Br + R$	6.6×10^{-10}	0
$CHBr_3 + OH$	$\longrightarrow \cdots \longrightarrow$	$3Br + R$	1.35×10^{-12}	600
$CHBr_3 + Cl$	$\longrightarrow \cdots \longrightarrow$	$3Br + HCl + R$	4.85×10^{-12}	850[a]

[a] Reaction not included in standard model setup.

Note that similarly to the idealized setup (Section 4.2.1) the intermediate reaction steps that lead to the formation of BrO_x are omitted here. Hossaini et al. (2010), who used a modified SLIMCAT version including these steps explicitly concluded that the intermediate products can be safely ignored with regard to the bromine chemistry. Table 4.3 lists the reactions that force the chemical equilibrium within the BrO_x family while Table 4.4 contains the reactions that control the partitioning among the non-reactive bromine species.

Note that some reactions listed in the Tables 4.2 to 4.4 are not included in the standard model setup. Sensitivity calculations with those reactions included show that their impact on the species relevant for this study is negligible in the UTLS region.

Table 4.3.: Gas phase reactions that interconvert the reactive inorganic bromine species Br and BrO. A-factor and E/R (see Equation 4.8) obtained from Sander et al. (2006).

Reactants		Products	A-factor	E/R
$Br + OClO$	$\longrightarrow$	$BrO + ClO$	2.6×10^{-11}	1300[a]
$Br + O_3$	$\longrightarrow$	$BrO + O_2$	1.7×10^{-11}	800
$BrO + O$	$\longrightarrow$	$Br + O_2$	1.9×10^{-11}	-230
$BrO + NO$	$\longrightarrow$	$Br + NO_2$	8.8×10^{-12}	-260
$BrO + OH$	$\longrightarrow$	$Br + HO_2$	1.7×10^{-11}	-250
$BrO + ClO$	$\longrightarrow$	$Br + OClO$	9.5×10^{-13}	-550
$BrO + ClO$	$\longrightarrow$	$Br + Cl + O_2$	2.3×10^{-12}	-260
$BrO + BrO$	$\longrightarrow$	$2Br + O_2$	1.5×10^{-12}	-230

[a] Reaction not included in standard model setup.

Table 4.4.: Gas phase reactions between reactive and non-reactive inorganic bromine species. A-factor and E/R (see Equation 4.8) obtained from Sander et al. (2006).

Reactants		Products	A-factor	E/R
BrO + ClO	$\longrightarrow$	BrCl + O_2	4.1×10^{-13}	-290
BrO + NO_2 + M	$\longrightarrow$	$BrONO_2$ + M		[a]
$BrONO_2$ + O	$\longrightarrow$	BrO + NO_3	1.9×10^{-11}	-215
HOBr + O	$\longrightarrow$	BrO + OH	1.2×10^{-10}	430
BrO + HO_2	$\longrightarrow$	HOBr + O_2	4.5×10^{-12}	-460
BrO + HO_2	$\longrightarrow$	HBr + O_3	4.5×10^{-12}	-460[b,c]
BrO + OH	$\longrightarrow$	HBr + O_2	1.7×10^{-11}	-250[b,d]
Br + HCHO	$\longrightarrow$	HBr + O_2	1.7×10^{-11}	800
Br + H_2O_2	$\longrightarrow$	HBr + HO_2	1.0×10^{-13}	>3000[b]
Br + HO_2	$\longrightarrow$	HBr + O_2	4.8×10^{-12}	310
HBr + OH	$\longrightarrow$	Br + H_2O	5.5×10^{-12}	-200
HBr + O^1D	$\longrightarrow$	Br + OH	1.5×10^{-10}	0
HBr + O	$\longrightarrow$	Br + OH	5.8×10^{-12}	1500

[a] Termolecular reaction. See Sander et al. (2006) for details and rate coefficients.
[b] Reaction not included in standard model setup.
[c] Minor reaction pathway (yield below 0.4%).
[d] Minor reaction pathway (yield below 3%).

4.3.2. Heterogeneous Chemistry

Heterogeneous reactions of halogenated species on aerosol or particle surfaces play an important role in ozone chemistry, especially in polar regions (Section 3.2.3). Therefore, the SLIMCAT chemistry scheme incorporates an equilibrium treatment of a set of reactions on liquid $H_2O/H_2SO_4/HNO_3$/HCl aerosols, solid NAT and ice particles, listed in Appendix B, Table B.2. The composition of liquid aerosols and the corresponding solubilities of HBr and HOBr are calculated using the analytical scheme of Carslaw et al. (1995a,b). NAT particles form according to the expression of Hanson and Mauersberger (1988) when they are thermodynamically possible. Both implementations are taken unchanged from Chipperfield (1999) and are not described in any further detail here. More relevant for this study is the uptake of halogenated species on ice particles which is, according to sensitivity calculations, the dominant process in the tropical UTLS (Section 6.1.2) and may lead either to eventual scavenging by sedimentation or activation by heterogeneous reactions. Therefore this part of the original SLIMCAT scheme was augmented in the course of this work to improve the representation of the involved processes. The reactions on ice particle surfaces involving bromine are listed in Table 4.5.

Ice particles form in a model grid box whenever the actual water mixing ratio exceeds the saturation mixing ratio of water vapor over ice, i.e. if the relative humidity is higher than 100% all excess water is in solid phase. This treatment is identical to idealized approach described in Section 4.2.2. Then, the uptake of gaseous HBr on ice (and likewise for HCl) is modeled using the partition coefficient K_{linC} for HBr (4.14×10^5 cm) from the recent recommendation of the IUPAC Subcommittee on Gas Kinetic Data Evaluation for Atmospheric Chemistry (Crowley et al., 2010):

$$[\mathrm{HBr}]_s = [\mathrm{HBr}]_g^{0.88} \cdot K_{linC} \cdot \bar{A} \tag{4.9}$$

Here, $\bar{A}$ denotes the available particle surface area density which is calculated from the

effective particle radius r_e and an assumed number density n_{ice} of 10 particles per cubic centimeter (Chipperfield, 1999):

$$\bar{A} = 4\pi \cdot r_e^2 \cdot n_{\text{ice}} \tag{4.10}$$

The effective particle radius r_e is approximated using the ice volume V_{ice} and n_{ice}:

$$r_e = \sqrt[3]{\frac{3 \cdot V_{\text{ice}}}{4\pi \cdot n_{\text{ice}}}} \tag{4.11}$$

Finally, the heterogeneous reaction rate k_h on the particle surface is calculated as product of uptake coefficient γ and the collision frequency ν (e.g., Rodriguez et al., 1989):

$$k_h = \gamma\nu \tag{4.12}$$

$$\nu = \frac{1}{4}\bar{A}\sqrt{\frac{8kT}{\pi M}} \tag{4.13}$$

with Boltzmann's constant k and the molecular weight M of the gas molecules. Sedimentation is calculated as well but is treated simply assuming a fixed mean ice particle radius of 10 µm to determine the fall velocity (about 1.5 km/day, Böhm, 1989). Note that it is assumed here that HBr is the only bromine species adsorbed on ice as it is currently not clear how and to what extent other species like HOBr and $BrONO_2$ are adsorbed as well (Crowley et al., 2010). As the original SLIMCAT scheme does not contain any explicit treatment of evaporation, all dissolved and adsorbed species are released back into gas phase instantaneously after the chemical integration step and the sedimentation calculation.

Table 4.5.: Heterogeneous activation reactions of solved/adsorbed bromine species on liquid aerosols, NAT and ice particles. Only the uptake coefficient γ for ice particle surfaces is given here, obtained from Sander et al. (2006).

Reactants		Products	γ
$HOBr(g) + HBr(s)$	$\longrightarrow$	$2Br(g) + H_2O(s)$	0.12
$HOBr(g) + HCl(s)$	$\longrightarrow$	$BrCl(g) + H_2O(s)$	0.3
$HOCl(g) + HBr(s)$	$\longrightarrow$	$BrCl(g) + H_2O(s)$	0.06
$BrONO_2(g) + HBr(s)$	$\longrightarrow$	$2Br(g) + HNO_3(s)$	0.3
$BrONO_2(g) + H_2O(s)$	$\longrightarrow$	$HOBr(g) + HNO_3(s)$	0.3
$BrONO_2(g) + HCl(s)$	$\longrightarrow$	$BrCl(g) + HNO_3(s)$	0.25
$ClONO_2(g) + HBr(s)$	$\longrightarrow$	$BrCl(g) + HNO_3(s)$	0.3
$N_2O_5(g) + HBr(s)$	$\longrightarrow$	$Br(g) + NO_2(g) + HNO_3(s)$	0.01[a]

[a] Reaction not included in standard model setup.

4.3.3. Photolysis

Photolysis rates in SLIMCAT are calculated using a scheme based on Lary and Pyle (1991), which was in turn an enhancement of the algorithm originally developed by Meier et al. (1982). The scheme's radiative transfer model calculates the contribution of four sources of radiation into any grid box: The direct solar flux, the diffuse omni-directional flux and the ground reflection of the direct solar and diffuse flux. The photolysis rate j_i for a tracer i is then calculated as:

$$j_i = \int F_{0\lambda} S_\lambda \phi_{\lambda i} \sigma_{\lambda i} \, \mathrm{d}\lambda \tag{4.14}$$

Here, $F_{0\lambda}$ is the solar flux incident at the top of the atmosphere, $\phi_{\lambda i}$ and $\sigma_{\lambda i}$ are the quantum efficiency and the absorption cross section for tracer i at wavelength λ, respectively. S_λ is the so called enhancement factor (Meier et al., 1982) which is defined as the quotient of the total flux F_λ integrated over all directions and the solar flux $F_{0\lambda}$. S_λ is a function of wavelength, solar zenith angle, altitude, ground albedo and the profiles of temperature and ozone.

The calculation of photolysis is one of the most computationally expensive parts of the chemistry scheme. To reduce the computational cost the scheme uses a 4-D look-up table[7] to interpolate precomputed j_i values to a particular location and time in the atmosphere. The required photochemical data to calculate the rates is generally obtained from the JPL 2006 recommendations (Sander et al., 2006). Table 4.6 lists the incorporated photolysis reactions involving bromine.

Table 4.6.: Photolysis reactions of bromine species included in the full chemistry scheme. R denotes the organic rest. The utilized parametrization of the absorption cross-sections is obtained from Sander et al. (2006).

Reactants		Products	Absorption cross-section parametrization
$CClBrF_2 + h\nu$	$\longrightarrow$	$Cl + Br + R$	Burkholder et al. (1991)
$CBrF_3 + h\nu$	$\longrightarrow$	$Br + R$	Burkholder et al. (1991)
$CH_3Br + h\nu$	$\longrightarrow$	$Br + R$	Simon et al. (1988)
$CH_2Br_2 + h\nu$	$\longrightarrow$	$2Br + R$	Gillotay et al. (1988)
$CHBr_3 + h\nu$	$\longrightarrow$	$3Br + R$	Gillotay et al. (1989)
$BrO + h\nu$	$\longrightarrow$	$Br + O$	Gilles et al. (1997)
$HOBr + h\nu$	$\longrightarrow$	$Br + OH$	Ingham et al. (1998)
$HBr + h\nu$	$\longrightarrow$	$Br + H$	Nee et al. (1986)
$BrONO_2 + h\nu$	$\longrightarrow$	$Br + NO_3$	Burkholder et al. (1995)
$BrCl + h\nu$	$\longrightarrow$	$Br + Cl$	Maric et al. (1994)

4.3.4. Chemical Integration Scheme

The core of the SLIMCAT scheme is the numerical solver for the chemical continuity equations. For a species i with the concentration n_i its chemical continuity equation can be written as:

$$\frac{dn_i}{dt} = P_i - L_i n_i = Q_i \tag{4.15}$$

with P_i and L_i the production and loss terms, respectively. For N species $\mathbf{n} = n_1, n_2, \ldots n_N$ at time t Equation 4.15 can be expressed in vectorial form as:

$$\frac{d\mathbf{n}}{dt} = \mathbf{Q}\left(t, \mathbf{n}(t)\right) \tag{4.16}$$

The common challenge when numerically integrating a given set of differential equations is to find the right balance between stability and accuracy on the one side and computational cost on the other. A simple Euler forward scheme of the form:

$$\mathbf{n}_{t+\Delta t} = \mathbf{n}_t + \Delta t \left.\frac{d\mathbf{n}}{dt}\right|_t \tag{4.17}$$

[7]The look-up table has the coordinates pressure, temperature, overhead ozone column and solar zenith angle.

is computationally inexpensive but is only applicable if the chemical lifetime of the particular species is long compared to the integration timestep Δt. Actually this scheme is used in SLIMCAT for the relatively long-lived source gases (e.g., Table 4.2) to save execution time.

For faster reactions the "semi-implicit symmetric" (SIS) method, originally developed by Ramaroson et al. (1992), is used. Here, Equation 4.16 is developed into the form:

$$\mathbf{n}_{t+\Delta t} - \mathbf{n}_t = \frac{\Delta t}{2} \left[\mathbf{Q} \left(t, \mathbf{n}(t) \right) + \mathbf{Q} \left(t + \Delta t, \mathbf{n}(t + \Delta t) \right) \right] \tag{4.18}$$

By expanding $\mathbf{Q} \left(t + \Delta t, \mathbf{n}(t + \Delta t) \right)$ in a Taylor series this equation can be solved and rearranged to get:

$$\mathbf{n}_{t+\Delta t} = \mathbf{n}_t + \frac{\Delta t}{2} \mathbf{J}_t \mathbf{n}_{t+\Delta t} \tag{4.19}$$

where $\mathbf{J_t}$ is the Jacobian matrix:

$$\mathbf{J}_t = \begin{pmatrix} \frac{\partial Q_1}{\partial n_1} & \frac{\partial Q_1}{\partial n_2} & \cdots & \frac{\partial Q_1}{\partial n_N} \\ \frac{\partial Q_2}{\partial n_1} & \frac{\partial Q_2}{\partial n_2} & \cdots & \frac{\partial Q_2}{\partial n_N} \\ \vdots & \vdots & \ddots & \vdots \\ \frac{\partial Q_N}{\partial n_1} & \frac{\partial Q_N}{\partial n_2} & \cdots & \frac{\partial Q_N}{\partial n_N} \end{pmatrix}$$

Therefore, to obtain the tracer concentrations at time $t + \Delta t$ one has to invert the matrix:

$$\mathbf{M} = \mathbf{I} - \frac{\Delta t}{2} \mathbf{J}_t \tag{4.20}$$

The inversion of a $N \times N$ matrix is costly[8] but comparisons by Ramaroson et al. (1992) show that generally the SIS method offers a better compromise between accuracy, stability and speed compared to other integration algorithms.

In this study, the integration timestep of the chemistry scheme is set to 15 minutes which is according to Chipperfield et al. (1993) the upper limit to adequately model the diurnal cycle. In general, the timestep of the CTM framework is set to 30 minutes when applying the full chemistry calculations, i.e. the chemistry scheme is invoked twice per model iteration.

4.3.5. Simulation Setup

The main simulation run using the full chemistry approach is named FC1 (see also Appendix A, Table A.1 for an overview of all conducted model runs). Like its idealized counterpart, ID1, it comprises the time span from 1989 to 2009 which allows direct comparisons between the two approaches. The initial tracer configuration is obtained from a previous run of a 2-D model with a similar chemistry scheme (Sinnhuber et al., 2003b) to reduce initialization artifacts. To capture long-term trends in source gas emissions the corresponding detrainment mixing ratios are time-dependent according to the estimates of WMO scenario A1 (Daniel and Velders, 2010). For the long-lived bromine source gases the timeseries is shown in Figure 3.1. However, the detrainment mixing ratios of the bromine VSLS are set uniformly to 1 pptv, analogous to the idealized setup. The atmospheric loading of H_2SO_4, required for the formation of sulfate aerosol, is obtained from a monthly 2-D climatology (by D. B. Considine, personal communication, 2009, prepared for WMO 2010 scenario REF1/REF2).

[8] Number of calculations is in the order of N^3 using a standard Gaussian elimination method.

To assess the impact of bromine VSLS on the stratospheric chemistry the reference run FC2 was conducted, lacking the source gases bromoform and dibromomethane but being identical to FC1 otherwise (Section 6.1.2).

Finally, FC3 was set up to measure the influence of heterogeneous processes on stratospheric bromine chemistry. Therefore, all heterogeneous reactions involving bromine (Table 4.5) are deactivated. The rest of the setup is identical to FC1 (Section 6.1.2).

Part III.

Results

5. Model Validation

This chapter concentrates mainly on the modeled transport in the TTL. Several proxies are used to evaluate the performance of the novel modeling approach, i.e. the usage of an explicit convective parametrization in an isentropic CTM. Firstly, convection in the model represented by the convective detrainment rate will be discussed in Section 5.1. The injection of bromine source gases into the TTL is detailed in Section 5.2 whereas the resulting product gas distribution is compared to observations in Section 5.3. The impact of convection on water vapor and ozone is discussed in Sections 5.4 and 5.5, respectively. Finally, the mean age of air in the model is evaluated in Section 5.6.

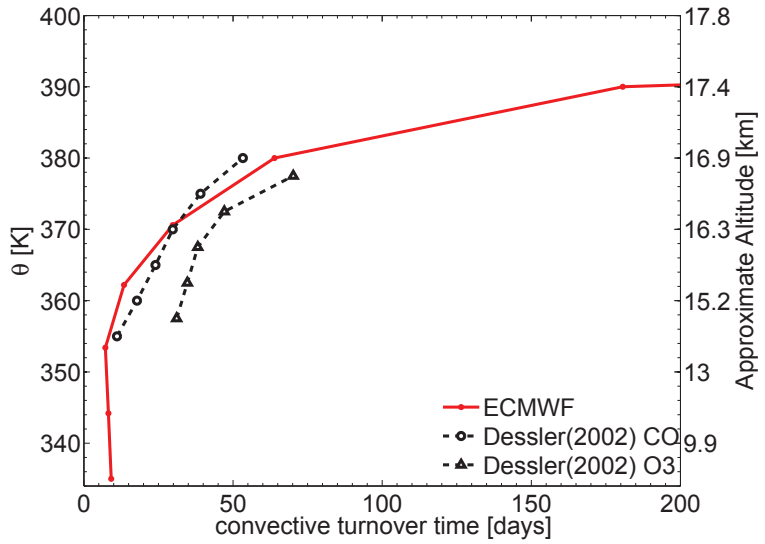

Figure 5.1.: Comparison of tropical convective turnover times derived from the ECMWF ERA-Interim updraft detrainment rate and those calculated by Dessler (2002) from CO and O_3 measurements. Adapted from Aschmann et al. (2009).

5.1. Convection

Convective transport is a key component of this modeling study and directly controls the distribution of VSLS in the UTLS. Since the convective parametrization in the model fundamentally relies on the external updraft detrainment rates from ERA-Interim the assessment of this quantity is essential for understanding transport processes in the tropopause.

Figure 4.4 shows a typical zonally averaged profile of the detrainment rate d_c in the tropics. The main convective outflow is located around 14 km, just below the LZRH, which is in agreement with previous studies (e.g., Fueglistaler et al., 2009a). Air masses that detrain below the LZRH generally subside again towards the surface, that means the

detrainment above the critical mark of about 15.5 km is important for the injection of tropospheric air masses into the UTLS. d_c decays rapidly with increasing altitude but as shown in Figure 4.4 there is still some detrainment above the cold point at around 17 km. With the utilized approach of convective transport this means a considerable amount of air is detrained at relatively high altitudes, and although there is ample evidence that overshooting deep convection can penetrate this level (e.g., Fueglistaler et al., 2009a, and references therein), it is unclear whether this frequent high reaching transport is a realistic representation. However, comparisons of the convective turnover time (i.e. the inverse of the detrainment rate) derived from ERA-Interim d_c with calculations made by Dessler (2002) based on CO and O_3 observations show excellent agreement up to 380 K (Figure 5.1) and are also in qualitative agreement with the findings of Folkins and Martin (2005).

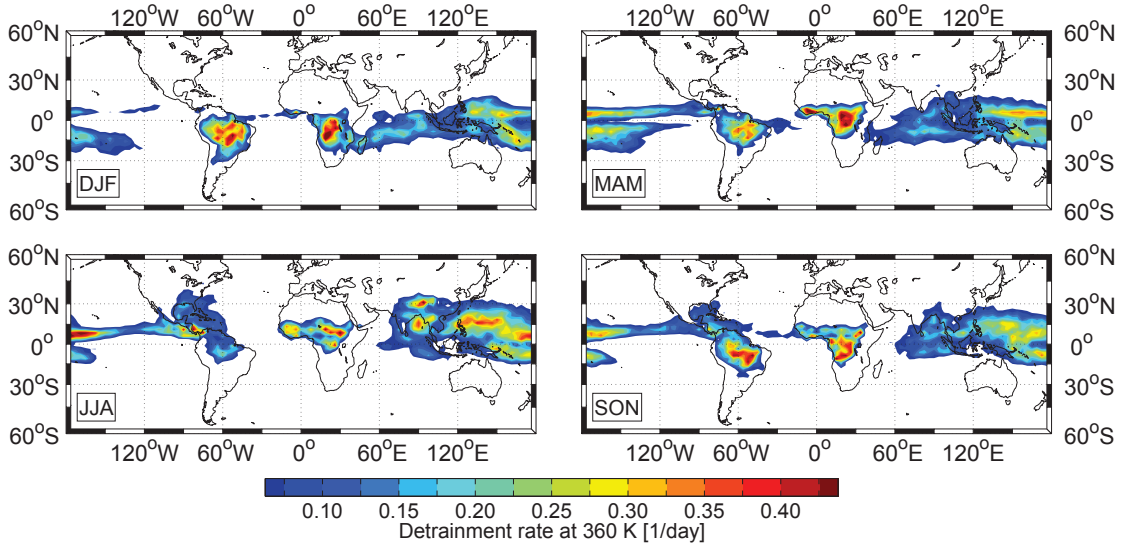

Figure 5.2.: ERA-Interim convective detrainment rate at 360 K (about 16 km) for December-January-February (DJF), March-April-May (MAM), June-July-August (JJA) and September-October-November (SON), averaged from 1989 to 2009.

The spatial distribution of convection above the LZRH is shown in Figure 5.2. In general, high-reaching convection is concentrated at the ITCZ with especially strong activity over the West Pacific region, in agreement with earlier studies (e.g., Gettelman et al., 2002b; Liu and Zipser, 2005). Although the major part of detrainment occurs above the ocean, strong hot spots are also located over South America and Central Africa. This confirms the findings of Jorgensen and LeMone (1989) who state that convection over land generally tends to produce higher vertical velocities compared to convection over the ocean which consequently results in more frequent and far-reaching overshoots. Furthermore, the ERA-Interim detrainment rate shows a strong Monsoon signal during boreal summer, i.e. increased convective activity over India, the Tibetan plateau and the Maritime Continent.

Finally, Figure 5.3 shows the development of d_c over time at different altitudes. At 350 K, i.e. at the level of main convective outflow, d_c shows a small negative trend up to 2006, followed by an increase for the next years. The increase is discernible at higher altitudes as well, but whether this is a realistic feature remains unclear. A distinctive feature is the exceptional strong El Niño event 1997/1998 which produced extensive overshoots and temporally shifted convective activity to higher altitudes. In Section 7.3, the relation of

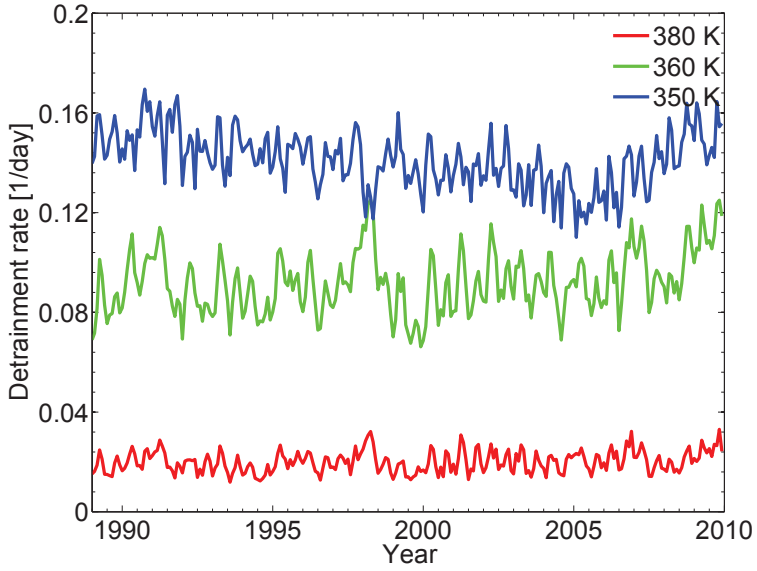

Figure 5.3.: Timeseries of tropical detrainment rate in 350 K (14 km), 360 K (16 km) and 380 K (17 km).

sea surface temperatures to convective activity and the consequences for the distribution of VSLS will be discussed in detail.

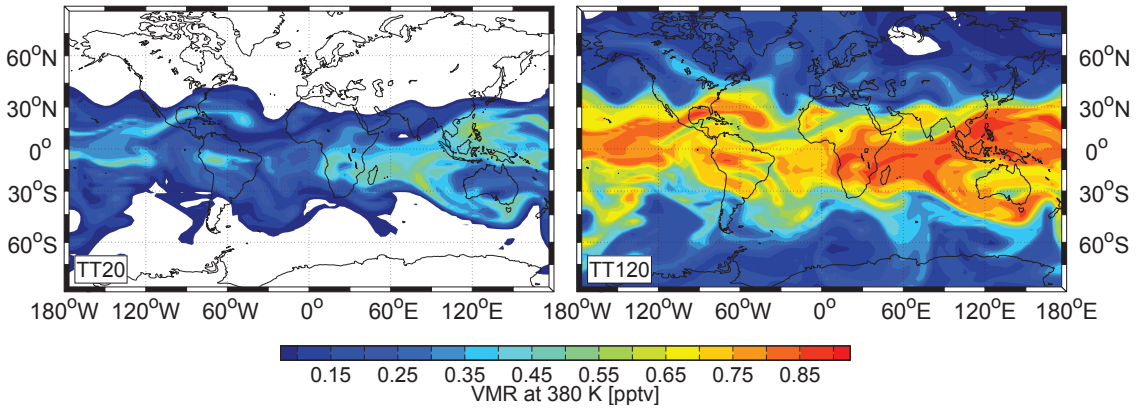

Figure 5.4.: Snapshot of TT20 (left) and TT120 (right) distribution of run ID1 at 380 K (about 17 km) on February 16, 2004.

5.2. Bromine Source Gases

Due to their short lifetime the distribution of VSLS in the TTL is mainly localized at areas where significant convective activity occurs. Figure 5.4 shows a snapshot of the modeled TT20/TT120 (i.e. $CHBr_3$, CH_2Br_2) abundance at 380 K, the top of the tropopause in the tropics. The distribution patterns of the shorter-lived TT20 are roughly similar to those of convective activity presented in Figure 5.2: the mixing ratio of the VSLS tracer peaks

at South America, Central Africa and the Maritime Continent/West Pacific, the regions showing substantial convection. In contrast, the distribution of TT120 is less localized. Although the patterns are similar to those of TT20 in principle, the mixing ratio of TT120 shows smaller relative variations in zonal direction due to its significantly longer lifetime. Clearly, horizontal transport is an important factor to consider in order to understand the distribution of VSLS in the TTL, which even applies for the shorter-lived species as the elongated plumes of TT20 indicate. The relative importance of convection and horizontal advection will be discussed in detail in Section 6.3.

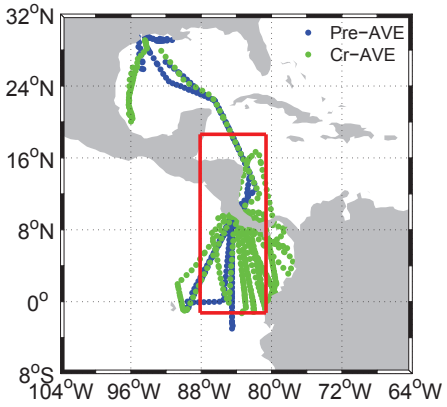

Figure 5.5.: Flightpath of the WB57 aircraft during the Pre-AVE and Cr-AVE campaign. Model and observational data have been averaged over the region denoted by the red box.

Direct comparison of modeled VSLS with observations in the TTL is difficult since there are few available measurements in this altitude region. Observations from two Aura Validation Experiment (AVE) campaigns with the NASA WB57 high-altitude aircraft are shown in Figure 5.6 and 5.7 together with modeled profiles (Aschmann et al., 2009). Both campaigns, Pre-AVE and Cr-AVE, were performed around 80-90°W at latitudes between 20°N and 3°S in January/February 2004 and 2006, respectively (Figure 5.5). There is in general good agreement between the idealized tracers of run ID1 and the observations, especially during the Pre-AVE campaign (Figure 5.6). The mixing ratios of TT20 between 10 and 16 km are higher compared to the measurements which may indicate that the simplistic assumption of a uniform detrainment mixing ratio of 1 pptv overestimates the emission of $CHBr_3$. During the Cr-AVE campaign the discrepancy between model and observations are larger. It is likely that these deviations are the result of strong interannual variations of VSLS emissions indicated by, e.g., Quack and Wallace (2003); Yokouchi et al. (2005); Quack et al. (2007a); Butler et al. (2007) which are not captured by the model. The other notable difference can be seen at the lowermost altitude levels where the modeled VSLS mixing ratios show a local maximum which is not supported by the observations. This is most likely an artifact introduced by the lower boundary of the model at 335 K or 8 km.

In general, the same applies for profiles of the full chemistry run FC1, shown in Figure 5.7, however, the deviations from the observational profiles are significantly larger compared to the idealized run. One important reason for this discrepancy is that the explicitly calculated degradation of $CHBr_3$ and CH_2Br_2 generally leads to longer photochemical lifetimes of the species compared to the idealized setup (Figure 3.3), especially in the

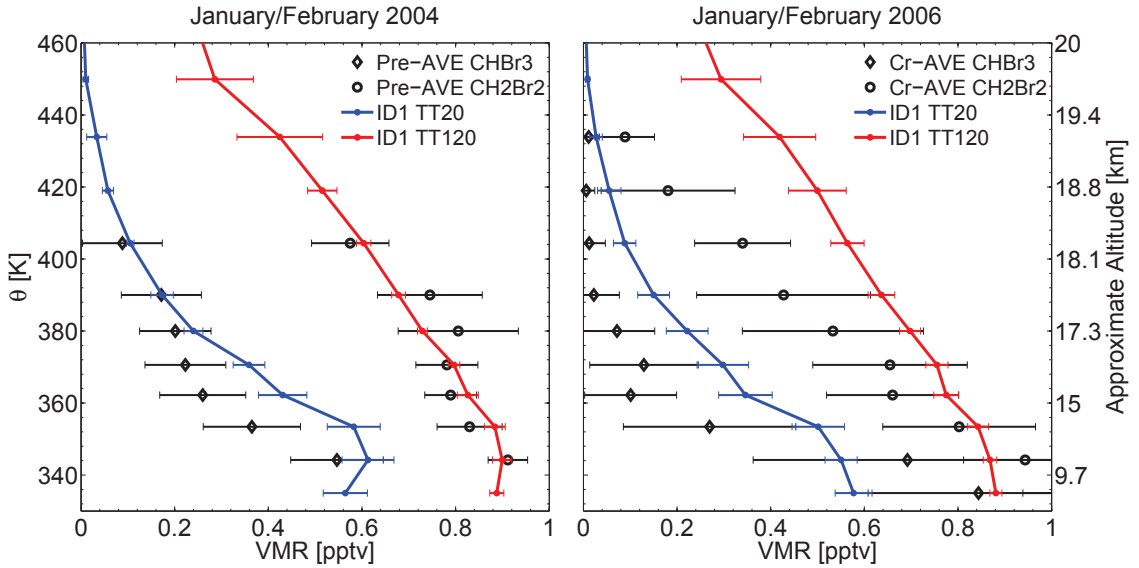

Figure 5.6.: Comparison of TT20 and TT120 of run ID1 with aircraft measurements of $CHBr_3$ and CH_2Br_2 from the Pre-AVE (left) and Cr-AVE (right) campaign. The observations were mostly performed at about 80–90°W, 20°N–3°S during January/February 2004 and 2006, respectively (see Figure 5.5). Model and observational data in this region have been averaged for this comparison. The error bars denote one standard deviation.

case of dibromomethane; thus the full chemistry setup is more sensitive to the assumed detrainment mixing ratio of VSLS. This becomes clear when reducing the detrainment mixing ratio of $CHBr_3$ and CH_2Br_2 by a factor of 0.5 and 0.85, respectively, as indicated by the dashed lines in Figure 5.7. With the source parameter scaled down, the agreement between model and observations improves drastically, though large deviations of modeled CH_2Br_2 during the Cr-AVE campaign still remain. Since the degradation of CH_2Br_2 in the tropospheric domain is strongly dependent on the OH-reaction, this might indicate that the variability of the hydroxyl radical distribution is not optimally represented in the full chemistry setup.

In addition, Figure 5.7 shows also the profiles of the long-lived bromine source gases, whose detrainment mixing ratio in the model varies with the WMO 2010 scenario A1 (Daniel and Velders, 2010, see also Figure 3.1). In general, there is excellent agreement between the modeled and observed profiles, although there is constant bias in the case of H1301 and CH_3Br. For CH_3Br, this bias can be mainly attributed to the globally uniform detrainment mixing ratio assumed in the model setup: according to Montzka and Reimann (2010), there is an inter-hemispherical difference in the CH_3Br source strength; in the Northern Hemisphere (NH), the average mixing ratio is approximately 1 pptv higher. Consequently, the globally averaged $[CH_3Br]_c$ underestimates the detrainment of CH_3Br into the NH by about 0.5 pptv which is consistent with the bias seen in Figure 5.7.

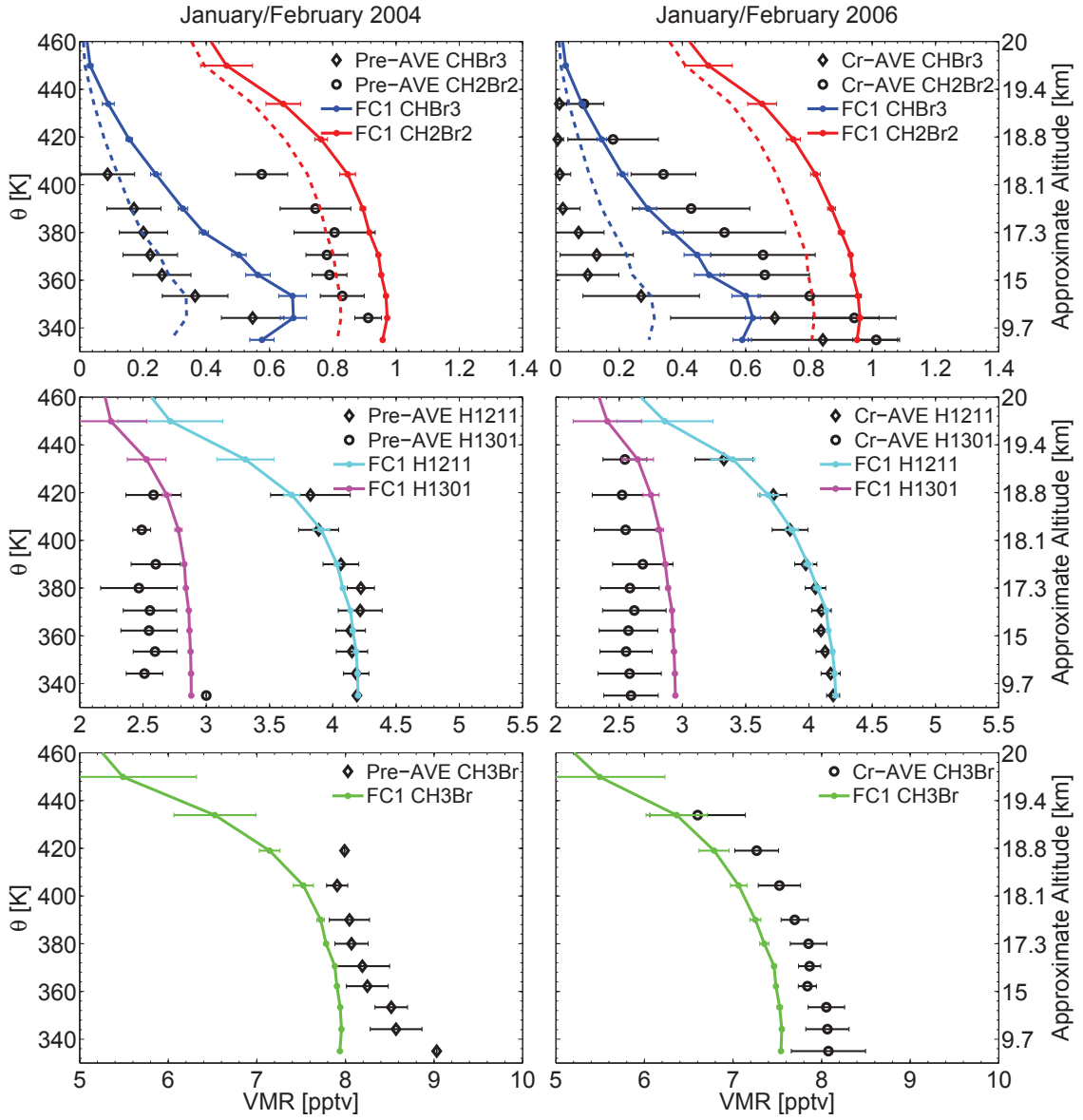

Figure 5.7.: Similar to Figure 5.6 but for the full chemistry run FC1. In addition to the VSLS $CHBr_3$ and CH_2Br_2 the profiles of the long-lived source gases ($CClBrF_2$/H1211, $CBrF_3$/H1301 and CH_3Br) are shown as well. The dashed lines denote profiles of $CHBr_3$ and CH_2Br_2 where the detrainment mixing ratio is scaled by 0.5 and 0.85, respectively.

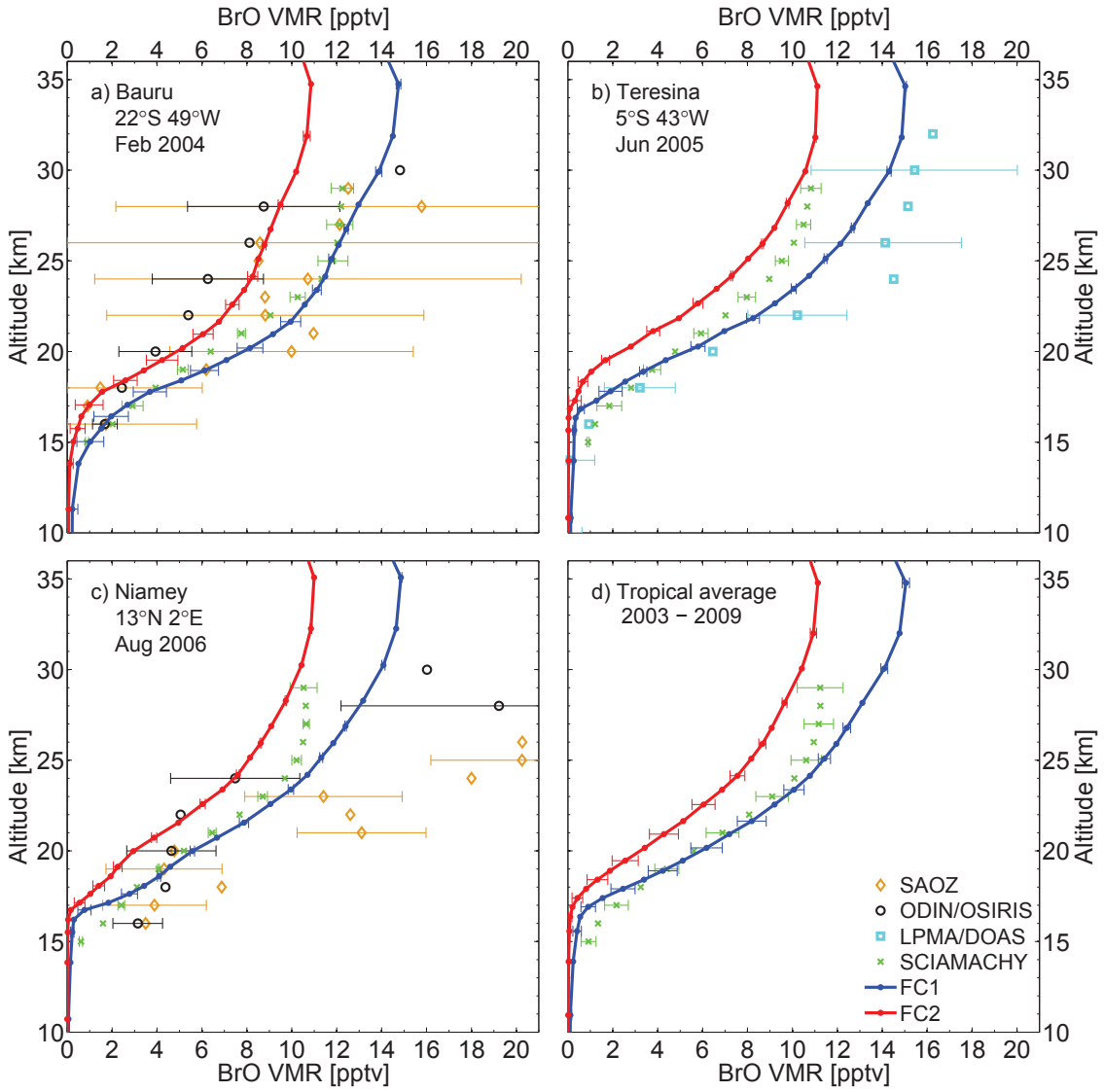

Figure 5.8.: Comparison of modeled and observed BrO, adapted from McLinden et al. (2010). The first three panels show local profiles from Bauro, Brazil (a), Teresina, Brazil (b) and Niamey, Niger (c). Panel d) shows tropical averaged profiles from 2003 to 2009. The SAOZ and LPMA/DOAS measurements are from balloon-borne instruments, conducted by Pundt et al. (2002) and Dorf et al. (2008), whereas the satellite data from ODIN/OSIRIS and SCIAMACHY is taken from McLinden et al. (2010) and Rozanov et al. (2010a), respectively.

5.3. Bromine Product Gases

The most important inorganic bromine product gases, which are commonly summarized as Br_y, are Br, BrO, HBr, HOBr, BrCl and $BrONO_2$ (see Figure 3.2). As shown in Section 3.2.2, about 50–70% of Br_y is actually BrO during daylight, which makes this species a useful proxy for stratospheric bromine. Figure 5.8 presents local daytime BrO measurements from different tropical sites together with model results from the full chemistry simulations FC1 and FC2. The only difference between those runs is that FC1 contains the two bromine VSLS $CHBr_3$ and CH_2Br_2 which are not included in run FC2 (Section 4.3.5). Panel a) shows local profiles at Bauru, Brazil (22°S, 49°W) in February 2004 from SAOZ balloon-borne measurements (Pundt et al., 2002), satellite data from ODIN/OSIRIS[1] (McLinden et al., 2010) and SCIAMACHY (Rozanov et al., 2010a). The profile of model run FC1 agrees well with the observations, especially with the SCIAMACHY and SAOZ data. The ODIN/OSIRIS instrument shows lower mixing ratios that are more similar to the model run FC2 without additional VSLS. Panel c) presents profiles from the same observational sources but for Niamey, Niger (13°N, 2°E) in August 2006. Here, model run FC1 and SCIAMACHY observations also generally agree between about 17 to 23 km. In the tropopause region, the satellite profile suggests higher mixing ratios than the model which is reversed above 23 km. However, the mixing ratios measured SAOZ and ODIN/OSIRIS are significantly higher than the previously mentioned profiles suggest, especially above 20 km altitude. Panel b) comprises data from balloon-borne LPMA/DOAS measurements conducted by Dorf et al. (2008) above Teresina, Brazil (5°S, 43°W) in June 2005 in addition to SCIAMACHY and model data. The balloon measurements show good agreement to run FC1, although there is a relatively constant offset of about 1–2 pptv present. The SCIAMACHY data shows the same divergence as described before, predicting higher mixing ratios in the tropopause and lower values in the middle stratosphere compared to the full chemistry run with VSLS. Finally, panel d) shows tropical averages of SCIAMACHY and model data between 2003 and 2009. The picture is essentially the same as for the local sites: the profiles agree generally well in the lower stratosphere and diverge further above and below.

In general, the standard full chemistry run FC1 with VSLS included agrees with the presented observational data, especially with the SCIAMACHY observations in the range between 17 and 23 km. With the exception of Niamey, the other observational sources also agree with the modeled profile in principle, although the deviations are generally larger.

5.4. Water Vapor

An adequate representation of water vapor in the tropical tropopause is an important prerequisite for modeling the possible loss of inorganic bromine due to washout or scavenging[2] (see Section 3.1.2). In the TTL, the averaged profiles of relative humidity with respect to ice (RH) obtained from the idealized and full chemistry setup (Figure 5.9) are in qualitative agreement with observations (e.g., Folkins et al., 2002; Sherwood et al., 2010), in particular the decrease of RH with decreasing altitude in the lower TTL. This decrease in RH results from the large-scale subsidence and associated adiabatic warming of air that was initially saturated at convective detrainment. The successful representation of this effect is thus only possible with the separation of slow large-scale descent and fast isolated

[1] Note that the ODIN/OSIRIS profiles are zonal averages at the corresponding latitude (McLinden et al., 2010).

[2] This section is based mainly on the work presented in Aschmann et al. (2009, 2011).

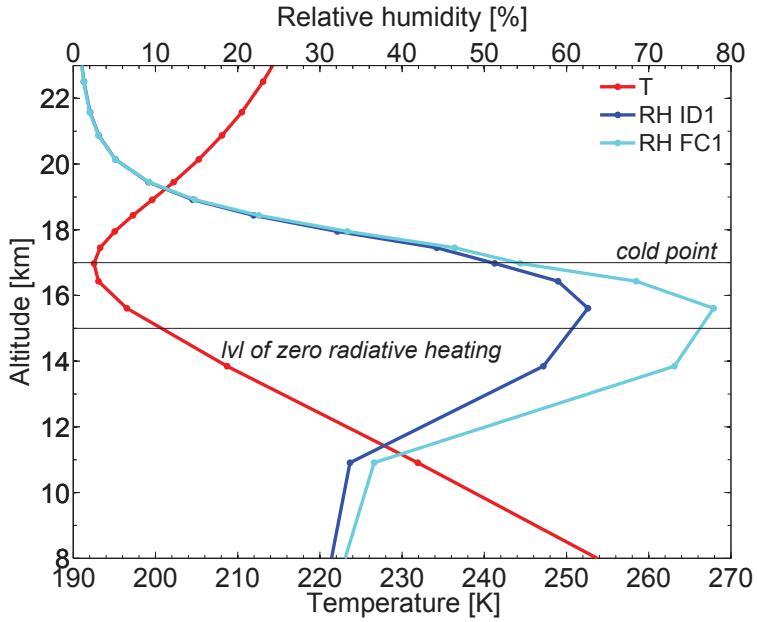

Figure 5.9.: Averaged tropical temperature (bottom abscissa) and relative humidity (top abscissa) profiles of run ID1 and FC1 for 2004. Adapted from Aschmann et al. (2009).

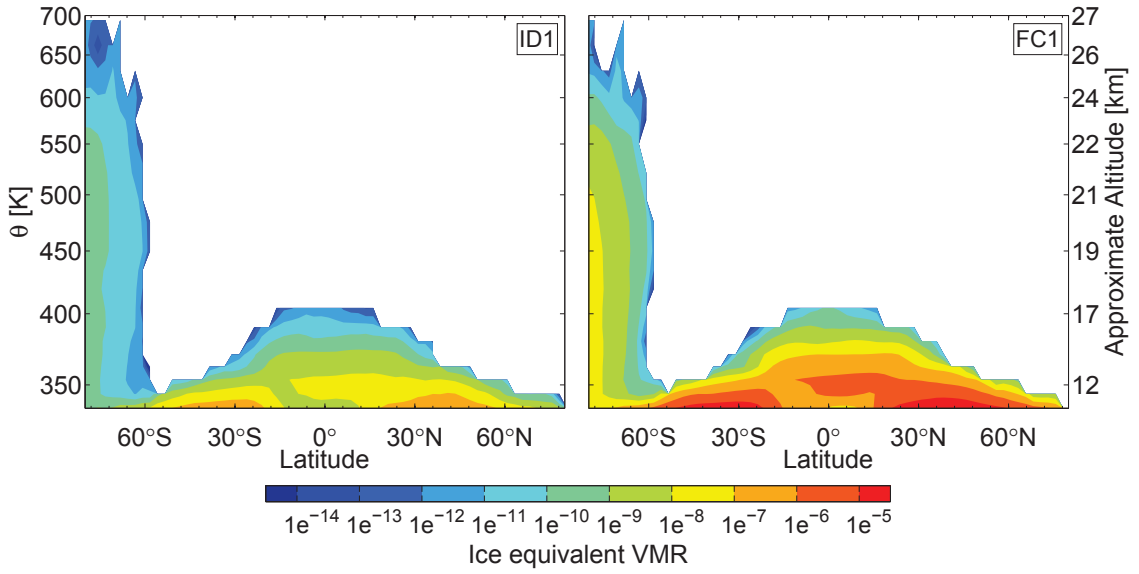

Figure 5.10.: Averaged equivalent gas phase volume mixing ratio of ice in run ID1 (left) and FC1 (right) for 2004. Adapted from Aschmann et al. (2011).

convective updrafts in the model.

The RH peaks at around 16 km which is slightly below the cold point (Figure 5.9). In this altitude region the air in the CTM gets effectively dehydrated, especially in local areas that show much higher values of RH, for example over the Indian Monsoon and

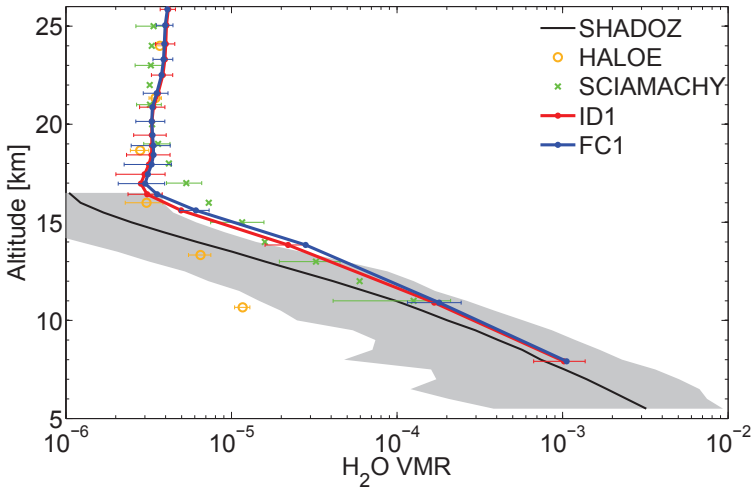

Figure 5.11.: Averaged tropical water vapor profiles derived from SHADOZ sonde measurements (Thompson et al., 2003), HALOE (Grooß and Russell, 2005) and SCIAMACHY (Rozanov et al., 2010b) observations and model runs ID1 and FC1 for 2004. The gray shading depicts the range between minimum and maximum values of the SHADOZ station ensemble (see Figure 5.13) whereas the black line marks the mean. The error bars denote one standard deviation.

West Pacific region during boreal summer, which is on the line with previous studies (e.g., Gettelman et al., 2002a; Fueglistaler et al., 2005; Read et al., 2008). Another indicator is the average amount of ice in run ID1 and FC1 presented in Figure 5.10, which concentrates predominantly in the tropical upper troposphere/tropopause region. The fraction of ice to total water abundance in the tropics is highest in the aforementioned altitude region, about 5–8% in run FC1. At high latitudes, the ambient meteorological conditions allow the formation of ice even up to 25 km altitude, i.e. Type II PSCs (e.g., McCormick et al., 1982; Solomon, 1999; Lowe and MacKenzie, 2008). Generally, the idealized run ID1 shows much lower values for ice than its full chemistry counterpart since it lacks the explicit treatment of ice particle sedimentation thus all ice is removed instantly upon formation. This effect can also be seen in the RH (Figure 5.9) and water vapor profiles (Figure 5.11) which show generally lower values for run ID1.

A more quantitative evaluation of the modeled water vapor is presented in Figure 5.11 using HALOE (Grooß and Russell, 2005) and SCIAMACHY (Rozanov et al., 2010b) satellite observations and SHADOZ balloon-borne sonde measurements (Thompson et al., 2003, see also Figure 5.13). Above the cold point up to the lower stratosphere the modeled profiles agree well with the HALOE data. This applies partly also for the comparison with the SCIAMACHY profile, however, due to the relatively coarse vertical resolution of the retrieval (2–5 km, Rozanov et al., 2010b) some distinctive features are smeared out, for example the minimum of water vapor at 17 km. At the lower part of the TTL there is a significant offset to the observations, especially compared to the sonde measurements. The water vapor mixing ratio obtained from the combined SHADOZ stations is up to a factor of three to four lower than the modeled profiles in the range between 12 and 17 km although there is a also large variability in the observations as indicated by the gray shading in Figure 5.11. The deviations to the SCIAMACHY observations are generally smaller. Since the shape of the profiles is very similar it is likely that there is a constant offset in the

modeled water vapor, probably introduced by the assumption that detraining air is always fully saturated (see Section 4.2.2, 4.3.2).

In the stratosphere, the modeled water vapor shows a clear "tape recorder signal" (Figure 5.12), i.e. the seasonal variation of humidity is conserved in ascending air parcels (e.g., Mote et al., 1995). Comparison with HALOE measurements show in general excellent agreement in the dry phases and also the speed of the tape recorder signal is well reproduced (Figure 5.12). But these comparisons reveal also that in both modeling approaches too much water (on average by about 1 to 1.5 ppm) is transported into the tropics at altitudes above 17 km during boreal summer. In the model calculations the 'moist head' of the tape recorder is located at about 18 km which is not supported by the HALOE observations. However, other measurements do indicate higher water vapor mixing ratios at 17 km and above during boreal summer (Dessler and Sherwood, 2004; Hanisco et al., 2007; Jiang et al., 2010). As stated above it is not clear if the discrepancy in water vapor between the model and HALOE observations is a result of too much convective transport above the cold point or whether the assumption that air detrains with 100% RH overestimates the flux of water into the stratosphere.

5.5. Ozone

Ozone can be utilized as useful means for evaluating the transport mechanisms of the CTM[3]. The linearized chemistry incorporated in the idealized run ID1 acts nearly identically throughout the tropics on a given level of potential temperature. Likewise, the convective detrainment mixing ratio is constant in this area, at about 20 ppbv. In addition, ozone in the altitude range between 15 and 20 km is relatively long-lived[4], compared to typical transport timescales (e.g., Brasseur and Solomon, 2005). Therefore, most of the ozone variations in the modeled TTL can be attributed to transport and convection. Figure 5.14 shows ozone profiles of tropical sonde stations of the SHADOZ project (Thompson et al., 2003, see also Figure 5.13) in comparison with corresponding data obtained from run ID1. In general, the modeled profiles match the observations despite the simple treatment in the model. However, especially the stations in South America and Central Africa show significantly larger ozone concentrations compared to the model. This becomes clear when considering that the ozone distribution in the free troposphere is not uniform throughout the tropics as assumed in the idealized setup. Thompson et al. (2003) showed that there exists a "wave-1" structure (e.g., Shiotani, 1992) in free tropospheric ozone with increased ozone mixing ratios between 50°W and 50°E, possibly due to ozone precursor emissions from biomass burning or other sources. In regions where the amount of free tropospheric ozone is similar, the modeled transport and convection are able to correctly reproduce the key features of the measured ozone distribution.

Further comparisons of modeled ozone also from the full chemistry setup are presented in Chapter 8, along with the impact of bromine VSLS on stratospheric ozone.

[3]This section is based mainly on the work presented in Aschmann et al. (2009).
[4]Under the assumption that there are no significant amounts of reactive halogens present.

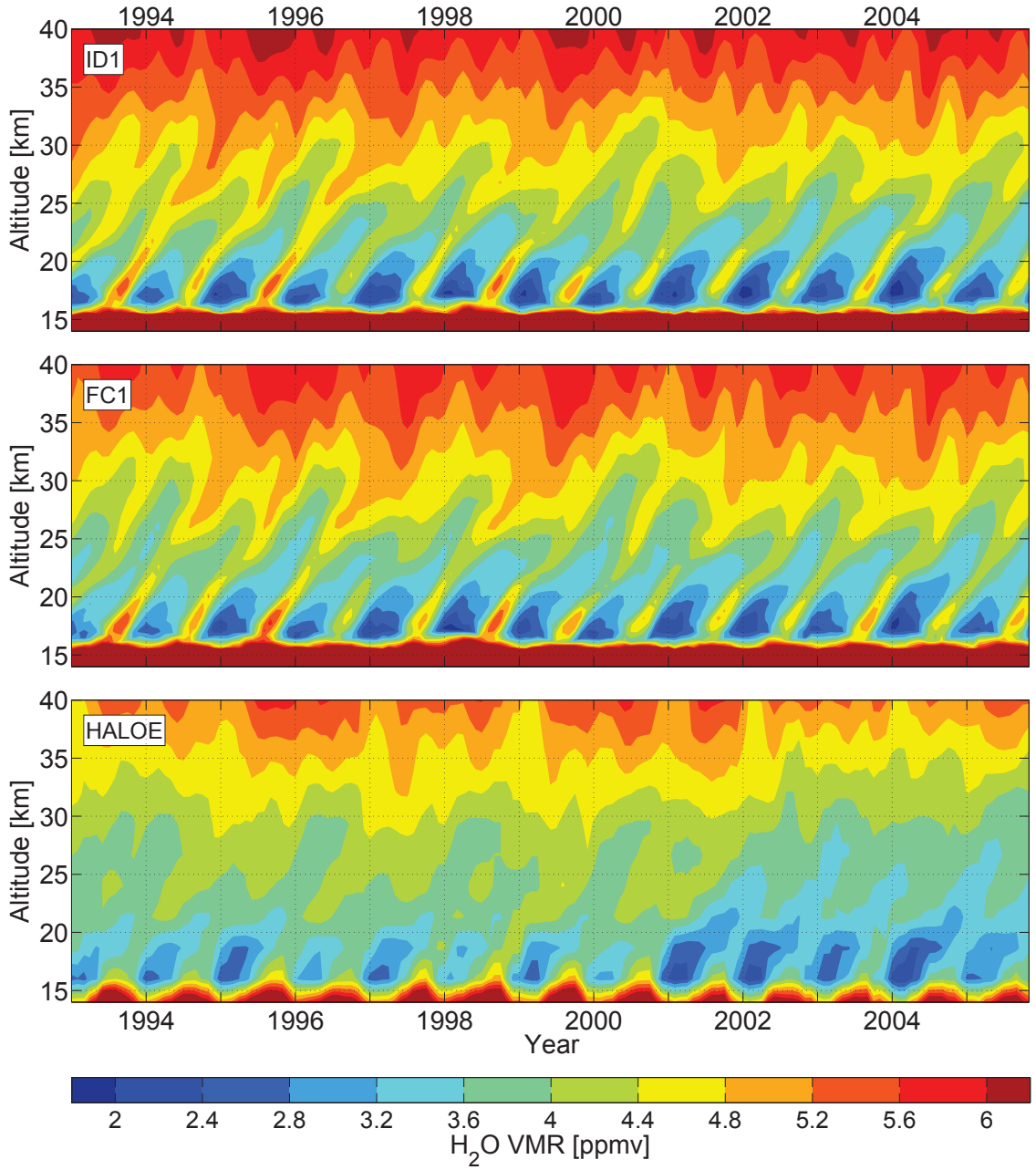

Figure 5.12.: Comparison of tropical water vapor mixing ratios ("tape recorder") of run ID1 (top), FC1 (center) and HALOE observations (bottom, Grooß and Russell, 2005). Adapted from Aschmann et al. (2011).

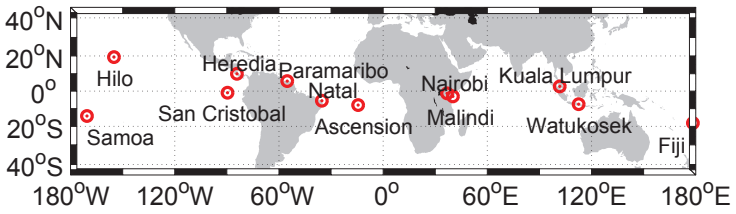

Figure 5.13.: SHADOZ sonde stations in the tropics (Thompson et al., 2003).

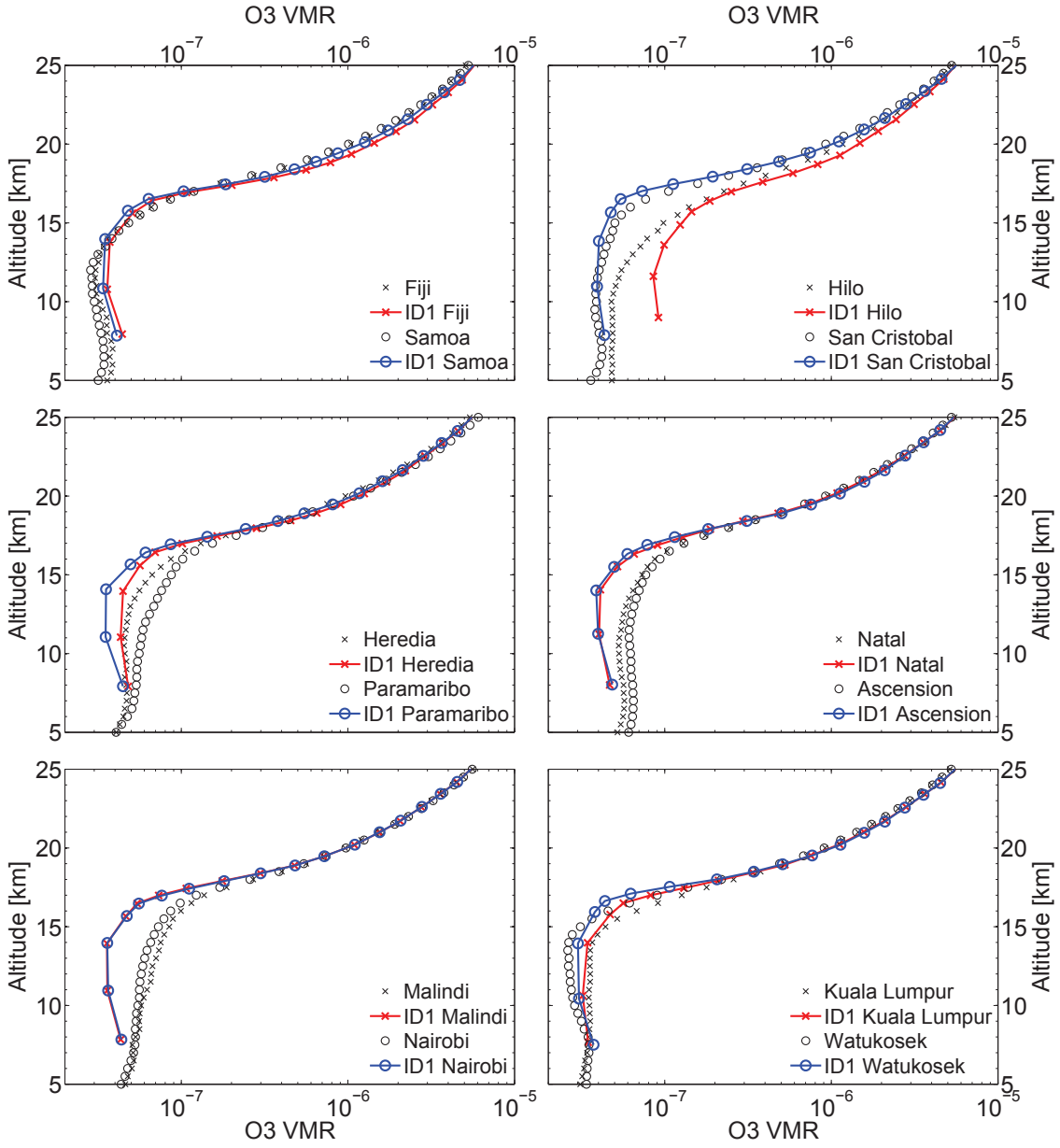

Figure 5.14.: Ozone profiles of individual SHADOZ stations (Figure 5.13) compared to model run ID1, averaged from 2000 to 2009.

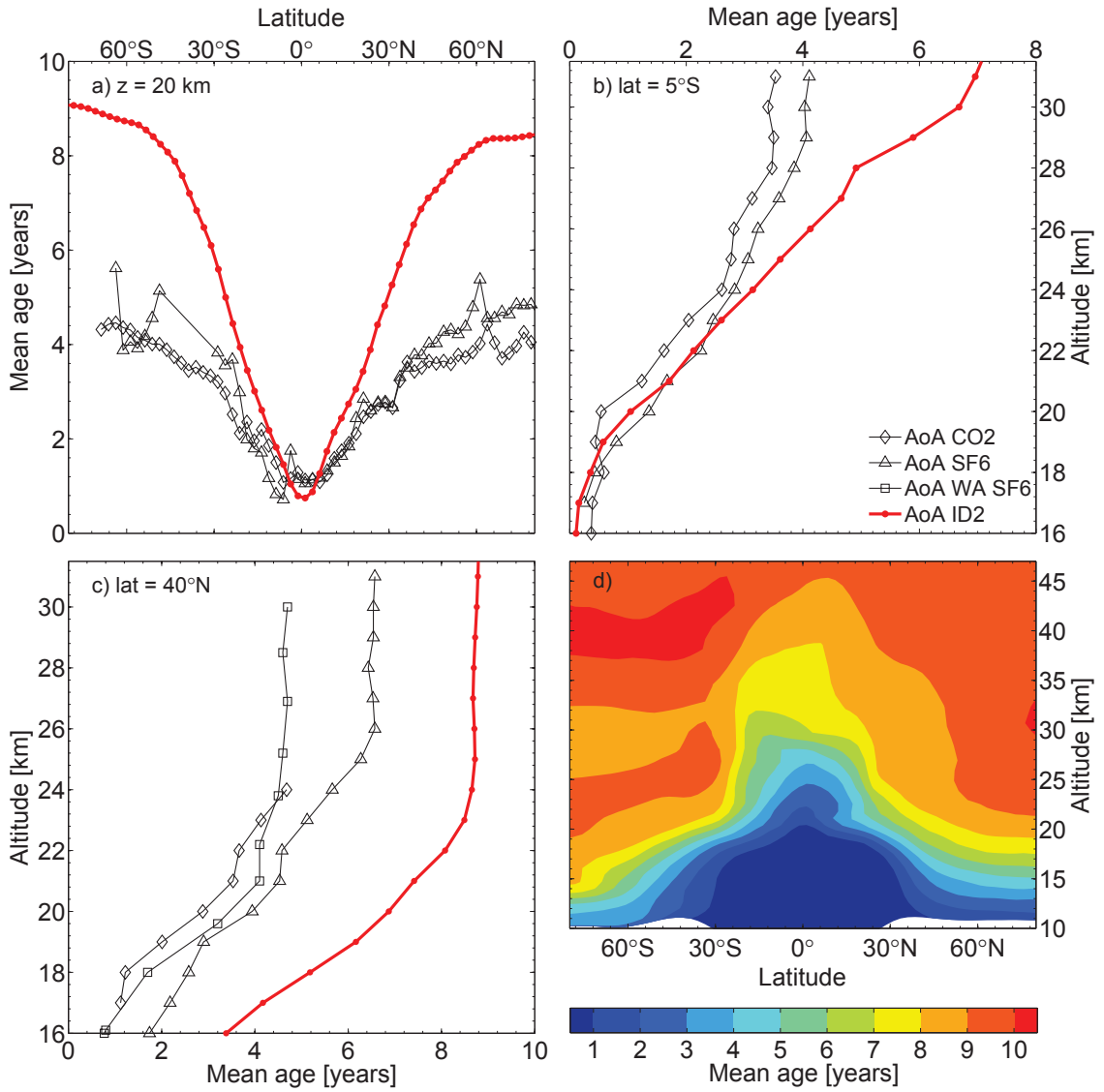

Figure 5.15.: Comparison of observed and modeled mean age of air, adapted from Waugh and Hall (2002): latitudinal profile at 20 km altitude (a), zonal averaged profile at 5°S (b) and 40°N (c). The symbols represent observations: mean age from in situ CO_2 (diamonds, Boering et al., 1996; Andrews et al., 2001), in situ SF_6 (triangles, Elkins et al., 1996; Ray et al., 1999), and whole air samples of SF_6 (squares, Harnisch et al., 1996). Panel d) shows a zonal cross-section of the modeled mean age of air.

5.6. Mean Age of Air

The general circulation in the CTM is investigated using a passive AoA tracer as described in Section 4.2.3. Figure 5.15 shows profiles of mean AoA obtained from observations of long-lived species such as CO_2 or SF_6 in comparison with model data of run ID2. In the tropics, the modeled AoA generally matches the observations up to 25 km. Furthermore, the average residence time of air parcels in the TTL, calculated from the mean heating rate between 360 to 380 K, is about 42 days, which is in good agreement with previous studies (e.g., Andrews et al., 1999; Krüger et al., 2009; Ploeger et al., 2010).

However, at higher latitudes or altitudes the modeled AoA is significantly higher in contrast to the observations. Even compared to a recent study of SF_6 distribution made by Stiller et al. (2008), which suggests a slightly higher overall mean age than the measurements presented in Figure 5.15, the modeled AoA deviates up to three years from the observational basis, especially in polar regions. Apparently, the velocity of the large-scale stratospheric flux in poleward direction (i.e. the Brewer-Dobson circulation, Figure 2.2) is underestimated in the model. It is currently not clear whether this effect is caused by the ERA-Interim input data or by the implementation of transport in the model. Although the primary focus of this study is on the tropical UTLS where the circulation speed is adequately represented, the deviations at higher latitudes/altitudes will affect the tropics due to mixing and must be taken into account.

5.7. Discussion and Conclusion

An initial validation of the model with observations of bromine source and product gases, water vapor and ozone shows in general good agreement (Sections 5.2–5.5). This means that the approach of dividing the vertical transport into a large-scale component constrained by diabatic heating rates on the one hand and convection in fast isolated updrafts on the other hand is an appropriate tool for studying processes in the tropical tropopause, in particular the impact of bromine VSLS. The modeled distribution of bromine source gases in the TTL agrees generally well with the available aircraft observations (Section 5.2), however, the assumption of a constant and uniform detrainment mixing ratio introduces a bias in the source gas profiles, reflecting the uncertainties in the source gas emissions. On the product gas side, BrO is used as proxy for stratospheric inorganic bromine in Section 5.3. The modeled profiles agree well with observations in general, taking into account that the uncertainty in the abundance of bromine source gases also propagates into the distribution of stratospheric Br_y.

Furthermore, there is some evidence from the ozone and water vapor comparisons that could indicate too much convective transport into the 16 to 18 km altitude region. However, a comparison of the convective turnover time scales in the TTL from the CTM with estimates from Dessler (2002) shows excellent agreement (Section 5.1), so it may also be that existing deviations from ozone and water vapor observations are a consequence of the inherent limitations in the treatment of these species.

The general circulation in the model is realistically reproduced in the tropical UTLS as shown by comparisons of the modeled phase speed in the water vapor tape recorder (Section 5.4), the residence time in the TTL and mean age of air (Section 5.5) with available observations. However, significant deviations are found in higher latitudes/altitudes suggesting that the strength of the Brewer-Dobson circulation is underestimated in the CTM. One consequence is that the model needs more time to reach a quasi-steady state, about 20 years, which was considered in the setup of the model runs (Section 4.2.4, 4.3.5).

Furthermore the response of the modeled atmosphere to changes is delayed. For example, this becomes evident when the emission of source gases varies over time, as described in Section 6.1.2 and 7.2. The impact of the underestimated poleward transport is also clearly discernible in the abundance of polar ozone, which will be discussed in Section 8.

6. Impact of VSLS on Stratospheric Bromine Loading

The contribution of bromine VSLS to stratospheric bromine loading is mainly dependent on three important processes. The first one is the (vertical) transport in the tropical UTLS region, which includes both the large-scale heating-rate-driven component and fast localized convection. As shown in the evaluation of the CTM's transport in Chapter 5, in general the distribution of long and short-lived source gases in the TTL is adequately reproduced. The second important process is the dehydration of tropospheric air masses during their ascent into the stratosphere. Soluble species are likely to be scavenged by falling water/ice particles during the dehydration process, however, important details of the TTL dehydration are not fully understood (see Section 2.3). The impact of dehydration on stratospheric bromine loading in the model will be discussed in Section 6.1. Finally, location and strength of VSLS emission may have significant influence on the contribution of short-lived source gases to stratospheric bromine. However, as pointed out earlier in Section 3.1.2, the few available measurements of VSLS emissions show large variations which introduces severe uncertainties in the assumed source strengths. Therefore, Section 6.2 presents a sensitivity study to identify the impact of a more refined emission scenario for bromine VSLS whereas Section 6.3 investigates the relative transport efficiency of different emission regions with regard to stratospheric bromine loading.

6.1. Dehydration and Heterogeneous Chemistry

Dehydration in the TTL is assumed to have a significant impact on soluble halogenated species and is subject to current research (e.g., Dvortsov et al., 1999; Sinnhuber and Folkins, 2006; Hossaini et al., 2010; Liang et al., 2010). A major part of Br_y at the base of the TTL is actually HBr and therefore highly soluble (e.g., Lary, 1996; Sinnhuber et al., 2002; Yang et al., 2005, see also Figure 3.4), thus the estimate of VSLS contribution to stratospheric bromine loading is highly sensitive to the implementation of uptake and scavenging in a model[1]. Moreover, dissolved or adsorbed bromine species may undergo heterogeneous reactions which are able to release active radicals again into the gas phase (e.g., von Glasow et al., 2004; Law and Sturges, 2007), introducing another process that has to be considered. This section is based mainly on the work presented in Aschmann et al. (2011).

As first step, the impact of these processes on the stratospheric bromine loading is illustrated by comparing the idealized and full chemistry approach for a single year, 2006. This particular year was chosen because it is in the last quarter of the covered time period of the conducted model runs, minimizing the effect of initialization artifacts. More important, 2006 is a year relatively unaffected by the El Niño Southern Oscillation that is typically accompanied by strong perturbations in sea surface temperature and convective activity (e.g., Ramanathan and Collins, 1991; Barsugli and Sardeshmukh, 2002; Chiang and Sobel,

[1]Note that due to the general absence of liquid water in the UTLS, the region of primary interest in this work, the terms "washout" and "scavenging" will be used in the following to refer to the uptake and loss of trace gases on falling ice particles rather on droplets, unless stated otherwise.

2002; Guilyardi et al., 2009) that would otherwise influence the results (see also Section 7.1).

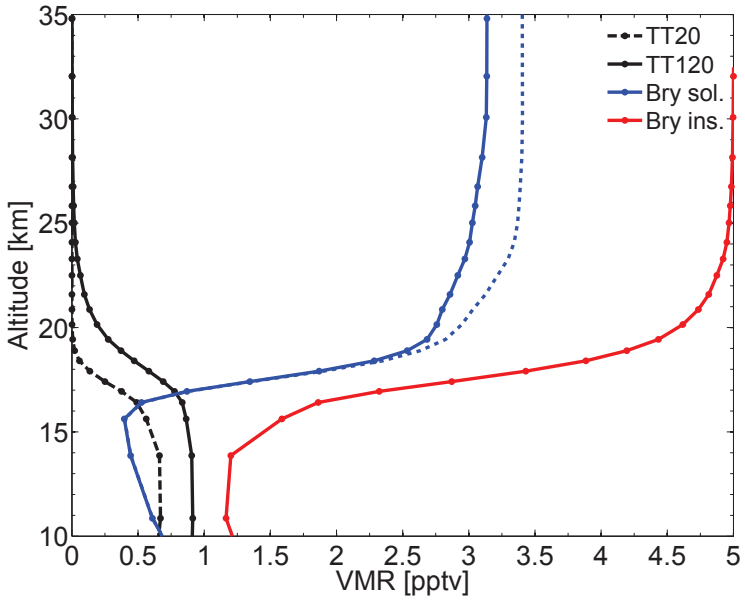

Figure 6.1.: Averaged tropical profiles of TT20, TT120 and soluble and insoluble Br_y (Br_y^{sol}, Br_y^{ins}) for 2006 from run ID1. The dotted blue profile marks Br_y^{sol} obtained from sensitivity run ID2 where washout of Br_y is restricted to within 40°N to 40°S. Adapted from Aschmann et al. (2011).

6.1.1. Idealized Setup

Figure 6.1 shows averaged tropical profiles for 2006 of bromine source and product gases of run ID1 illustrating typical distributions. The suggested stratospheric bromine loading is in the range of 3.14 pptv for the totally soluble tracer Br_y^{sol} up to 5 pptv for the totally insoluble tracer Br_y^{ins}. Since both source gases, TT20 and TT120, detrain with 1 pptv each and produce upon their decay Br_y corresponding to their number of included bromine atoms[2], a maximum of 5 pptv of bromine is available from VSLS. This means that at least 62% of all Br_y^{VSLS} is not affected by scavenging. Considering the sources gases individually, TT20 and TT120 contribute about 1.58–3 pptv and 1.56–2 pptv to Br_y^{VSLS}, respectively. Clearly, TT20 is more affected by dehydration than TT120 due to its shorter lifetime.

The average amount of Br_y^{VSLS} entering the stratosphere by source or product gas injection (SGI and PGI, see Section 3.1.2) can be estimated from the distribution of source and product gases at 380 K, defined as the top of the TTL. Figure 6.2 shows that SGI is the major pathway for VSLS into the stratosphere: At 380 K, the mixing ratio of TT20 is roughly 0.37 pptv, which represents 1.11 pptv Br_y^{VSLS}. Likewise, TT120 has an average mixing ratio of about 0.77 pptv at the same altitude, being equal to 1.54 pptv Br_y^{VSLS}. Consequently, the impact of PGI for both VSLS ranges from 0.47–1.89 pptv for TT20 and 0.02–0.46 pptv for TT120. The SGI of bromine VSLS sums up to 2.65 pptv while the cumulative PGI is in the range of 0.49–2.35 pptv. These results agree well with the recent

[2] i.e. one unit of TT20 and TT120 yields three and two units of Br_y, respectively.

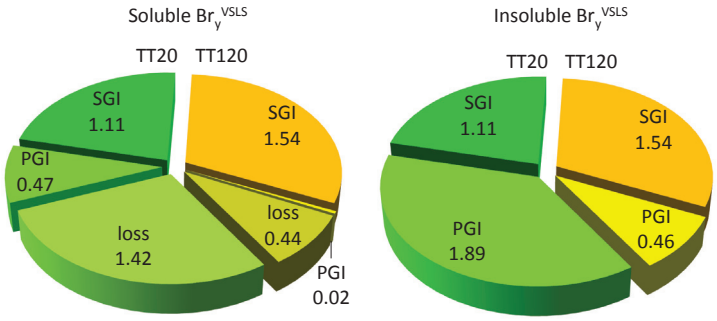

Figure 6.2.: Overview of average source (SGI) and product gas injection (PGI) of TT20 and TT120 in run ID1, in the case of a totally soluble (left) and insoluble Br_y tracer (right). The numbers represent the mixing ratios (pptv) of equivalent Br_y^{VSLS} with respect to TT20/TT120 (see text).

WMO report (Montzka and Reimann, 2010) which gives a range of 0.7–3.4 pptv for SGI and 0.4–4.2 pptv for PGI of bromine VSLS.

Furthermore, the magnitude of PGI varies with the amount of water vapor in the TTL, thus the distribution of Br_y^{sol} shows a clear tape recorder signal (Figure 6.3). Br_y^{sol} in the TTL peaks during boreal summer and undergoes a minimum in boreal winter, the mixing ratio at 380 K/17 km ranging from about 0.8 to 1.8 pptv. Further above the abundance of Br_y^{sol} increases with altitude to typical values of 2.8 to 3.2 pptv depending on the tape recorder phase. In general these phases remain discernible up to 30–35 km altitude. A detailed analysis of interannual variations of dehydration and its impact on stratospheric bromine loading is given in Section 7.1.

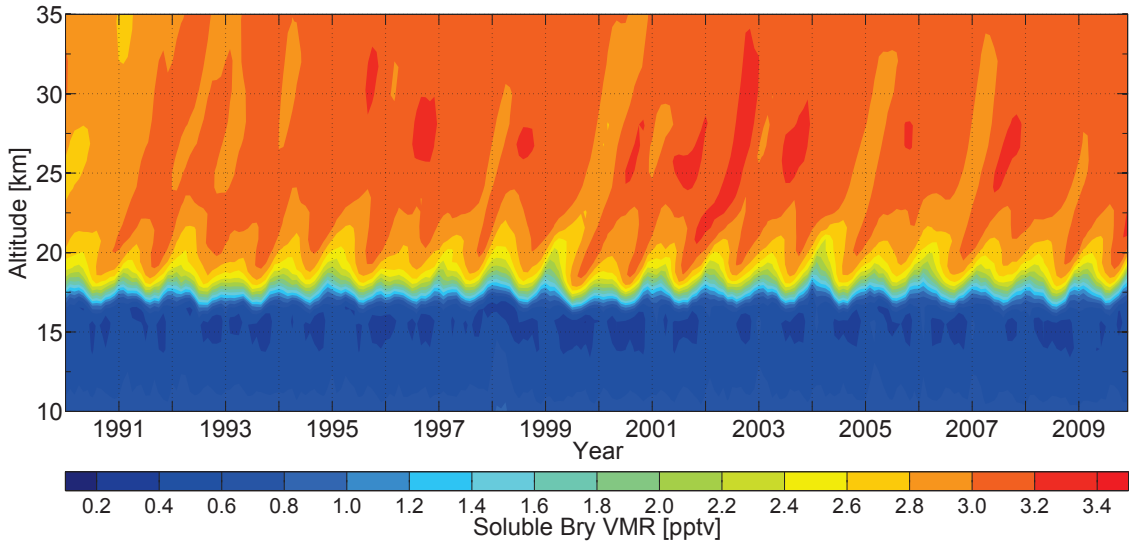

Figure 6.3.: Distribution of tropical Br_y^{sol} from run ID1 over time. Adapted from Aschmann et al. (2009).

Another aspect that influences the stratospheric bromine loading due to VSLS is the assumption regarding the partitioning of Br_y. In the idealized setup, Br_y is either considered totally soluble or insoluble throughout the atmosphere. In comparison, Figure 6.4 shows the percentage of HBr to the total amount of Br_y for the full chemistry run FC1. The fraction of soluble inorganic bromine is large only at the base of the tropical tropopause and diminishes rapidly with increasing altitude and latitude which is supported by earlier studies (e.g., Lary, 1996; Sinnhuber et al., 2002; Yang et al., 2005). Since the Br_y^{sol} tracer is designed to be affected uniformly by dehydration this significantly overestimates the impact of washout especially near the South Pole which is shown in Figure 6.5: the left panel illustrates the drastic decrease of Br_y^{sol} in the southern polar region in standard run ID1, which influences also the tropical mixing ratios by meridional transport. The right panel shows the result of the sensitivity calculation ID2 where the scavenging of Br_y is restricted to within 40°N to 40°S. Switching off the scavenging process at higher latitudes increases the lower limit of the contribution of VSLS from 3.14 to 3.4 pptv (dotted profile in Figure 6.1).

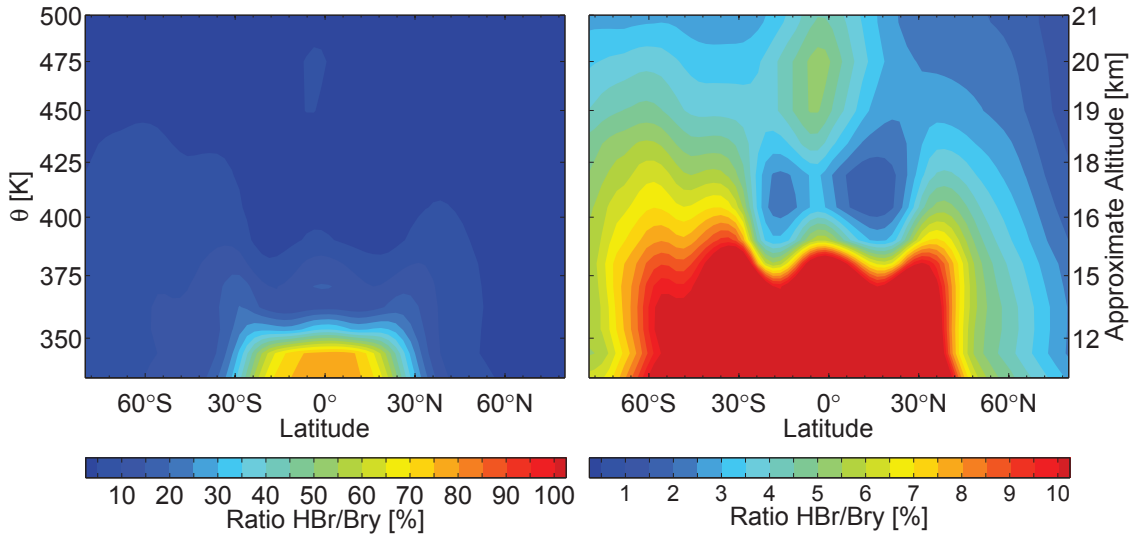

Figure 6.4.: Averaged ratio of HBr to Br_y for 2006 obtained from run FC1. The left panel covers the range from 0–100% whereas the right panel shows the detailed structures in the range from 0–10%.

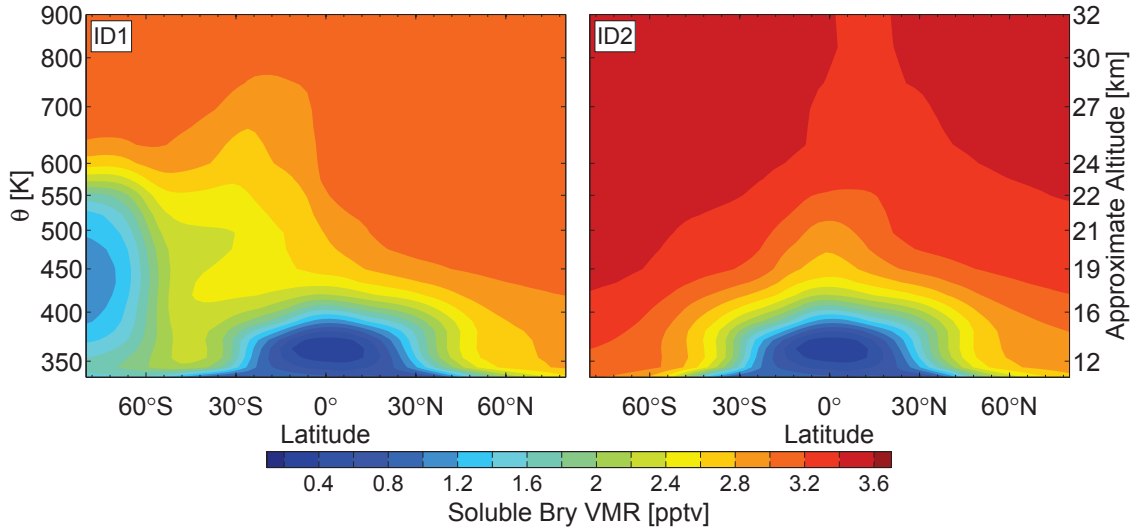

Figure 6.5.: Annual mean distribution of Br_y^{sol} in 2006 for standard run ID1 (left) and sensitivity run ID2 (right) where washout of Br_y is restricted to within 40°N to 40°S.

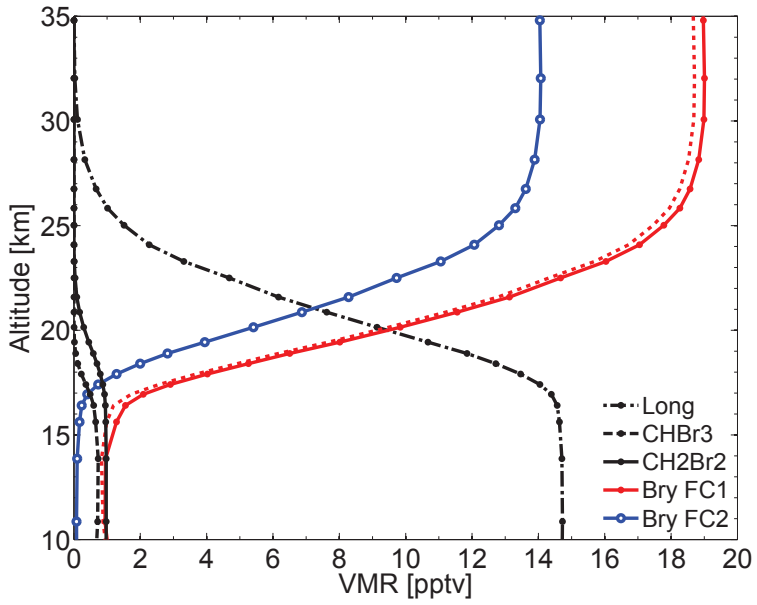

Figure 6.6.: Averaged tropical profiles of long (CH_3Br, Halon-1211, Halon-1301) and short-lived bromine source gases ($CHBr_3$, CH_2Br_2) and the inorganic bromine product gases Br_y (Br, BrO, HBr, HOBr, $BrONO_2$, BrCl), for 2006 of run FC1. The blue Br_y profile denotes the reference run FC2 which does not contain VSLS. The red dotted Br_y profile is derived from the sensitivity calculation FC3 where VSLS are included but the heterogeneous activation reactions (see Table 4.5) are switched off. Adapted from Aschmann et al. (2011).

6.1.2. Full Chemistry Setup

The full chemistry setup incorporates long-lived source gases that define the background concentration of bromine in the stratosphere. Moreover, emissions of the long-lived source gases are changing over time (Section 4.3.5) which makes the assessment of the impact of VSLS on stratospheric bromine loading more complicated. To identify this background the reference run FC2 was conducted which does not include bromine VSLS but is identical to the standard run FC1 otherwise.

Figure 6.6 shows the averaged tropical profiles of bromine source and product gases in 2006 for the full chemistry runs. During 2006, the average detrainment mixing ratio of long-lived source gases (CH_3Br, $CClBrF_2$, $CBrF_3$) is about 14.81 pptv (see Figure 3.1). At the top of the tropopause (380 K), the mixing ratio of these source gases is 14.39 pptv in comparison to 0.4 pptv of Br_y^{Long}, derived from the reference run FC2. This means the loss of Br_y^{Long} due to scavenging is negligible with 0.02 pptv (0.018 pptv not rounded) as the long-lived source gases are primarily photolyzed above altitudes where dehydration is important (e.g., Sander et al., 2006; Hossaini et al., 2010). Consequently, about 14.79 pptv of bromine originated from long-lived species enters the stratosphere in this particular year. However, as shown in Figure 6.6, the mixing ratio of Br_y in the stratosphere peaks at about 14.07 at 32 km altitude (run FC2) and decreases slowly with increasing height to about 13.75 pptv at 53 km. This effect is caused by the variable "emission" (to be precise: the changing detrainment mixing ratio) of the long-lived bromine species. The relatively slow transport in the stratosphere compared to the troposphere introduces a time lag in the mixing ratio of Br_y, i.e. some parts of the stratosphere still contain older air parcels with less inorganic bromine which reduces the overall mixing ratios of these species. Note that this effect is likely to be exaggerated by the slow stratospheric circulation in the model as described in Section 5.6.

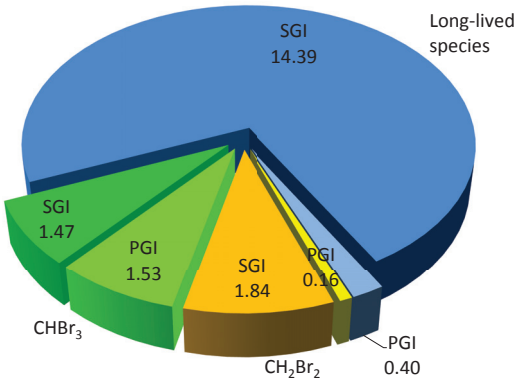

Figure 6.7.: Overview of average source (SGI) and product gas injection (PGI) of bromine long and short-lived source gases in run FC1. The numbers represent the mixing ratios (pptv) of equivalent Br_y. Note that the fraction of Br_y lost to dehydration (combined for all source gases about 0.02 pptv) is omitted here to maintain readability.

In run FC1 the mixing ratio of the additional VSLS is 0.49 pptv and 0.92 pptv at 380 K for $CHBr_3$ and CH_2Br_2, respectively, which equals 1.47 pptv and 1.84 of Br_y^{VSLS} (see Section 6.1.1). Both species detrain with a mixing ratio of 1 pptv, each. The amount of inorganic bromine at 380 K is 2.09 pptv. Considering that 0.4 pptv of Br_y is originated

from long-lived source gases (see above), 1.69 pptv are produced by VSLS. The sum of these individual values gives 5 pptv of additional bromine (4.998 pptv not rounded) from VSLS, which is practically the entire amount of VSLS detrained in the model. Apparently the effect of dehydration and scavenging on stratospheric bromine loading is negligible in the full chemistry setup. This leads to a total bromine loading of about 19.79 pptv for 2006, however, the stratospheric values of Br_y are generally lower, around 19 pptv, due to mixing with older air masses as described in the previous paragraph.

Figure 6.7 gives an overview of SGI and PGI of bromine source gases in run FC1. Obviously SGI dominates for the long-lived species, but also for the VSLS the relative importance of SGI is important, accounting for 49% and 92% of Br_y^{VSLS} regarding $CHBr_3$ and CH_2Br_2, respectively. Compared to the idealized setup the values for SGI are higher, 1.47 pptv to 1.11 pptv for $CHBr_3$ and 1.84 to 1.54 pptv for CH_2Br_2, reflecting the longer local photochemical lifetimes of VSLS in the TTL in the full chemistry approach (Figure 3.3). The cumulative values for SGI and PGI for short-lived substances are 3.31 pptv and 1.69 pptv, respectively; well in range of the estimate of the WMO report (SGI: 0.7–3.4 pptv, PGI: 0.4–4.2 pptv, Montzka and Reimann, 2010).

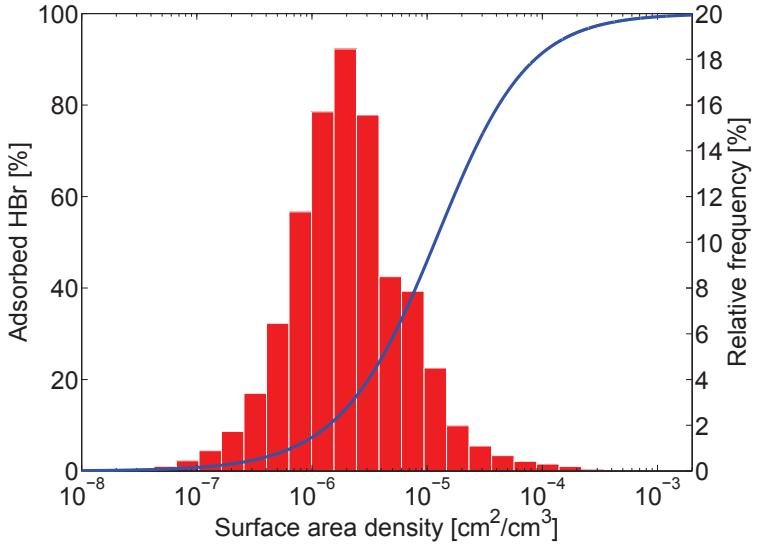

Figure 6.8.: Relation between available ice particle surface area density in a model grid box and the resulting fraction of adsorbed HBr on ice to total HBr derived from Equation 4.9 (blue line, left ordinate). The red bars indicate the relative frequency of occurrence of surface area density values in the tropical tropopause (20°N to 20°S, 330 K to 380 K) for 2006 of run FC1 (right ordinate). The fraction of adsorbed HBr is lower than 46% in 95% of all calculated surface area densities. Adapted from Aschmann et al. (2011).

The presented results suggest that dehydration has apparently no significant effect on stratospheric bromine loading, in contrast to the findings of previous studies (e.g., Dvortsov et al., 1999; Warwick et al., 2006; Sinnhuber and Folkins, 2006; Hossaini et al., 2010). This has several reasons. First, the mixing ratio of HBr in the transient altitude range between the level of zero radiative heating and the cold point is relatively small (about 0.15 pptv), the average fraction of HBr to Br_y below 5% (Figure 6.4). Consequently, the majority of inorganic bromine at this altitude is actually insoluble with respect to ice which is the

most important particle surface in the TTL in the model (see below). Note that it is assumed here that only HBr is adsorbed on ice. The SLIMCAT chemistry scheme includes heterogeneous reactions for HOBr and $BrONO_2$ on ice surfaces as well (Table 4.5), however, as it is currently not clear how and to what extent HOBr and $BrONO_2$ are adsorbed on ice (Crowley et al., 2010), the uptake of these species is not explicitly modeled in contrast to HBr. The partitioning between HBr and Br_y in the chemistry scheme is controlled mainly by the gas phase reactions in Table 4.4 , the heterogeneous reactions in Table 4.5 and the uptake and sedimentation on ice.

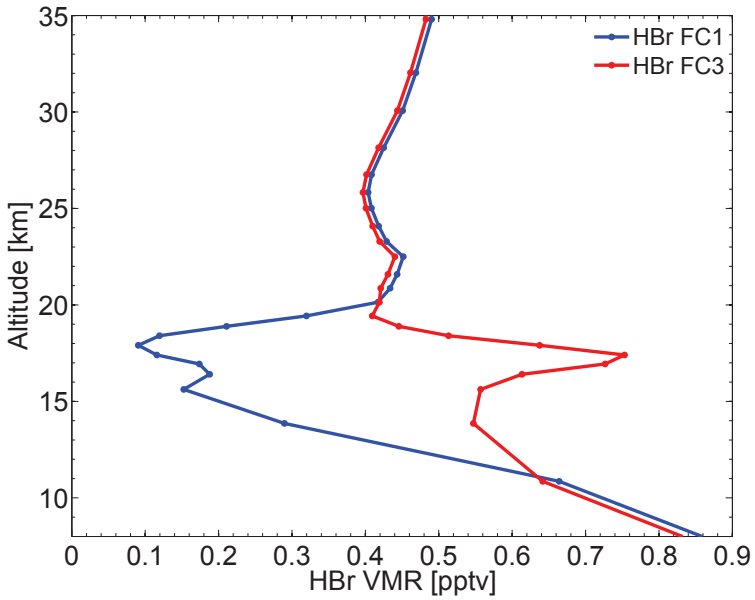

Figure 6.9.: Tropical profiles of HBr from the standard full chemistry run FC1 (blue) and the sensitivity calculation FC3 without heterogeneous activation (red) for 2006. Adapted from Aschmann et al. (2011).

Furthermore, the fraction of adsorbed HBr on ice is relatively small as well. Figure 6.8 shows the relation of available ice particle surface area density and the resulting fraction of adsorbed HBr to total HBr according to Equation 4.9 and the relative frequency of occurrence of surface area density values in the tropical tropopause region for 2006: in 95% of all model grid boxes where ice forms the percentage of HBr on ice is significantly lower than 46%, thus limiting the possible impact of scavenging directly.

In addition, a major part of HBr on ice undergoes heterogeneous activation that releases reactive bromine back into gas phase, supporting the assumption of Fitzenberger et al. (2000). To investigate this effect the sensitivity run FC3 was conducted, being identical to standard run FC1 but without the heterogeneous reactions for HBr on all particle surfaces as listed in Table 4.5. Figure 6.9 presents tropical HBr profiles for both runs. In the standard setup, the mixing ratio of HBr drops rapidly between 15 and 17 km altitude; a distinctive feature that is also discernible in the zonal cross section in Figure 6.4. The heterogeneous chemistry effectively depletes adsorbed HBr and releases bromine into gas phase. In contrast, the mixing ratio of HBr in the UTLS is up to four times higher in the sensitivity calculation without heterogeneous activation. Here, the partitioning of Br_y is shifted towards HBr which in turn leads to increased loss of bromine due to scavenging; the resulting profile for Br_y (Figure 6.6) is about 0.36 pptv lower than in the standard run.

Consequently, 4.64 out of 5 pptv of bromine originating from VSLS are able to enter the stratosphere when heterogeneous activation is ignored. An additional sensitivity calculation shows that 96% of the observed effect can be attributed to heterogeneous reactions on ice particles, in comparison to 3% and 1% for heterogeneous reactions on liquid aerosol and NAT particles, respectively. This supports the assumption that ice particles are the most important surface for heterogeneous chemistry in the TTL.

Finally, adsorbed HBr is not washed out instantaneously but sediments slowly downwards, i.e. it is possible that a significant part evaporates again and eventually reaches the stratosphere. This effect explains the local maximum of HBr at around 17 km in run FC3 (Figure 6.9): repeated sedimentation, evaporation and eventual ascent accumulates the available HBr in a small vertical range. In fact the model likely overestimates the impact of sedimentation in assuming a fixed fall velocity based on an average particle radius of 10 µm. According to Figure 6.8 most ice particles are actually smaller (about 0.5 to 2 µm).

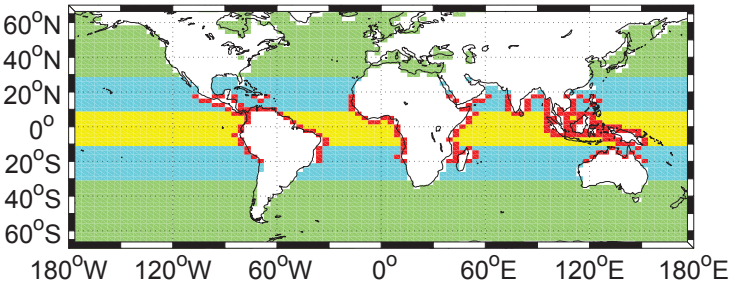

Figure 6.10.: VSLS emission scenario for run ID3 adapted from Warwick et al. (2006); Liang et al. (2010): the detrainment mixing ratio of TT20 is 1 pptv in latitudes above 30°N/S (green area), 0.7 pptv between 10°–30°N/S (cyan), 1.5 pptv between 10°N–10°S (yellow) and 2 pptv on the coastlines between 20°N–20°S (red). The values for TT120 in the same areas are 1.1, 0.9, 1.1 and 1.3 pptv, respectively. There is no detrainment of VSLS over land (white areas).

6.2. Spatial Distribution of VSLS Sources

Strength and spatial distribution of the sources of bromine VSLS remain uncertain to this day. The available measurements of these species are scarce and show large spatial and seasonal variations (e.g., Carpenter and Liss, 2000; Quack and Wallace, 2003; Yokouchi et al., 2005; Quack et al., 2007a; Butler et al., 2007). Effort has been invested into source parametrizations that incorporate the available observational data (e.g., Palmer and Reason, 2009) or correlate the abundance of VSLS to specific phytoplankton functional groups (e.g., Quack et al., 2007b), but the resulting climatologies still contain significant deficiencies. Recently, several top-down estimates of $CHBr_3$ and CH_2Br_2 emission have been used to assess the impact of VSLS (e.g., Warwick et al., 2006; Kerkweg et al., 2008; Liang et al., 2010). In general, these scenarios suggest that a major part of the emissions occur in the tropical ocean, especially in coastal areas (Table 3.2).

To study the impact of a more detailed VSLS emission/detrainment scenario on stratospheric bromine loading the sensitivity run ID3 was conducted. Generally, it uses the idealized setup of standard run ID1 and the restriction of Br_y^{sol} washout to within 40°N to 40°S of run ID2. However, the detrainment mixing ratios for TT20 and TT120 (the

idealized tracers representing bromoform and dibromomethane) are spatially varied as depicted in Figure 6.10, based loosely on the emission scenarios of Warwick et al. (2006) and Liang et al. (2010). The detrainment mixing ratios are especially high in a zonal band between 10°N to 10°S and on the tropical coast lines whereas detrainment of VSLS over land is ignored in this scenario (d_c is zero for both species). The average tropical detrainment mixing ratio for TT20 and TT120 is 0.96 pptv and 0.81 pptv, respectively.

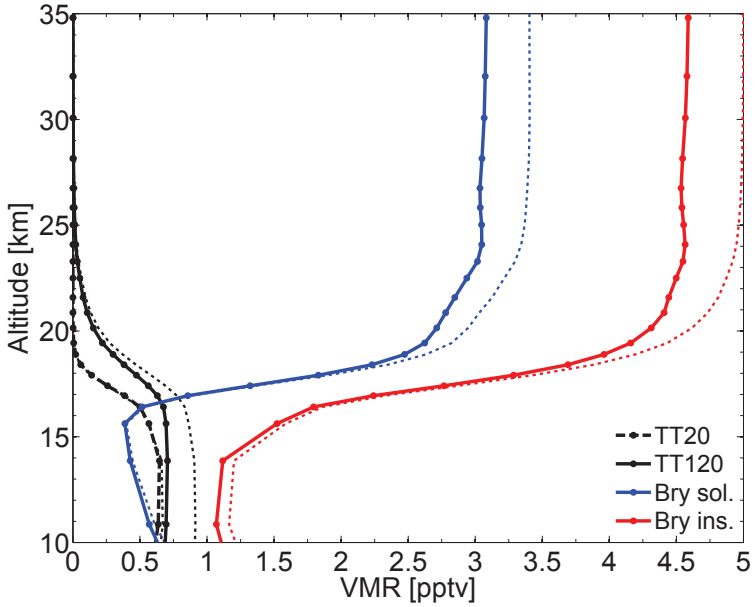

Figure 6.11.: Averaged tropical profiles of TT20, TT120 and soluble and insoluble Br_y (Br_y^{sol}, Br_y^{ins}) for 2006 from run ID3. This run is identical to ID2 except for the detrainment mixing ratio distribution of TT20 and TT120 (see Figure 6.10). In comparison, the dotted lines denote the tracer profiles obtained from ID2.

Figure 6.11 presents a comparison of bromine source and product gases in the TTL for runs ID3 and ID2. The main difference is located in the TT120 profile of run ID3, which is approximately 0.2 pptv lower than its counterpart of ID2 in the TTL region. This value matches the difference of average tropical detrainment mixing ratio of TT120 in run ID3 (0.81 pptv) to the assumed uniform value of 1 pptv in run ID2. Furthermore, taking into account the difference of the detrainment mixing ratios of TT20 (0.96 pptv vs. 1 pptv for ID3 and ID2, respectively) one would expect that the stratospheric Br_y^{ins} abundance in run ID3 is about 0.5 pptv lower than in ID2. In fact, the Br_y^{ins} profile of run ID3 reaches about 4.55 pptv in the stratosphere, i.e. the difference is only slightly smaller (5 pptv for run ID2). Naturally, the difference of the Br_y^{sol} profiles is shifted to lower values (3.08 pptv to 3.4 pptv for ID3 and ID2, respectively), since the impact of the different detrainment mixing ratios is reduced by the loss of inorganic bromine due to scavenging. Apparently the amount of stratospheric bromine is predominantly sensitive to the averaged tropical emission of VSLS[3], while the spatial distribution of the sources plays a minor role only. This confirms the findings of Schofield et al. (2011) who come to a similar conclusion using a trajectory model with different emission scenarios.

In contrast to the averaged tropical mixing ratios of VSLS and Br_y, the local abundance

[3]To be precise, the detrainment mixing ratio of VSLS.

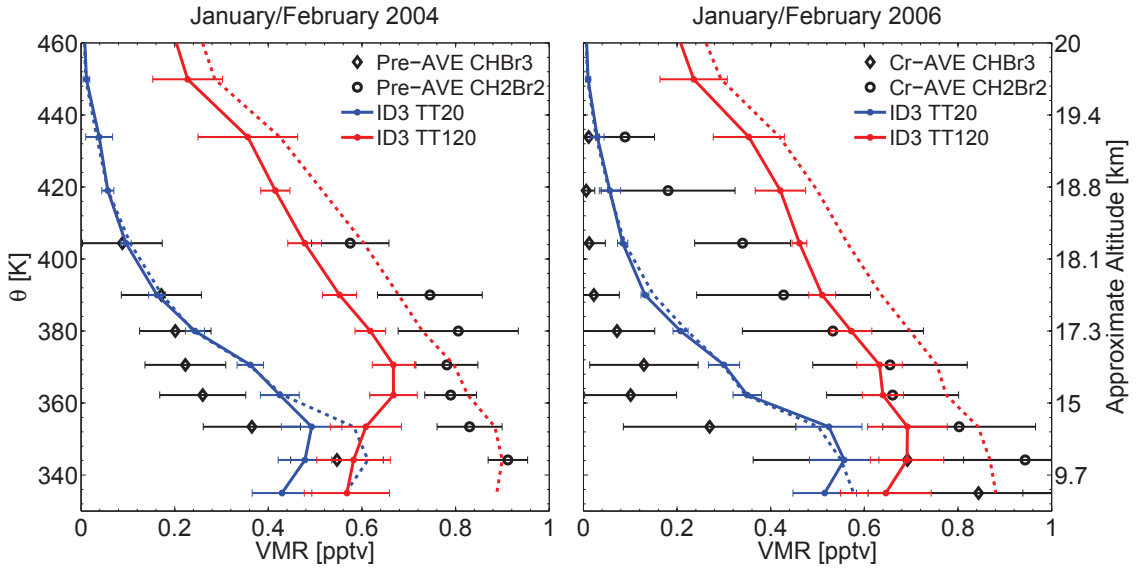

Figure 6.12.: Comparison of TT20 and TT120 with aircraft measurements of $CHBr_3$ and CH_2Br_2 from Pre-AVE (left) and Cr-AVE (right) campaign like in Figure 5.6 but for run ID3. For comparison, the dashed lines denote the corresponding profiles for run ID1.

of source gases is more affected by the utilized detrainment scenario. Figure 6.12 shows the profiles of TT20/TT120 in comparison with aircraft measurements of bromoform and dibromomethane similar to Figure 5.6 and the profiles from run ID1. Both VSLS show generally lower values in the sensitivity run, with the most distinctive difference located at the base of the tropopause (10–15 km). According to transport efficiency analysis presented in Section 6.3, approximately 40% of the air in this region and altitude is detrained above the American continent (Figure 6.15). Since the detrainment mixing ratio of both VSLS is zero above land in run ID3, the abundance of bromine source gases is significantly reduced in the vertical region where continental air masses dominate. At higher altitudes, the impact of continental detrainment decreases thus the differences between the profiles of run ID1 and ID3 nearly diminish in the case of TT20, and approach an approximately constant offset in the case of TT120, introduced by the difference between the averaged tropical detrainment rates in both runs.

In general, the agreement with the observational data does not improve in run ID3, especially the reduction of source gases below 15 km is not supported by the measurements. This highlights the importance of continental detrainment for the bromine abundance in the troposphere and lower tropopause. Although the major source of bromine VSLS is assumed to be in the ocean (see above), it is likely that a significant amount of source gases is transported landward in the boundary layer which cannot be explicitly calculated in the model. At higher altitudes the impact of continental detrainment diminishes, as the profiles of both VSLS are becoming mainly dependent on the average tropical detrainment mixing ratio, which is especially distinctive for the shorter-lived TT20.

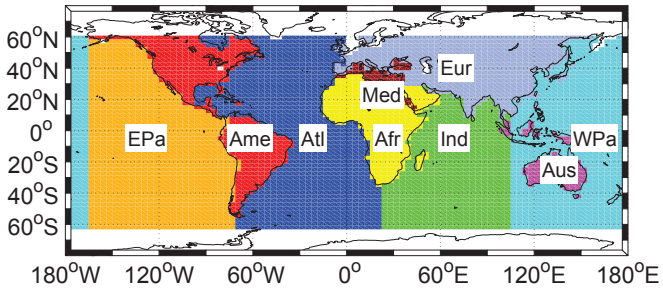

Figure 6.13.: Map of the nine different source regions in run ID4. The regions are from left to right: Eastern Pacific (EPa), America (Ame), Atlantic (Atl), Mediterranean plus Black and Red Sea (Med), Africa plus Arabian Peninsula (Afr), Eurasia (Eur), Indian Ocean (Ind), Australia plus Maritime Continent (Aus), Western Pacific (WPa). Adapted from Aschmann et al. (2009).

6.3. Transport Efficiency of Individual Source Regions

Deep convection in the TTL generally tends to concentrate along the ITCZ, however, the strength of convective activity is not evenly distributed across the tropics but forms local hot spots (e.g., Gettelman et al., 2002b; Liu and Zipser, 2005; Berthet et al., 2007, see also Section 5.1). This has large impact on the transport of VSLS into the TTL since the injection of short-lived species is directly related to the convective activity in the particular region.

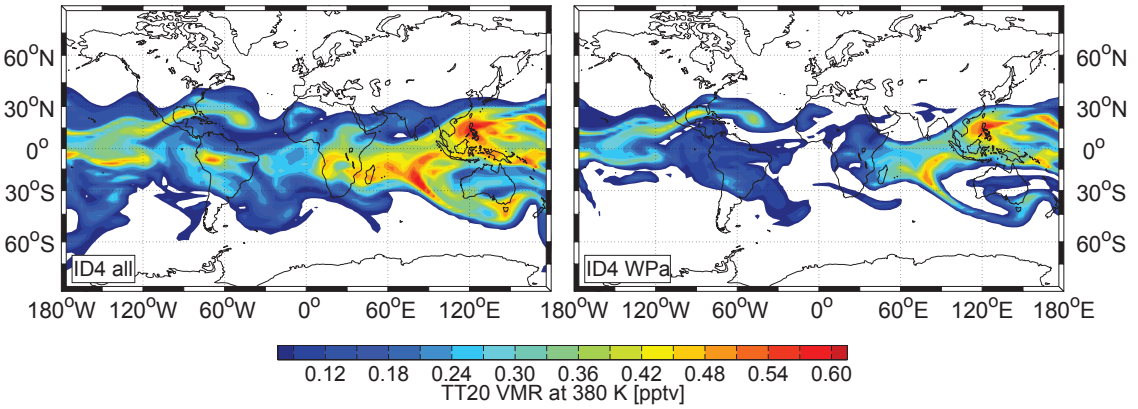

Figure 6.14.: Snapshot of the TT20 distribution of run ID4 at 380 K (about 17 km) on February 16, 2004. The left panel shows the sum of all individual TT20 tracers (corresponds to left panel of Figure 5.4) whereas the right panel shows the Western Pacific tracer, only.

To investigate the differences in the transport efficiency of individual regions with respect to VSLS the run ID4 was conducted[4]. As shown in Figure 6.13, it comprises nine different source areas which roughly resemble Earth's oceans and land masses. Each region is associated with a group of four tracers, which corresponds to the standard idealized setup

[4]This section is based mainly on the work presented in Aschmann et al. (2009).

(Section 4.2): two source gases (TT20 and TT120) and the product gas tracer in a soluble and insoluble variant (Br_y^{sol}, Br_y^{ins}). The detrainment mixing ratio of both VSLS is 1 pptv in the particular region and zero outside. Note that by design this approach can only reveal the differences of the transport efficiency in the individual regions. As indicated before (Section 6.2), it is likely that there will be large differences in the source strengths of VSLS among the investigated regions (see also Butler et al., 2007). These differences are completely ignored in this approach by assuming an identical detrainment mixing ratio for each source region.

Figure 6.14 clearly illustrates the importance of horizontal transport even for tracers with a lifetime of only a few days: the left panel shows an arbitrary snapshot of the combined TT20 distribution of all sources regions at 380 K, being practically identical to the corresponding figure for run ID1 (Figure 5.4, left panel). In contrast, the right panel shows the TT20 distribution for the Western Pacific source region, only, i.e. the amount of TT20 at the top of the tropopause that was originally detrained above this region. Naturally, the highest concentrations are located above the emission region but there are also significant mixing ratios thousands of kilometers away above Central America and the Atlantic. Furthermore, a large fraction of total TT20 in the TTL is apparently originated from the Western Pacific, which will be investigated more quantitatively below.

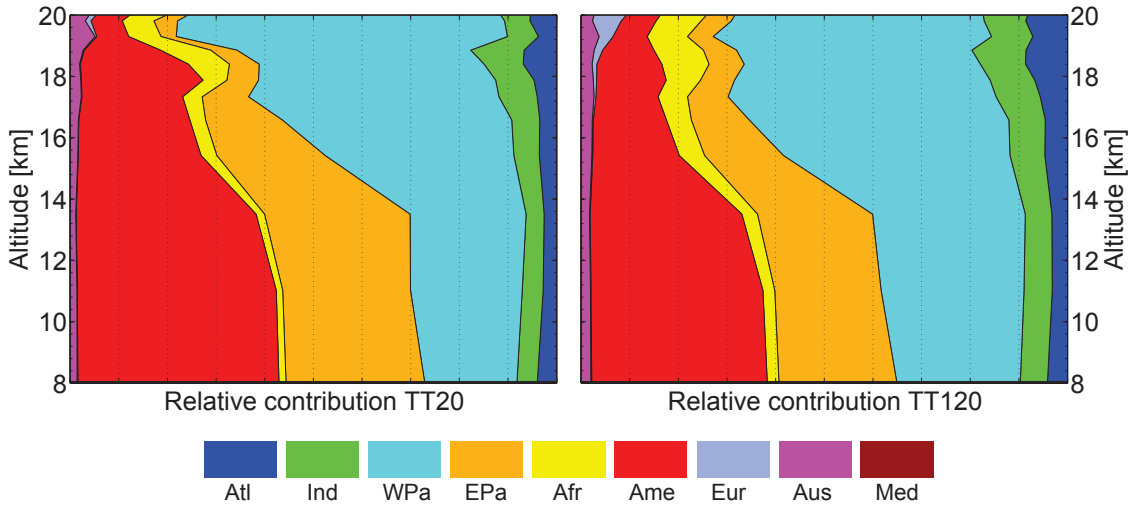

Figure 6.15.: Relative contribution of individual source regions to the total amount of TT20 (left) and TT120 (right) in January/February 2004 above 80–90°W, 20°N–3°S (area of the Pre-AVE campaign, see Figure 5.5), obtained from run ID4. Each tick mark on the abscissa represents 10% relative contribution. Adapted from Aschmann et al. (2009).

Considering these facts it is interesting to return again to the Pre-AVE measurements above Central America conducted in early 2004 as discussed in Section 5.2. It was already shown, that the model is generally able to reproduce the observed profiles of bromoform and dibromomethane in this particular region (Figure 5.6). With the individual source tracers of run ID4 it is possible to investigate the relative contribution of the different regions to these profiles. Figure 6.15 shows the contribution of the different source regions to the total amount of TT20/TT120 in the before mentioned Pre-AVE area, plotted against height. At lower altitudes mainly three regions contribute to the amount of TT20/TT120,

America, East and West Pacific. However, at the top of the tropopause the Western Pacific clearly dominates all other regions, contributing up to 67% and 51% of TT20 and TT120, respectively. Consequently, a major part of the VSLS measured above Central America during the Pre-AVE campaign was likely originated from the Western Pacific.

As generalization, Figure 6.16 shows the averaged relative contribution of the individual source regions to TT20/TT120 in the whole tropics. The picture is similar to the local example presented above: at lower altitudes the relative contribution is roughly equal for most of the source regions whereas at the top of the TTL the Western Pacific is clearly identified as the most important area which contributes about 52% to the total TT20 abundance. As expected, the effect is slightly smaller for TT120 (47%) due to its longer lifetime which reduces the impact of individual source regions. Apparently, the Western Pacific and the Maritime Continent are the main regions where substantial high-reaching (i.e. above the level of zero radiative heating) convection occurs. The combined contribution of all oceanic source regions peaks around 75% at the top of the tropopause for both VSLS. Thus oceanic regions, in particular the Western Pacific, represent the most important transport pathway into the stratosphere, in agreement with earlier studies (e.g., Gettelman et al., 2002b; Notholt et al., 2005; Liu and Zipser, 2005; Brioude et al., 2010; Pisso et al., 2010). An interesting feature is the increase of relative contribution of the continental source regions (Africa, America, Eurasia, Australia) at the top of the TTL. Although the effect is small and the absolute abundance of VSLS, especially of TT20, is very low above 18 km, this might indicate that the rare occurrences of very high-reaching convection are predominantly found over land, as stated by Jorgensen and LeMone (1989).

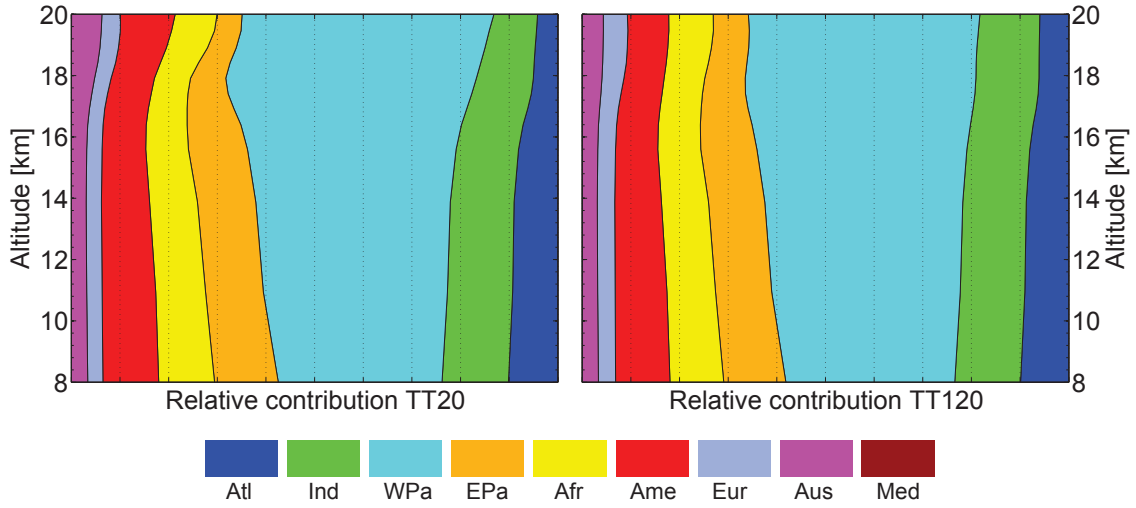

Figure 6.16.: Relative contribution of individual source regions to the total amount of TT20 (left) and TT120 (right) averaged over the tropics. Adapted from Aschmann et al. (2009) and reproduced for WMO 2011 report.

6.4. Discussion and Conclusion

This chapter investigates the impact of the VSLS bromoform and dibromomethane on stratospheric bromine loading with emphasis on the effect of dehydration (Section 6.1), the spatial distribution of VSLS sources (Section 6.2) and the regional transport efficiency

(Section 6.3).

The estimated contribution of these short-lived species to the stratospheric bromine loading is 3.14/3.4 to 5 pptv for the idealized setup (ID1/ID2) and 5 pptv for the full chemistry setup, assuming that both VSLS detrain with 1 pptv each. These values are in agreement with observations ranging from 3 pptv (Sinnhuber et al., 2005) to 5 and 5.2 pptv (McLinden et al., 2010; Dorf et al., 2008) to 8.4 pptv (Sioris et al., 2006). Compared to other modeling studies the estimations made in this study are rather at the higher end. Considering only bromoform, the estimated contributions to stratospheric bromine range from 0.8 to 1 pptv (Dvortsov et al., 1999; Nielsen and Douglass, 2001) to 0.5 to 3 pptv (Sinnhuber and Folkins, 2006). When taking both bromoform and dibromomethane into account recent studies suggest a contribution of 2.4 to 2.8 pptv (Hossaini et al., 2010; Gettelman et al., 2009) up to 4.8/5 pptv (Schofield et al., 2011; Liang et al., 2010). Warwick et al. (2006) suggest an even higher value of 6 to 7 pptv but considers five short-lived bromocarbons.

Table 6.1.: Overview of the contribution of VSLS to stratospheric bromine loading (SBL) and the impact of dehydration in different modeling studies. The columns give the average tropical mixing ratio of available bromine in the form of VSLS and the stratospheric bromine loading due to VSLS. The ratio of both values represents the loss of bromine due to dehydration. Adapted from Aschmann et al. (2011).

Study	Available VSLS [pptv]	SBL due to VSLS [pptv]	Loss due to dehydration
Hossaini et al. (2010)	6	2.4	60%
Schofield et al. (2011)	7.7	4.8	38%
Liang et al. (2010)	7	5	5/30%[a]
ID1	5	3.14	37%
ID2[b]	5	3.4	32%
FC1	5	>4.99	<0.2%
FC3[c]	5	4.64	7%

[a] 30% of Br_y from VSLS is lost in total. The fraction of Br_y lost above 500 hPa is 5%.
[b] Washout of Br_y^{sol} restricted to within 40°N/S.
[c] No heterogeneous activation reactions.

One key question is the impact of dehydration and scavenging on soluble inorganic bromine species. Depending on the representation of these processes in the model the estimated contribution of VSLS to bromine loading differs significantly. Table 6.1 gives an overview of the contributions of bromine VSLS to stratospheric bromine dependent on the applied dehydration mechanism in recent modeling studies together with the results from this study. Hossaini et al. (2010) assume a constant washout lifetime of 10 days for Br_y, resulting in a loss of 60% of bromine originated from VSLS. In the approach of Schofield et al. (2011), 85% of Br_y is removed at the cold point, resulting in a loss of 38% of bromine contributed by VSLS. The idealized setup, which uses a comparable simple approach for dehydration, suggests a loss of 32–37% of bromine produced by VSLS. In contrast to the simple dehydration mechanisms, Liang et al. (2010) use a detailed wet and dry deposition scheme to calculate the loss of Br_y. They state that 30% of Br_y produced by VSLS is removed by wet scavenging, however, 85% of this wet removal occurs below 500 hPa (5–6 km). Consequently, about 5% of Br_y produced by VSLS is scavenged above 500 hPa.

These findings are consistent with the results of the full chemistry setup, if heterogeneous activation is ignored (about 7% loss). Taking into account the heterogeneous chemistry lowers the loss of Br_y to almost zero thus rendering the influence of dehydration in the UTLS on bromine loading insignificant.

The impact of a spatially varied detrainment scenario for bromine VSLS on stratospheric bromine similar to those applied in, e.g., Warwick et al. (2006); Kerkweg et al. (2008); Liang et al. (2010); Schofield et al. (2011) is found to be rather small (Section 6.2). The abundance of VSLS is sensitive to differences in the detrainment mixing ratio mainly in the troposphere and lower tropopause; further above the source gas profiles are predominantly dependent on the average tropical detrainment mixing ratio. Consequently, the impact of the detrainment scenario on inorganic bromine at the top of the TTL is also only minor, which is in agreement with Schofield et al. (2011) who come to a similar conclusion using a trajectory model with different emission scenarios.

Finally, the transport efficiency of different regions regarding VSLS is investigated in Section 6.3. The Western Pacific is clearly identified as the most important source region for VSLS transport, contributing up to about 50% of TT20/TT120 at the top of the TTL under the assumption of a uniform detrainment mixing ratio. This confirms the findings of earlier studies (e.g., Gettelman et al., 2002b; Liu and Zipser, 2005; Brioude et al., 2010; Pisso et al., 2010) that the Western Pacific and the Maritime Continent are the most important pathways into the TTL and eventually the stratosphere, especially for short-lived substances.

7. Long-term Variability of Stratospheric Bromine

The estimations of stratospheric bromine loading due to VSLS given in the previous chapter represent a snapshot of a specific point in time. However, as indicated before (e.g., tape recorder signal of inorganic bromine, Figure 6.3), the amount of bromine in the UTLS undergoes distinctive cycles as the major controlling mechanisms, convective activity, dehydration and advection are not in a static equilibrium. Therefore, this chapter focuses on the interannual variability of stratospheric bromine loading and the involved processes. Section 7.1 presents tropical averaged timeseries of the most important variables that control the amount of Br_y^{VSLS} in the TTL. The temporal development of modeled stratospheric bromine is compared to satellite observations in Section 7.2. Finally, Section 7.3 presents two extraordinary distinctive ENSO seasons that are investigated to explore the impact of a strong perturbation in convective transport on stratospheric bromine in detail.

7.1. Variations of VSLS Injection into the Stratosphere

The balance between the processes controlling bromine loading is not static but rather varies significantly with ambient meteorological conditions[1]. To illustrate the connection between the most important variables the following sections present timeseries of tropical ECMWF ERA-Interim sea surface temperature (SST) and detrainment rate d_c, bromine short-lived source gases, inorganic bromine product gases and total bromine abundance (i.e. the sum of source and product gases) and the corresponding monthly anomalies from 1990 to 2009 (1989 was discarded to reduce spin-up effects) for run ID1 and FC1. The values for d_c are averages over the altitude range being most relevant for bromine in the UTLS: from the level of zero clear sky radiative heating at approximately 350 K (15.5 km), which marks the transition from large-scale subsidence to large-scale upwelling (e.g., Corti et al., 2005; Sinnhuber and Folkins, 2006), to the cold point at about 380 K (17 km) where major parts of tropopause air get effectively dehydrated (e.g., Gettelman et al., 2002a; Fueglistaler et al., 2005). The cold point is also commonly regarded as a likely upper altitude limit for deep convection (e.g., Dessler, 2002; Fueglistaler et al., 2009a). For the tracer timeseries 380 K is picked for the same reasons: almost all detrainment and dehydration (in the tropics, Figure 5.10) occurs below this level so tracers at this altitude are likely to enter the stratosphere with their current mixing ratio at 380 K.

7.1.1. Idealized Setup

Firstly, Figure 7.1 illustrates the relation between sea surface temperature and convective activity in the ECMWF ERA-Interim reanalysis: as expected, higher SSTs lead in general to intensified convection denoted by higher values of d_c (correlation coefficient between the two timeseries is $r = 0.53$) which is in line with real world observations (e.g., Ramanathan and Collins, 1991). Secondly, the calculations show clearly a tight coupling of bromine

[1]This section is based mainly on the work presented in Aschmann et al. (2011).

source gas abundance in the UTLS and detrainment rate ($r = 0.69$ for d_c/TT20 and d_c/TT120). Quantitatively, this affects mostly the short-lived species TT20, for example its mixing ratio at 380 K increases by about 20% during the exceptional strong El Niño event 1997/98. For TT120 the magnitude of this effect is smaller (e.g., about 6% during 1997/98) due to its relatively long lifetime.

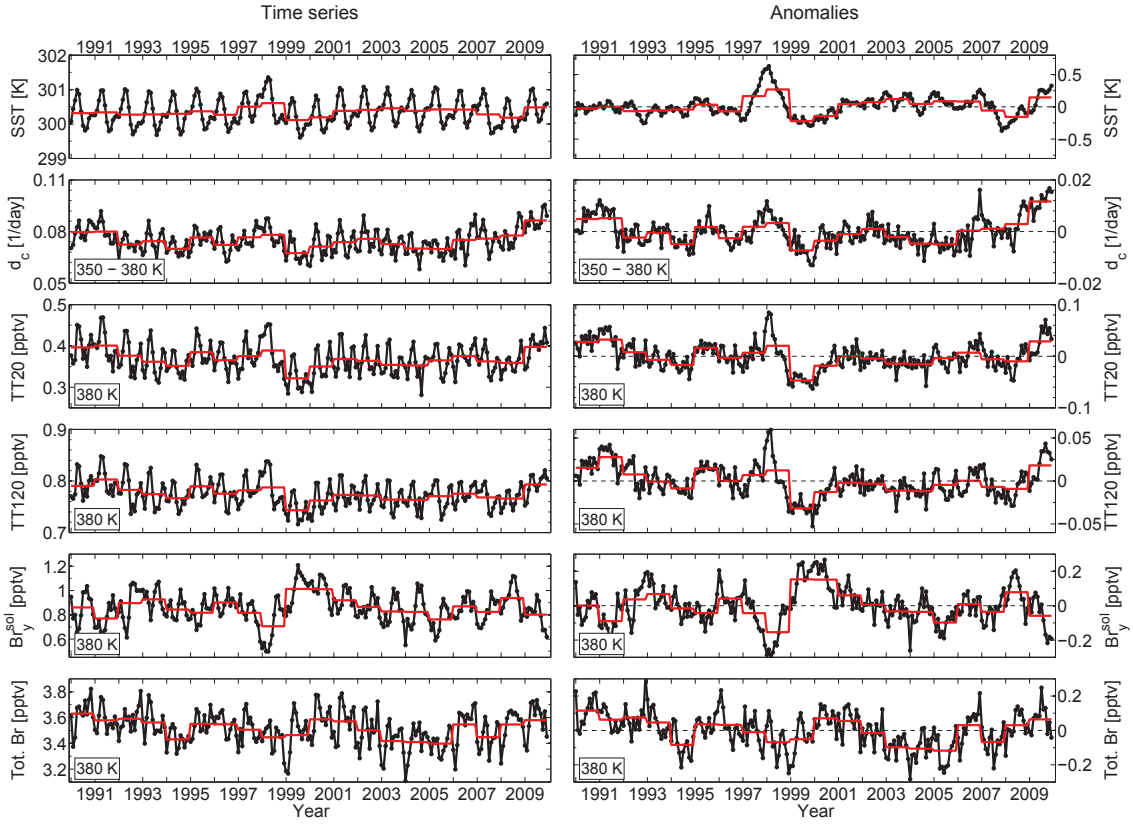

Figure 7.1.: Monthly timeseries of tropical sea surface temperature SST, detrainment rate d_c, the VSLS TT20 and TT120, $\mathrm{Br_y^{sol}}$ and total bromine (left panels) and the corresponding anomalies (right panels) from 1990 to 2009 obtained from run ID1. The values represent the top of the TTL (380 K, about 17 km) for the tracers or the average of the range between the level of zero radiative heating and the cold point (350–380 K) for d_c. The red lines denote the corresponding yearly average. Adapted from Aschmann et al. (2011).

However, for the product gas $\mathrm{Br_y}$ the situation is more complex. The insoluble variant (not shown here) has no sink in the model (Section 4.2.1) but is diluted by detraining air ($[\mathrm{Br_y}]_c = 0$ pptv), leading to a robust anti-correlation to the detrainment rate ($r = -0.70$). Since the insoluble $\mathrm{Br_y}$ tracer is inert and all bromine VSLS eventually end up as $\mathrm{Br_y}$, the mixing ratio of total bromine converges to a fixed value, in the case of the applied setup 5 pptv. That means variations in convective activity cannot alter the amount of total bromine once it reaches its equilibrium value of 5 pptv. In contrast, the soluble $\mathrm{Br_y}$ tracer is subject to washout as described in Section 4.2.1, which introduces an additional process that disrupts the anti-correlation to d_c ($r = -0.40$ for $\mathrm{Br_y^{sol}}/d_c$). Consequently, total bromine abundance cannot reach equilibrium but varies with the amount of source gases and the scavenging efficiency. This process is due to the model's treatment of dehydration

mainly controlled by relative humidity in the UTLS region, i.e. local water vapor content and temperature. Which process dominates depends on the ambient conditions. Actually there is a weak correlation of total bromine with d_c ($r = 0.44$ for total Br/d_c) which may lead to the conclusion that the additional injection of bromine source gases during strong convection tends to outweigh the decrease due to scavenging, however, there are also short periods where total bromine is anti-correlated to convective activity.

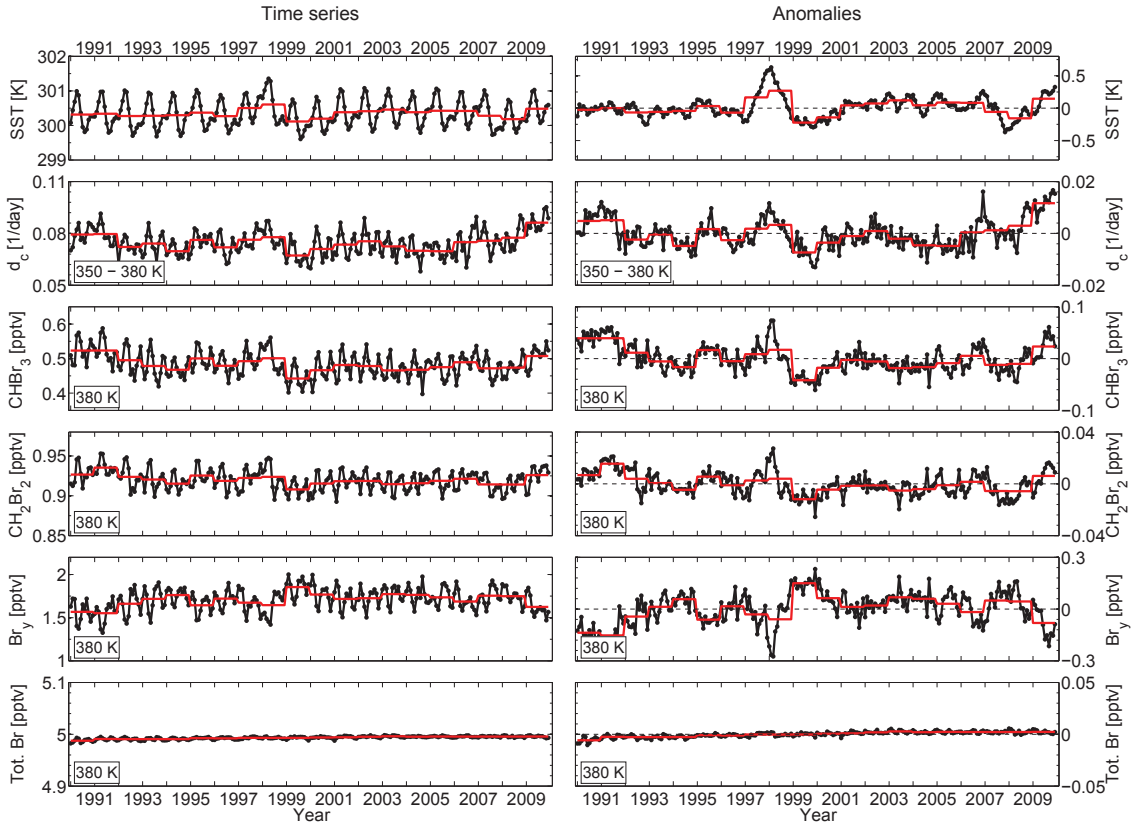

Figure 7.2.: Tropical timeseries and anomalies of sea surface temperature, detrainment rate, bromine VSLS, inorganic and total bromine, similar to Figure 7.1 but for full chemistry run FC1. Note: the values for Br_y and total bromine are actually the difference of standard run FC1 and the reference run FC2 without VSLS to isolate the impact of the short-lived substances. Adapted from Aschmann et al. (2011).

7.1.2. Full Chemistry Setup

The corresponding timeseries for run FC1 are presented in Figure 7.2. The picture for the bromine VSLS, bromoform and dibromomethane, is essentially the same as in the idealized setup (Section 7.1.1). Both are correlated to d_c ($r = 0.59$, 0.61 for $d_c/CHBr_3$, d_c/CH_2Br_2) and bromoform is also more affected quantitatively than dibromomethane.

The pronounced difference to the idealized setup manifests in the mixing ratio of Br_y/total bromine at 380 K. To remove the influence of the variable long-lived source gases (Section 4.3.5), the timeseries of Br_y/total bromine in Figure 7.2 actually shows the difference between the reference run FC2 without VSLS and the standard full chemistry

setup as already described in Section 6.1.2. As stated earlier the model suggests that virtually the entire amount of bromine originating from VSLS is able to reach the UTLS region at 380 K. Temporal variations in convective activity and washout efficiency do not have a significant effect; after about two years of spin-up time the mixing ratio of total bromine stays at 5 pptv. In return, Br_y acts as the insoluble product gas tracer discussed in Section 7.1.1: since total bromine has reached the equilibrium value of 5 pptv, Br_y is clearly anti-correlated to convection ($r = -0.62$ for d_c/Br_y) thus balancing out the changing amount of available source gases. Apparently the loss of soluble inorganic bromine species in the tropopause by uptake on ice is negligible in the full chemistry approach as stated in Section 6.1.

Results from the sensitivity calculation FC3 without heterogeneous activation presented in Figure 7.3 show that uptake of soluble Br_y on ice causes an average loss of total bromine of about 0.3 pptv that increases up to 0.5 pptv, for example, during the El Niño season 1997/98 which is roughly 25% to 30% of the Br_y originating from VSLS at 380 K. Interesting to note is the time lag of the total bromine loss during the aforementioned El Niño season: in the idealized setup with instantaneous washout the major loss of total bromine occurs at December 1997 (Figure 7.1) in contrast to the full chemistry run FC3, where the minimum is reached around May 1998. This delay is most likely caused by the repeated cycle of adsorption, sedimentation and ascent as described in Section 6.1.2, which is not present in the idealized setup where loss due to scavenging occurs instantaneously. Another notable difference to the idealized approach is revealed in the La Niña season at the end of 1999. The idealized run shows a small minimum in total bromine of about 0.1 pptv (Figure 7.1) whereas the loss in the full chemistry run is doubled. Apart from these two major events the effect of dehydration on total bromine is generally smaller in the full chemistry sensitivity run than in the idealized setup.

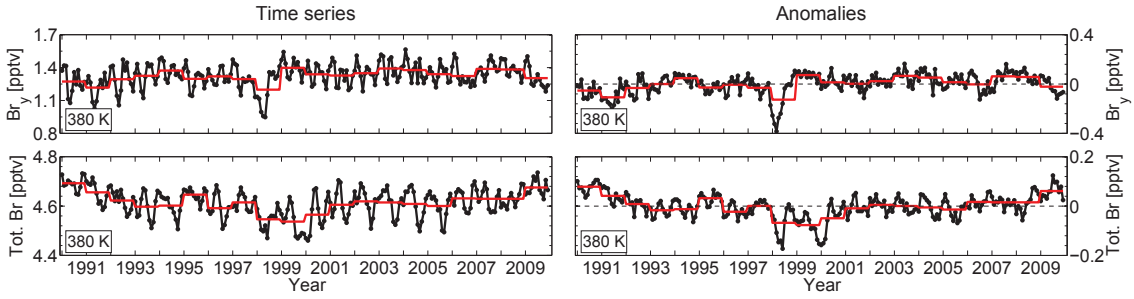

Figure 7.3.: Tropical timeseries and anomalies of Br_y and total bromine as in Figure 7.2 but from sensitivity run FC3 without heterogeneous activation.

7.2. Temporal Development of Stratospheric Bromine Loading

The only currently available multi-year timeseries of bromine observations in the UTLS stems from SCIAMACHY, which measures BrO in the range between 15 and 29 km (Rozanov et al., 2010a, see also Section 5.3). Thus, the full chemistry simulation offers the opportunity to compare the modeled temporal development of stratospheric bromine with observations, as it explicitly calculates the partitioning of Br_y. Figure 7.4 presents timeseries of BrO obtained from simulation runs with and without VSLS (FC1, FC2) and SCIAMACHY observations at the tropics and high latitudes at 17 and 27 km altitude. To

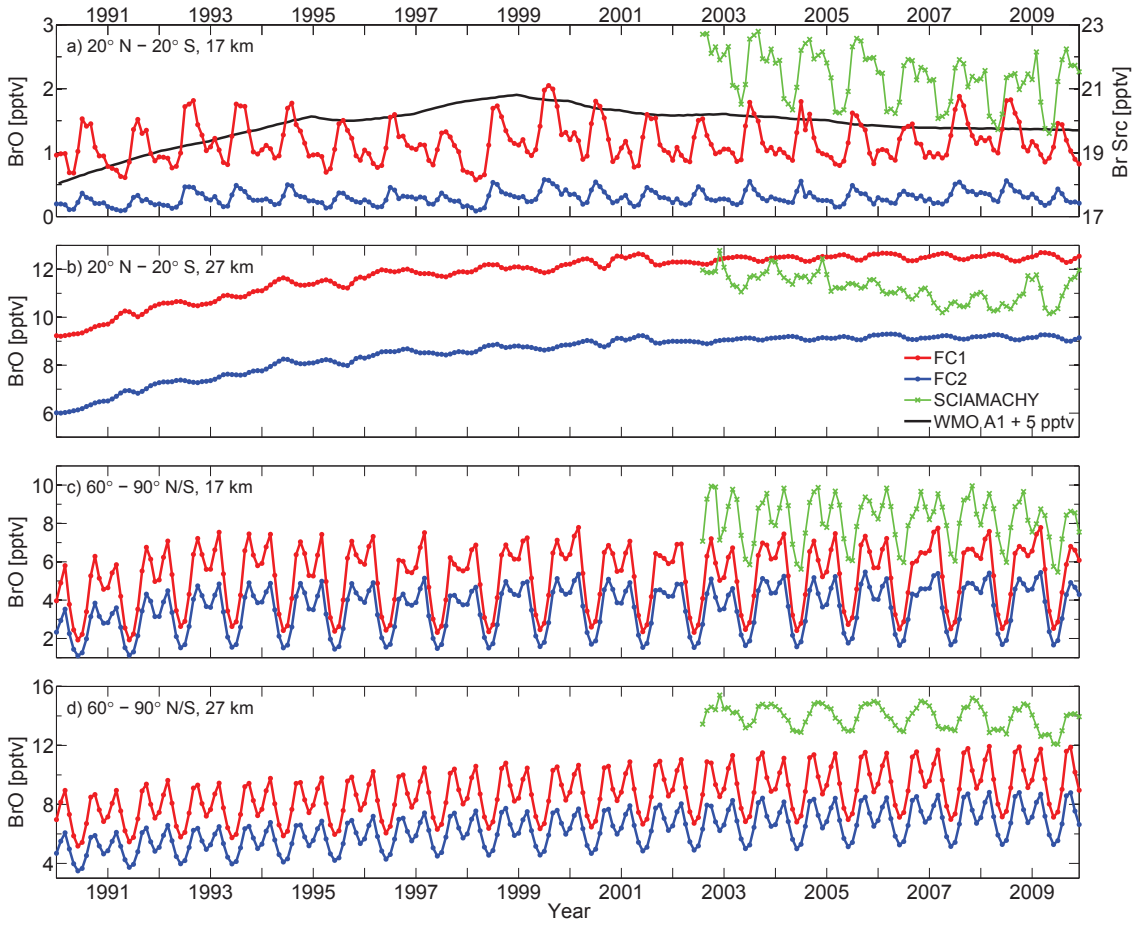

Figure 7.4.: Timeseries of BrO from simulation FC1, FC2 and SCIAMACHY (Rozanov et al., 2010a) at the tropics and high latitudes at 17 and 29 km. The model results are given at SCIAMACHY local time to ensure comparability. In addition, panel a) shows the detrainment mixing ratio of all bromine source gases in the model, i.e. the long-lived species according to WMO scenario A1 (Daniel and Velders, 2010) plus 5 pptv from VSLS.

ensure direct comparability, the model output is shown here at the SCIAMACHY local time. In addition, the black line denotes the detrainment mixing ratio of all bromine source gases included in the model, i.e. the two VSLS that contribute constantly 5 pptv and the long-lived species, whose detrainment mixing ratio varies according to the WMO scenario A1 (see Figure 3.1; Daniel and Velders, 2010). In panel a), i.e. at the top of the tropical tropopause at 17 km (approximately 380 K, in analogy to Figure 7.2), hardly any trend of modeled BrO is discernible: only 10% of total bromine at this altitude is in the form of Br_y, as the majority of bromocarbons is still intact. Furthermore, the difference between run FC1 and FC2 reveals that about 75% of BrO is contributed by VSLS at 17 km, whose detrainment mixing ratio stays constant over time. The interannual variability of the BrO mixing ratio can be attributed to the variation of convective activity. As indicated in the previous section, Br_y is anti-correlated to d_c and SST and one can expect the same for BrO. In fact, the anti-correlation between modeled BrO and SST is relatively high ($r = -0.80$). SCIAMACHY BrO shows a similar anti-correlation to SST ($r = -0.69$),

however, in addition it exhibits a notable decrease, about −3.3%/yr in the period between 2003–2010. Since the decrease in long-lived source gases as projected by the WMO scenario is only about −0.4%/yr in the same period, this change cannot be solely related to these species.

This becomes especially clear at higher altitudes and latitudes, as shown in the panels b)–d): Here, the model suggests a positive trend of BrO almost over the entire time span which is not supported by the observations. It is likely that the modeled BrO distribution responds too slowly to changes in the long-lived source gases due to the underestimated Brewer-Dobson circulation (see Section 5.6). Furthermore, distortions caused by initialization artifacts cannot be entirely ruled out. However, these arguments alone can hardly explain the discrepancy between the model and observations. If the observations do not contain a large systematic error, this effect must be caused by a possible unknown mechanism or a poorly represented process in the model which causes a stronger variability of stratospheric bromine than previously expected.

One possibility is the inter-hemispherical difference in the emission of the most abundant bromocarbon, CH_3Br. As indicated by Montzka and Reimann (2010), the mixing ratios of CH_3Br are found to be higher in the Northern Hemisphere, by about 1–2 pptv in the years between 1996–2008, which is not included in the model. Therefore, changes in the exchange between the Northern and Southern Hemisphere for example by ENSO or other dynamical processes could possibly impact the abundance of stratospheric bromine. Another important factor to consider here is the variability of VSLS emissions, which is completely ignored in the model. As stated before (Section 3.1.2), the observed mixing ratios of VSLS vary dramatically in the boundary layer, therefore it is definitely possible that the variability of stratospheric bromine is predominantly controlled by short-lived species. In addition, SCIAMACHY shows generally larger values of BrO compared to model run FC1 (except in the tropical stratosphere), that means the contribution of VSLS may easily exceed the assumed 5 pptv. However, little is currently known about the temporal development of VSLS sources, which makes it difficult to prove this assumption. Definitely, more research is needed to address this important question.

7.3. Spatial Anomalies during El Niño/La Niña Seasons

The special circumstances during the ENSO seasons offer the opportunity to investigate the impact of convective transport and dehydration on stratospheric bromine under extreme conditions[2]. As already stated in Section 7.1, the ENSO phases are accompanied by anomalies in sea surface temperature and changes in convective activity, predominantly in the Pacific region (e.g., Ramanathan and Collins, 1991; Barsugli and Sardeshmukh, 2002; Chiang and Sobel, 2002; Guilyardi et al., 2009). The following sections illustrate the impact of an intense perturbation in convective transport, presenting spatial anomaly maps of sea surface temperature, convective detrainment, bromine VSLS and inorganic and total bromine for the exceptional strong El Niño/La Niña seasons 1997/98 and 1999.

7.3.1. Idealized Setup

Figure 7.5 shows the spatial anomaly distribution of the aforementioned variables for the El Niño/La Niña seasons 1997/98 and 1999, respectively. For the El Niño season 1997/98 there is an increase of SST in the equatorial East Pacific and to a lesser extent in the western part of the Indian Ocean. Convective activity generally intensifies in these areas

[2]This section is based mainly on the work presented in Aschmann et al. (2011).

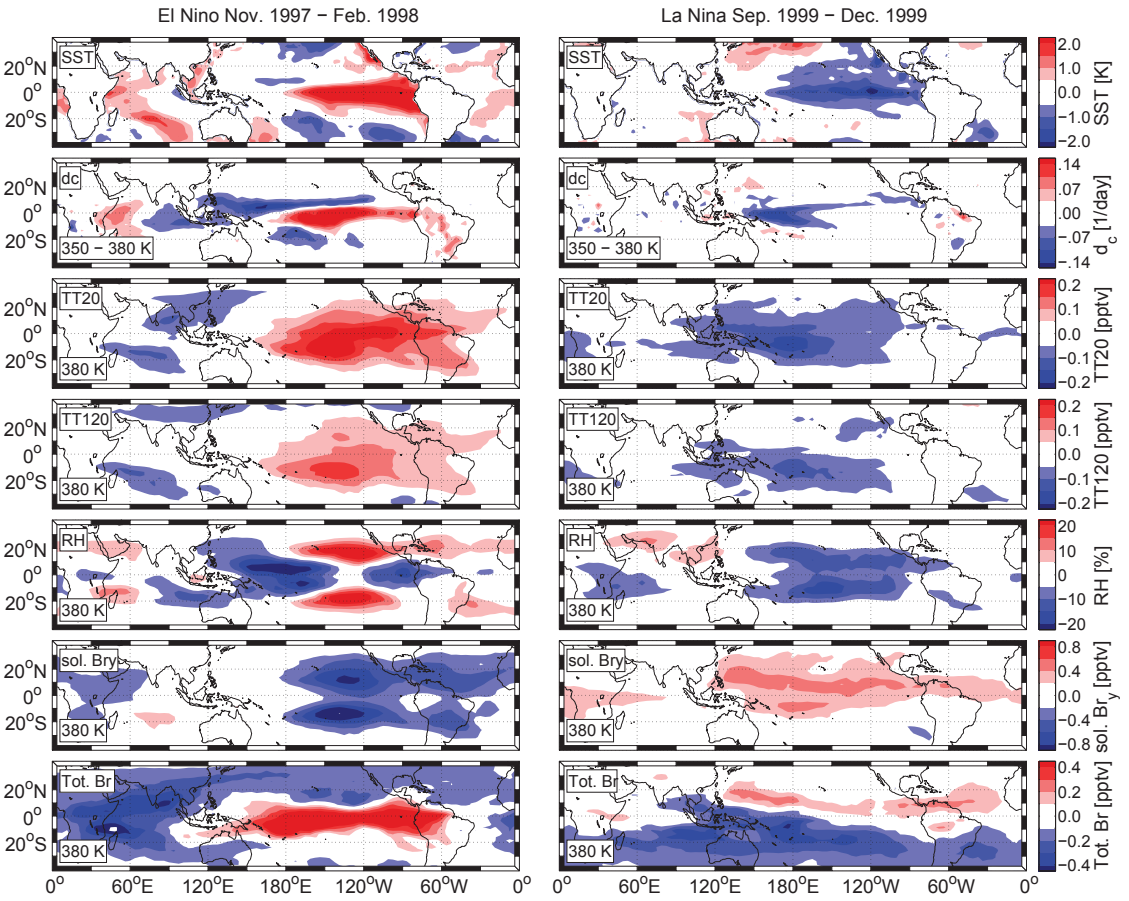

Figure 7.5.: Averaged anomalies of sea surface temperature SST, detrainment rate d_c, the VSLS TT20 and TT120, relative humidity RH, Br_y^{sol} and total bromine. The small boxes denote the corresponding potential temperature level. Left: Averages over El Niño season November 1997 to February 1998. Right: Averages over La Niña season September 1999 to December 1999. Adapted from Aschmann et al. (2011).

although there is also a decrease of d_c over the Maritime Continent. This dipole-type structure is also discernible in the distribution of the bromine source gases, TT20 and TT120, but the increase outweighs the loss considering the whole tropics. Interestingly, the mixing ratios of both source gases are actually dropping over the Western Indian Ocean although d_c shows a positive anomaly there which might be a transport-related effect. The relative humidity as indicator for scavenging efficiency shows two zonal bands of strong positive anomalies at 20°N/S disrupted by an extensive negative anomaly over the Western Pacific stretching as equatorial band eastward. Mixing ratios of Br_y^{sol} are significantly reduced in areas with positive anomalies of relative humidity, exceeding the effect of Br_y reduction due to dilution by detraining air.

The interpretation of the distribution of the total bromine anomalies is more complex. During El Niño 1997/98, the main features of the distribution, i.e. the strong positive anomaly over the equatorial Pacific next to the negative anomaly over the Indian Ocean, generally correspond to the patterns of TT20 and TT120. However, as explained in the previous section (Section 7.1.1), the amount of total bromine is also directly controlled

by the scavenging efficiency, which may outweigh the effect of source gas injection. The positive anomaly of total bromine in the equatorial pacific and the negative anomaly in the Indian Ocean are examples where these two factors coincide: an increase in source gases is accompanied by an decrease of relative humidity (i.e. scavenging efficiency). However, at 20°N/S, this is not the case and total bromine is reduced due to increased washout, although both source gases show a positive anomaly at this latitude (in the Pacific region).

In principle, the La Niña season 1999 shows a similar picture with inverted sign for the detrainment rate and the source gases. However, there are notable differences, the most important is the missing dipole-type structure of the previous El Niño season. This leads to a roughly uniform negative anomaly for the source gases and relative humidity in the Pacific region, whereas Br_y^{sol} shows a corresponding positive anomaly. The distribution of total bromine is split up in a small northern positive anomaly and an extensive negative anomaly in the South. The northern anomaly can be explained with the exceptionally low scavenging efficiency in this region which restricts washout of Br_y^{sol}, however, this explanation is not applicable for the Southern Hemisphere (SH) where total bromine is reduced in spite of the low scavenging efficiency. It is likely that the reduced amount of source gases outweighs the impact of scavenging in this region. Furthermore, it is possible that the negative anomaly is intensified by transport of Br_y-depleted air from other areas, for example from India or the northern part of the Maritime Continent, where a positive anomaly of relative humidity exists.

7.3.2. Full Chemistry Setup

The spatial anomaly patterns of the full chemistry run FC3 for the prominent El Niño/La Niña seasons 1997/98 and 1999 are presented in Figure 7.6. The run FC3 is chosen here, because it is on the one hand identical to the standard run FC1 with regard to the source gases and the relative humidity. On the other hand, as shown in Section 7.1.2, there is no discernible effect of dehydration on stratospheric bromine in run FC1, as heterogeneous activation nullifies its impact, thus run FC3 without these reactions offers the opportunity to study the isolated effect of dehydration. In addition, to remove the influence of changing long-lived source gases and focus on bromine VSLS, the difference of run FC3 and FC2 (without VSLS) is shown for Br_y and total bromine.

The anomaly patterns for the two VSLS and the relative humidity are very similar in shape and magnitude to the idealized setup (Figure 7.5) during both seasons. The main differences between the two approaches is present in the anomalies of inorganic and total bromine. There is a certain resemblance in the patterns of those tracers compared to the idealized approach, however, the magnitude differs significantly, especially in the case of total bromine where FC3 shows a much smaller effect. These differences are caused by the treatment of dehydration in the full chemistry setup. In contrast to the idealized run ID1, the removal of inorganic bromine due to adsorption on ice is neither complete (only HBr is removed) nor instantaneous. This treatment limits the impact of dehydration and furthermore introduce a time lag, e.g. the major loss of total bromine during El Niño season 1997/98 occurs five months later in FC3 compared to ID1 (Section 7.1.2). The uniform decrease of total bromine during La Niña 1999 in contrast to the partial increase in the idealized run can be also explained by these differences. Since the effect of dehydration is smaller and delayed in the full chemistry setup, illustrated by the weak anomalies of Br_y during the La Niña season, the uniform negative anomaly is mainly forced by the decrease in source gas abundance.

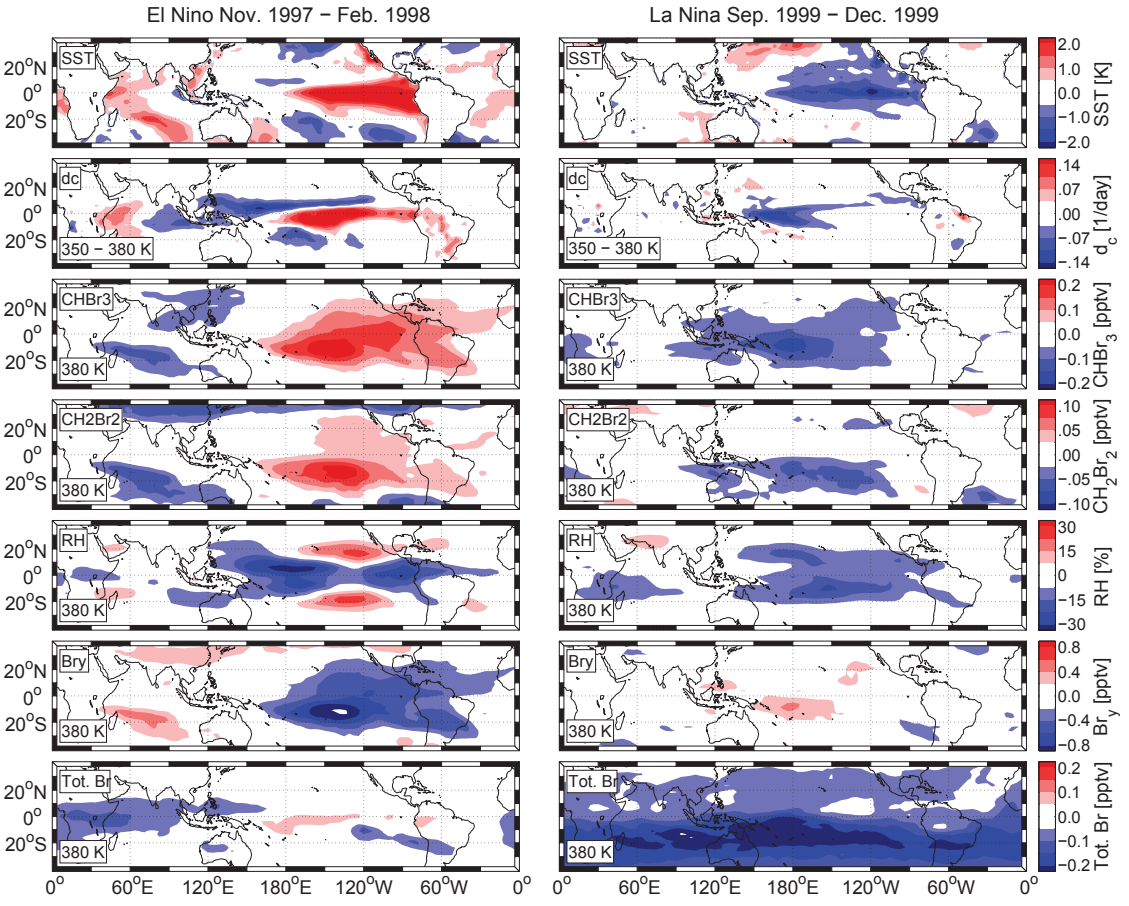

Figure 7.6.: Averaged anomalies for sea surface temperature, detrainment rate, bromoform, dibromomethane, relative humidity and inorganic and total bromine for the El Niño season 1997/98 (left) and La Niña season 1999 (right) as in Figure 7.5 but for the full chemistry run FC3 without heterogeneous activation. Note: the values for Br_y and total bromine are actually the difference of run FC3 and the reference run FC2 to show the impact of dehydration and short-lived substances (see also Section 7.1.2). Adapted from Aschmann et al. (2011).

7.4. Discussion and Conclusion

In this chapter, the long-term variability of stratospheric bromine is investigated using 21-year timeseries obtained from the idealized and full chemistry runs (Section 7.1) and comparisons to available observations (Section 7.2). The impact of the intense perturbations in convective activity during ENSO phases is discussed in Section 7.3.

In general, there is a tight coupling of sea surface temperatures and convective activity in the conducted model runs (Section 7.1). Although the strongest variations of SST and d_c are predominantly located in the Pacific region (e.g., Figure 7.5), the mixing ratios of bromine source and product gases are affected in the whole TTL, as the (Western) Pacific region has been identified to be the most important gateway into the stratosphere (Section 6.3). The abundance of the bromine VSLS bromoform and dibromomethane at the top of the TTL is highly correlated with convective activity, especially in the case of the shorter-lived bromoform. In contrast, Br_y is generally anti-correlated to d_c due

to convective dilution, however, this is strongly dependent to the utilized treatment of dehydration in the model. Likewise, the impact of varying deep convection on total bromine loading in the stratosphere is also very sensitive to the implementation of the dehydration mechanism. In the full chemistry setup, total bromine is practically unaffected by moderate changes in the convective detrainment rate (Figure 7.2). In turn, the more "aggressive" idealized approach suggests that on average more bromine reaches the stratosphere during strong convective events and vice versa, but that is not necessarily the case for local areas because the scavenging efficiency plays also an important role, which is mainly controlled by ambient temperature and water vapor content, i.e. relative humidity. Of course, in reality convection and relative humidity are not independent but form a complex interaction (e.g., Sherwood and Dessler, 2001; Gettelman et al., 2002b; Jain et al., 2006; Fueglistaler et al., 2009a; Tost et al., 2010) which cannot be captured in detail by the simplified treatment of convection in the model.

Comparisons between modeled BrO and SCIAMACHY observations reveal that the satellite data shows a negative trend during 2003–2010 which exceeds the expected decrease of long-lived bromine source gases by a factor of 8 and is not reproduced by the model (Section 7.2). It is currently not entirely clear what causes this discrepancy but a likely explanation could be that the variability of BrO in the UTLS region is largely controlled by the changing emissions of VSLS which is not included in the model.

The ENSO phases offer an interesting opportunity to study the impact of bromine VSLS under varying conditions of convective activity (Section 7.3). Several processes simultaneously control the amount of bromine at the top of the TTL. The first is directly related to convective transport. An increase of convection leads in general to an increase of source gases in the TTL, resulting in rising concentrations of total bromine and vice versa. However, the total amount of bromine becomes increasingly insensitive to variations in convective transport if it converges to its possible maximum, i.e. if the loss of bromine becomes negligible, which is the case for the insoluble Br_y tracer in the idealized setup and the inorganic bromine species in the standard full chemistry setup (e.g., Section 7.1). The second process is dehydration, which is in part connected to convection (see above). The formation of ice is controlled by the ambient temperature and content of water vapor, which is similar for both modeling approaches. In the idealized setup, where dehydration is approximated as instantaneous mechanism that immediately removes all ice and adsorbed Br_y, the resulting distribution of total bromine can be clearly identified as a superposition of the anomaly patterns of convectively injected source gases and the dehydration efficiency represented by the relative humidity (Figure 7.5). In the full chemistry setup without heterogeneous activation this relationship is not as clear (Figure 7.6), since the loss of inorganic bromine due to dehydration is not instantaneous in contrast to the quasi-instantaneous convective transport. These different timescales introduce a time lag in the response of total bromine. Finally, the last important process is the large-scale advection. Its impact is closely connected to the dehydration process, as it enables air masses to be transported in or out of areas where efficient dehydration occurs ("cold trap" hypothesis, e.g., Holton and Gettelman, 2001; Fueglistaler et al., 2005, 2009a), however, this is difficult to quantify as it does not produce distinctive features as the two previous processes.

The presented results confirm a tight coupling between SST, convective activity, abundance of bromine VSLS in the TTL and, depending on the modeling approach, stratospheric total bromine. Considering an increase SST in a changing climate (e.g. Rayner et al., 2003; Kumar et al., 2004; Dong et al., 2009), this will likely alter the amount of VSLS reaching the stratosphere (e.g., Dessens et al., 2009). In addition, Butler et al. (2007) found a positive correlation between the oceanic emissions of bromine VSLS and SST, that

means it is possible that an increase of SST not only makes the transport of VSLS into the stratosphere more efficient, but the emission of these species will increase as well.

8. Impact of VSLS on Stratospheric Ozone

The catalytic destruction of ozone caused by reactive halogens is a key process in the stratospheric ozone chemistry, as outlined in Section 3.2.3. This applies in particular for bromine, which is according to Sinnhuber et al. (2009) on average about 64 times more efficient in the depletion of ozone than an equal amount of chlorine. Therefore, this chapter evaluates the impact of short-lived bromine source gases on stratospheric ozone abundance. Firstly, Section 8.1 compares the modeled ozone with available observations. In a second step, the actual ozone decrease caused by bromine VSLS is investigated in Section 8.2.

8.1. Comparison of Modeled and Measured Ozone

In this section, the ozone distribution in the model is evaluated using observational data. Panel d) of Figure 8.1 shows a zonal cross section of O_3 mixing ratio of run FC1 for 2006, which represents a typical distribution of ozone (e.g., Brasseur et al., 1999): Low mixing ratios in the troposphere/tropopause region (typically below 100 ppbv), a strong gradient between approximately 15 and 25 km that lead to a local maximum in the stratosphere around 25 to 35 km altitude. The highest mixing ratios, around 10 ppmv, can be found above the tropics at around 30 km, where most stratospheric O_3 is produced.

A more quantitative comparison is given in the panels a) to c) in Figure 8.1, representing O_3 profiles in the tropics, mid and high latitudes of run ID1 and FC1, SHADOZ sonde measurements (Thompson et al., 2003) and SCIAMACHY satellite observations (Rozanov et al., 2007). In the tropics, both modeling approaches significantly underestimate the ozone abundance in the UTLS region compared to the observations (about 30–70%). It is possible that the assumed detrainment mixing ratios for O_3 are too low which would lead to a reduction of ozone in the TTL caused by convective dilution. Furthermore, run FC1 predicts lower mixing ratios at the top of the stratosphere, in contrast to the idealized setup that shows only slightly higher values than the SCIAMACHY observations. In between, the amount of modeled O_3 generally agrees with the observations, although especially the full chemistry setup overestimates the amount of ozone around 20 to 25 km. At mid and high latitudes the picture is similar for the middle and upper stratosphere, however, here the model simulations drastically overestimate the O_3 abundance in the UTLS by up to 60–80%. Since both modeling approaches show a similar behavior this deviation is most likely a transport effect, probably caused by the too slow Brewer-Dobson circulation in the model (Section 5.6).

Figure 8.2 presents zonal cross sections of total column ozone (TO3) from multiple modeling approaches and observations for different seasons in 2006. In addition to the model runs ID1 and FC1, the ozone data set of Kiesewetter et al. (2010a) is shown here who used the B3DCTM in an approach similar to the idealized setup but also assimilated O_3 observations from the SBUV satellite-borne instrument into their model. Note that since the model does not explicitly contain the troposphere, an ozone climatology from Fortuin and Kelder (1998) is used to calculate the column contribution from lower altitudes. Furthermore, observational data from SCIAMACHY and the merged TOMS/SBUV data set (Stolarski and Frith, 2006) is shown. The modeled TO3 obtained from run FC1 agrees

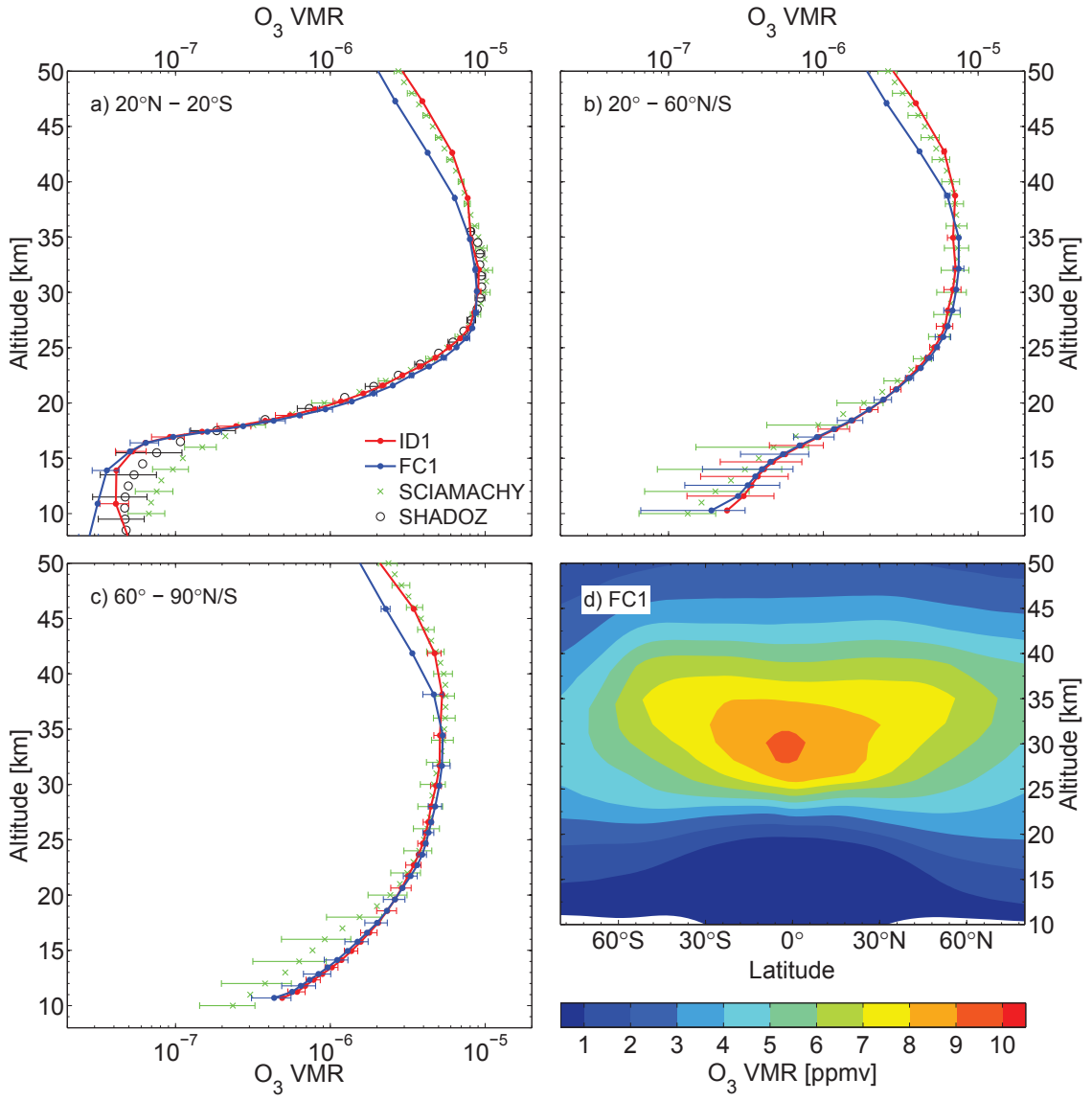

Figure 8.1.: Comparison of averaged ozone profiles from model runs ID1/FC1 and SHADOZ (Thompson et al., 2003) and SCIAMACHY (Rozanov et al., 2007) observations for the tropics (a), mid and high latitudes (b and c) for 2006. The error bars denote one standard deviation. Panel d) shows a zonal cross section of modeled ozone (run FC1) for the same year.

well with the observations and the assimilated data set. The largest deviations can be found during springtime in the Northern and Southern Hemisphere (MAM and SON), where the major loss of ozone occurs in the corresponding polar vortex (e.g., Brasseur et al., 1999). In both cases the full chemistry approach tends to overestimate the impact of ozone depletion and suggests lower TO3 values compared to the observations. The idealized run ID1 shows larger deviations in general, especially in the NH. There is an offset in the calculated TO3 which is about 20 DU in the tropics, increasing up to 50 DU in the northern polar region.

Table 8.1.: Correlation coefficients between timeseries of total column ozone of run ID1/FC1 and TOMS/SBUV and SCIAMACHY observations at different latitudinal ranges (Figure 8.3).

	Run	r_{TOMS}	r_{SCIA}
Tropics	ID1	0.84	0.72
	FC1	0.90	0.85
Mid lat	ID1	0.34	0.19
	FC1	0.57	0.53
High lat	ID1	0.58	0.84
	FC1	0.67	0.88

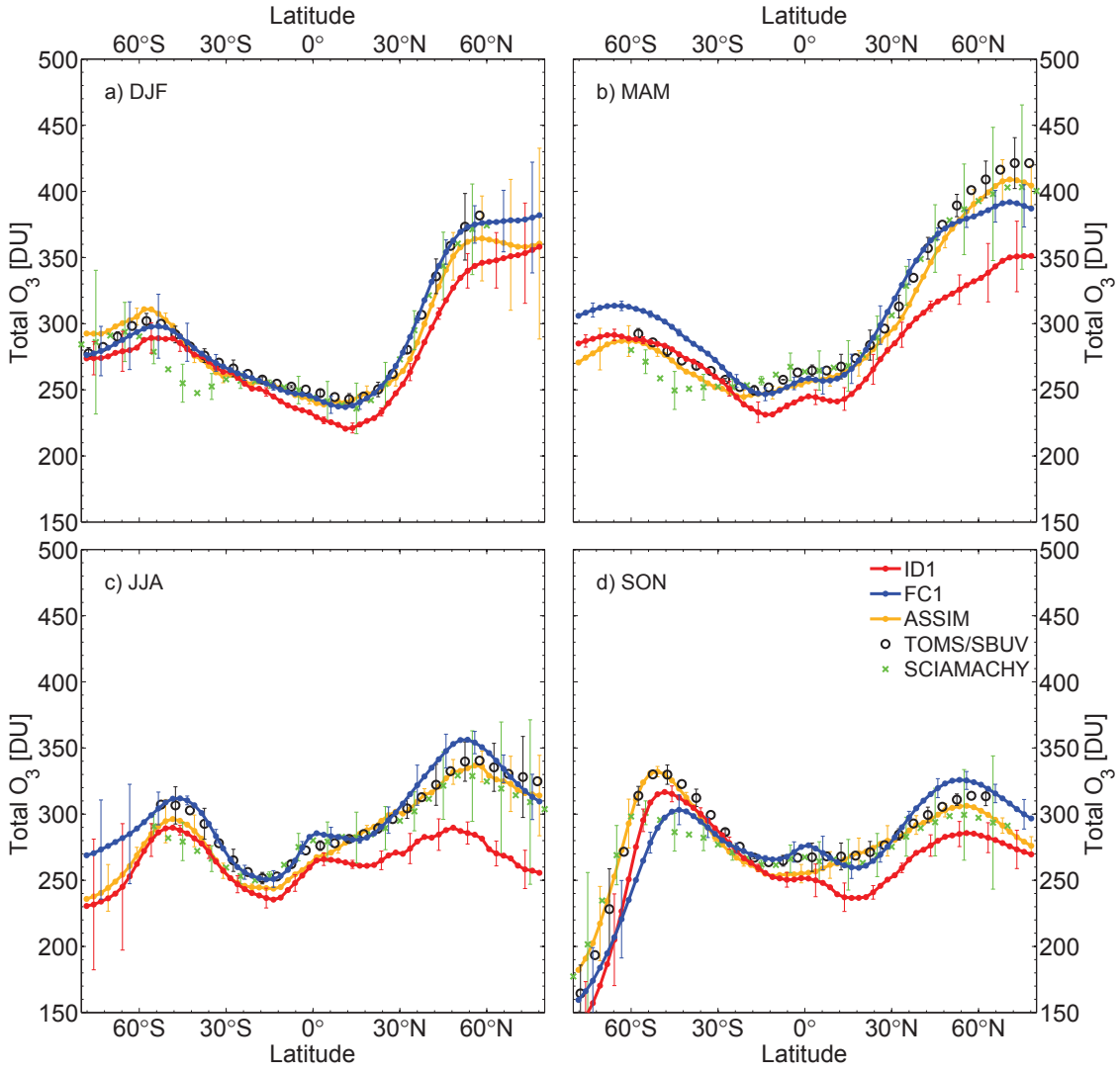

Figure 8.2.: Comparison of total column ozone obtained from model runs ID1/FC1, assimilated O_3 data set by Kiesewetter et al. (2010a), TOMS/SBUV (Stolarski and Frith, 2006) and SCIAMACHY (Rozanov et al., 2007) observations for different seasons (DJF, MAM, JJA, SON) in 2006. The error bars denote one standard deviation.

The temporal evolution of TO3 is illustrated in Figure 8.3. Shown are timeseries for the tropics, mid and high latitudes from the model runs ID1 and FC1, together with satellite data from TOMS/SBUV and SCIAMACHY. The correlation coefficients between the model and the observational data is summarized in Table 8.1. In the tropics, the model agrees well with the observational data, although both approaches show a nearly constant offset that is reached after about 10 years of spin-up time. In case of the idealized setup, TO3 is about 20 DU units lower than the satellite measurements suggest. The offset of the full chemistry setup is smaller (5 DU) and also the correlation of this run with the observational data is higher compared to the idealized approach. At mid latitudes, the idealized setup has problems to reproduce the annual cycle of TO3. The offset-corrected values are similar to the TOMS/SBUV data, however, the correlation to the satellite measurements is low (0.34). In contrast, TO3 from the full chemistry setup shows a higher correlation to the TOMS/SBUV data set (0.57), but the offset-corrected values after the 10 years of spin-up time are generally lower than the observations suggest. However, these values agree better with the SCIAMACHY observations, which are also lower compared to the TOMS/SBUV data set. TO3 from run ID1 is not only higher compared to SCIAMACHY, there is furthermore almost no correlation between the two data sets (0.19) in this latitudinal range. Finally, at high latitudes both modeling approach are able to replicate the annual cycle and also the loss of TO3 during austral spring is quantitatively well reproduced[1]. However, both runs show a smaller recovery of ozone during austral summer and autumn; the predicted values of TO3 are significantly lower compared to the satellite observations, especially for TOMS/SBUV. Since this feature exists both in the linearized and full chemistry scheme this is a strong indication that the overall poleward circulation and therefore the poleward O_3 flux is systematically underestimated in the model, as already stated in Section 5.6.

[1]Taking into account the offset correction.

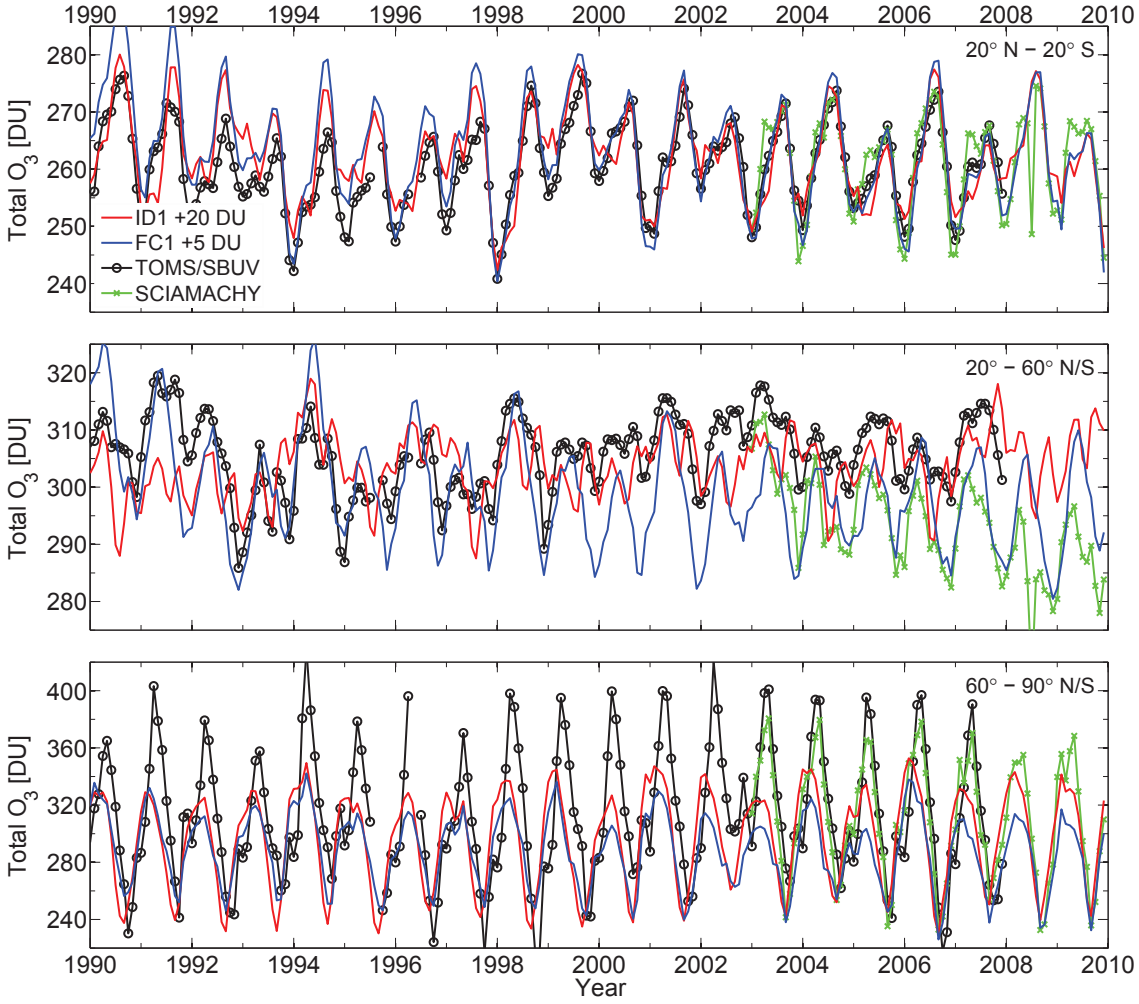

Figure 8.3.: Timeseries of total column ozone obtained from model run ID1/FC1, TOMS/SBUV (Stolarski and Frith, 2006) and SCIAMACHY (Rozanov et al., 2007) in the tropics (top), mid (center) and high latitudes (bottom). For comparison, the values of run ID1 and FC1 are offset by 20 and 5 DU, respectively.

8.2. Ozone Loss Due to VSLS

In contrast to the idealized setup ozone in the full chemistry approach is sensitive to the amount of bromine in the model. By comparing the standard run FC1 with VSLS included to the reference run FC2 without VSLS it is possible to identify the impact of the additional bromine on stratospheric ozone. As stated in Section 6.1 and 7.1, one can safely assume that practically the entire amount of bromine originated from VSLS is able to reach the stratosphere in the standard full chemistry setup, that means stratospheric bromine loading in run FC1 is increased by 5 pptv compared to run FC2.

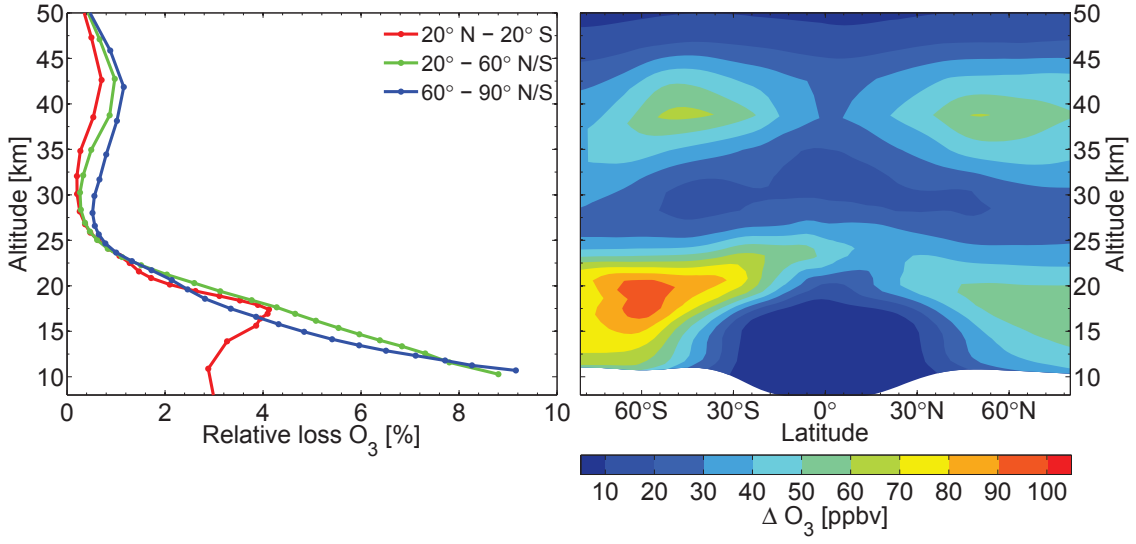

Figure 8.4.: Relative loss of ozone due to additional bromine VSLS (5 pptv) in the tropics, mid and high latitudes (left panel), calculated from run FC1 (with VSLS) and FC2 (without VSLS) for 2006. The right panel shows the absolute difference of ozone of run FC1 and FC2.

Figure 8.4 reveals the relative and absolute difference in the O_3 profiles between run FC1 and FC2 averaged over 2006. The largest ozone losses occur around 50° to 70°N/S between 15 to 20 km, a region where heterogeneous activation of halogens plays an important role for ozone depletion (e.g., Brasseur and Solomon, 2005). Ozone mixing ratios are reduced by a maximum of 0.1 ppmv in the southern high latitudes compared to a maximum of 0.06 ppmv in the North, which corresponds to about 3 to 6 % relative ozone loss compared to run FC2. The impact of the additional bromine is also discernible near the stratopause around 40 km, where ozone loss by gas phase chemistry dominates (e.g., Brasseur and Solomon, 2005). Here, the ozone mixing ratio is decreased by about 0.06 ppmv in both hemispheres, equal to about 1.5% relative loss. In the tropics, the ozone reduction is generally small. Only at the lower stratosphere around 22 km the amount of ozone is reduced due to mixing with air parcels from higher latitudes.

The seasonal variation of the relative and absolute TO3 loss due to VSLS in 2006 is depicted in Figure 8.5. As the differences in the ozone profiles suggest (Figure 8.4), the maximum TO3 loss occurs in the southern high latitude region from the end of austral winter to austral spring. The O_3 column is reduced by about 5–8 DU, i.e. 2.5–3.5% loss compared to run FC2 without additional bromine. In the NH, the ozone loss is less intense,

ranging from 4 to 5 DU (1.5%) during DJF and MAM. Mixing reduces TO3 in the tropics by about 2 DU during all seasons. In comparison, the global annually averaged loss of TO3 due to VSLS is about 3.5 DU, corresponding to a relative loss of approximately 1.3%.

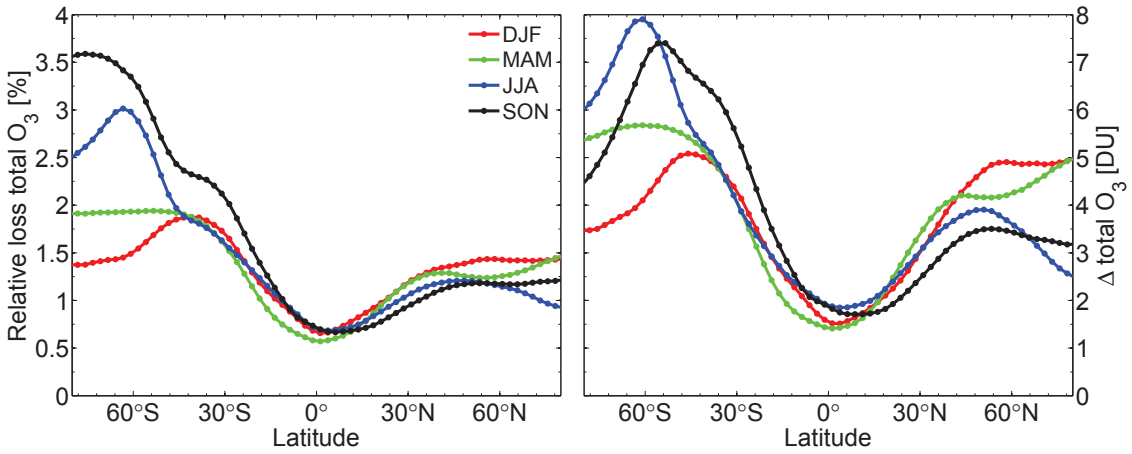

Figure 8.5.: Seasonal variations of relative (left panel) and absolute loss (right panel) of total column ozone due to additional bromine VSLS (5 pptv) calculated from run FC1 (with VSLS) and FC2 (without VSLS) for 2006.

The temporal evolution of TO3 loss due to VSLS over the complete modeled time span is presented in Figure 8.6. The most prominent feature is the alternating decrease of column ozone at high latitudes following the corresponding polar night. The peak amplitude of the springtime signal is about 6–9 DU in the NH and 11–14 DU in the SH. During the following months, the springtime perturbation in column ozone is still discernible as it propagates relatively intact into the mid latitudes producing a pattern comparable to the water vapor tape recorder depicted in Figure 5.12. It takes approximately 3–4 months for the perturbation to reach the tropics where it disperses. The strongest and most extensive signal can be seen in the years after the eruption of Mt. Pinatubo in June 1991. The volcano injected enormous amounts of sulfuric particles into the atmosphere that significantly contribute to ozone depletion (e.g., McCormick et al., 1995). Since the abundance of H_2SO_4 in the full chemistry setup relies on an external data set (see Section 4.3.5), the impact of the increased aerosol loading after the eruption is also visible in the model. The peak amplitude of TO3 depletion by additional bromine of VSLS origin is not increased, but the spatial and temporal extent of the signal is enlarged in both hemispheres. For example, in the years from 1992 to 1994, the SH springtime signal is able to penetrate deep into the tropics; furthermore TO3 remains significantly reduced even during austral summer and autumn where ozone typically recovers.

8.3. Discussion and Conclusion

This chapter compares the modeled ozone distribution with several satellite-borne observations (Section 8.1). In a second step, the impact of additional bromine contributed by VSLS on stratospheric ozone is investigated in Section 8.2.

Both modeling approaches are generally able to reproduce observed ozone profiles in the tropics, mid and high latitudes (Figure 8.1). The relative deviations in the middle strato-

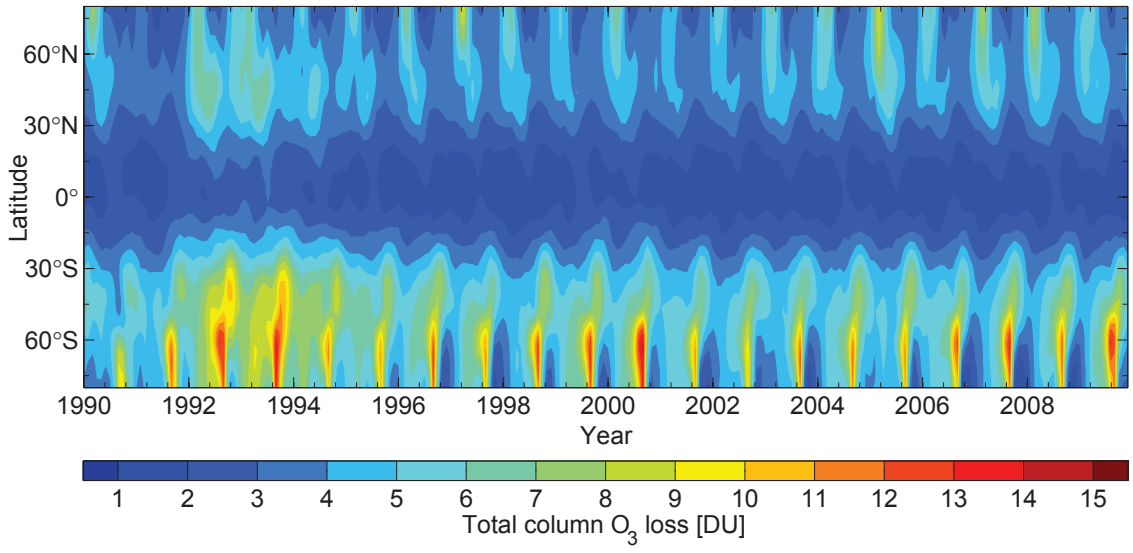

Figure 8.6.: Temporal evolution of total column ozone loss due to additional bromine VSLS (5 pptv) calculated from run FC1 and FC2.

sphere are generally lower than 15% compared to SCIAMACHY observations. However, at altitudes where the absolute ozone concentration is low, i.e. in the troposphere and to a lesser extent near the stratopause, there are larger discrepancies between the model and the observations, ranging from 30–70%. Total column ozone is well reproduced by the full chemistry run FC1, compared to TOMS/SBUV and SCIAMACHY data (Figures 8.2, 8.3). In contrast, the idealized setup generally shows lower values for TO3, particularly in the NH. Both modeling approaches tend to underestimate the ozone recovery at high latitudes in the hemisphere-specific summer and autumn seasons which is another indicator for the too slow meridional circulation in the model.

The impact of additional bromine originated from VSLS on stratospheric ozone is investigated using the two full chemistry runs FC1 and FC2. The only difference between those runs is that FC1 incorporates 5 pptv of additional bromine in the form of $CHBr_3$ and CH_2Br_2 which is not included in FC2. The major loss of ozone due to VSLS can be observed at high latitudes between 15 and 20 km altitude, ranging up to 60 and 100 ppbv in the Northern and Southern Hemisphere, respectively, which corresponds to about 3–6% of the annual average of the local ozone mixing ratio (Figure 8.4). When considering the loss of total column ozone, the maximum decrease is about 6–9 DU in the NH and 11–14 DU in the SH during the corresponding spring time season, being equal to a decrease of 1.5 and 3.5% relative to the annual average, respectively (Figures 8.5, 8.6). These results agree well with the findings of Feng et al. (2007) who used a similar approach and predict an average impact of 5 pptv additional bromine of about 10 DU at mid latitudes.

9. Conclusions

The final chapter of this thesis summarizes the main results in Section 9.1. Possible future work and scientific questions are outlined in Section 9.2.

9.1. Summary

In the course of this work, the existing chemistry transport model B3DCTM, originally developed by Sinnhuber et al. (2003a), was modified and extended to study the impact of very short-lived bromine source gases on stratospheric bromine loading. Multiple modeling approaches have been applied to study important processes and mechanisms related to the transport of VSLS in a physically motivated framework (Chapter 4).

An initial validation shows that the developed modeling approach is able to realistically reproduce the interplay of horizontal advection, localized deep convection and large-scale diabatic heating-rates in the tropical upper troposphere/lower stratosphere in general (Chapter 5). The modeled distribution of bromine source and product gases agrees reasonably well with available observations, taking into account the large uncertainties in the source strength of short-lived species. Comparisons between a simple parametrized ozone tracer and sonde measurements confirm that the spatial variability of convective updrafts is adequately represented in the model; also the modeled water vapor distribution, which is mainly dependent on convective detrainment and the applied dehydration mechanism, shows generally good agreement with observations. However, there is also strong evidence that the model tends to underestimate the large-scale meridional circulation. This becomes especially clear when considering the mean age of air at high latitudes/altitudes, which is significantly older compared to observations or other models.

When assuming that convectively detrained air contains both 1 pptv of bromoform and dibromomethane, the two most important bromine VSLS, which is consistent with the recent WMO recommendation for these species (Montzka and Reimann, 2010), the different modeling approaches predict an increase of stratospheric bromine ranging from 3.1 to 5 pptv (Chapter 6). An important question that is subject to current research is the impact of dehydration on inorganic bromine at the tropopause, which may be scavenged by falling ice particles. The conducted modeling runs show that at least 50% of the detrained VSLS are able to reach the stratosphere intact as source gas, which is insoluble and therefore unaffected by dehydration; in contrast, the other half already decays into inorganic bromine within the TTL and is susceptible to scavenging. A simple modeling approach, relying on idealized bromine source and product gas tracers, predicts that 3.1 out of 5 pptv of bromine originated from VSLS is able to reach the stratosphere when assuming total solubility of inorganic bromine, i.e. the complete amount of Br_y is removed whenever dehydration occurs in a model grid box. However, when applying a more realistic setup with detailed chemistry including a parametrization for adsorption and sedimentation the model suggests that virtually the entire amount of bromine contributed by VSLS reaches the stratosphere, in contradiction to most earlier modeling studies which assumed a flat washout mechanism for inorganic bromine. The main reasons for this discrepancy are that the fraction of HBr to Br_y – according to the current state of research the only bromine species which is

efficiently adsorbed on ice – is small in the TTL, generally lower than 5%. Furthermore, the partitioning of gas and solid phase HBr is inclined towards the gas phase, i.e. on average only about 30–40% of HBr is adsorbed on ice. Finally, heterogeneous reactions release the small amount of bromine that is actually adsorbed, rendering dehydration to be insignificant for inorganic bromine in the full chemistry setup.

Source strength and distribution of bromine VSLS remain highly uncertain to this day. This study contributes to current research by investigating the impact of a more refined emission scenario for VSLS on stratospheric bromine, which is similar to typical scenarios used in earlier modeling studies. The results suggest that the amount of bromine reaching the stratosphere is not very sensitive to the spatial distribution of VSLS sources. Furthermore, the transport efficiency of individual source regions is evaluated by dividing the model domain in different areas. According to the model calculations, the Western Pacific alone contributes about 50% to the total VSLS distribution in the TTL, being clearly identified as the most important source region for short-lived species.

The long-term variation of VSLS injection into the stratosphere is analyzed over a time span of 21 years (Chapter 7). There is a robust correlation between sea surface temperature, convective activity and the amount of bromine source gases in the TTL. This connection becomes especially clear during the El Niño/La Niña seasons which induce a strong perturbation in sea surface temperatures and convection patterns. However, the impact on total bromine loading in the model depends on the applied dehydration mechanism. In case of the full chemistry setup, where dehydration has no discernible effect on Br_y, total bromine is insensitive to changes of convective activity, as the complete amount of bromine provided by source gases is able to reach the stratosphere anyway. In contrast, the idealized setup, where dehydration removes a certain part of inorganic bromine, suggests a weak but statistically significant correlation between convective activity and stratospheric bromine.

Interestingly, comparisons with long-term SCIAMACHY measurements show that the observed negative trend of BrO is much larger than expected from the decrease of long-lived source gases. This discrepancy is currently subject to intensive research but if drastic systematic errors could be ruled out this might indicate that another previously undetected or underestimated process affects the abundance of stratospheric bromine, for example strong variability in the emissions of VSLS.

In the final part of this work, the modeled ozone distribution is compared to observations (Chapter 8). The modeled ozone profiles agree well with observations, except near the boundaries of the model, i.e. in the troposphere and at the stratopause, where the deviations are larger. The seasonal and interannual variability of total column ozone is also well reproduced, especially in the full chemistry setup which only shows a small constant offset of about 5 DU compared to the observations. In a second step, the impact of the additional bromine contributed by VSLS on stratospheric ozone is investigated. The maximum loss of ozone in the model due to 5 pptv of additional bromine occurs in the high latitudes of the Southern Hemisphere during austral spring and accounts for about 11–14 DU, which corresponds to 5–7% of the annually averaged total ozone column in this region. The global effect on total ozone is smaller, around 3.5 DU (1.3%).

9.2. Outlook

The conducted study raises some important questions that should be considered in further research. One important result of this work is that dehydration has apparently no impact on inorganic bromine in the TTL when using a more complex scheme instead of a simple

washout mechanism commonly used in earlier models. This should be verified by a more detailed microphysical representation of the associated processes, for example an explicit treatment of ice crystal growth with spectral size distribution, that would affect the adsorption of gaseous species as well as sedimentation and evaporation.

Furthermore, the representation of convection in the model is relatively simple and is artificially hampered by the lack of an explicitly modeled troposphere and boundary layer. It would be advisable for a future study to extend the model down to the surface using a hybrid vertical coordinate approach to overcome this limitation.

A central question is whether the injection of short-lived bromine source gases into the stratosphere will respond to global warming and an associated increase of sea surface temperature in the future. The analysis of VSLS transport during El Niño perturbations conducted in this study is a first step and could be further investigated by either using future projections from long-running general circulation models as input for the CTM presented here or by migrating the applied modeling approach to a chemistry climate model.

Arguably the most challenging task is to achieve a realistic representation of VSLS sources in the model. All current simulation studies about VSLS share the common problem that the strength and distribution of VSLS sources is highly uncertain, relying predominantly on top-down estimates. Sophisticated source parametrizations, for example based on satellite-borne chlorophyll observations, may help to solve this problem, however, the current research in this direction is still in its early stages.

To conclude, one can state that this study provides some new insights on the impact of VSLS on stratospheric bromine but raises new questions at the same time. Definitely, more work has to be done to better our understanding of these processes, especially against the background of a possible future climate change.

Appendix A.

List of Conducted Simulation Runs

Table A.1.: Overview of conducted model runs with idealized and full chemistry setup. Refer to Section 4.2.4 and 4.3.5 for details.

	Name	Description
Idealized	ID1	Standard setup, 6 tracers
	ID2	Restricted washout, additional AoA tracer, 7 tracers
	ID3	Emission scenario for VSLS, 6 tracers
	ID4	Regional emission for VSLS, 38 tracers
F. Chem.	FC1	Standard setup, 59 tracers
	FC2	Reference run w/o VSLS, 57 tracers
	FC3	No heterogeneous reactions, 59 tracers

Appendix B.

Reactions Included in SLIMCAT Chemistry Scheme

B.1. Gas Phase Reactions

$$O + O + M \longrightarrow O_2 + M \quad (B.1)$$
$$O + O_2 + M \longrightarrow O_3 + M \quad (B.2)$$
$$O + O_3 \longrightarrow 2\,O_2 \quad (B.3)$$
$$O(^1D) + O_3 \longrightarrow 2\,O_2 \quad (B.4)$$
$$O(^1D) + N_2 \longrightarrow O + N_2 \quad (B.5)$$
$$O(^1D) + O_2 \longrightarrow O + O_2 \quad (B.6)$$
$$O(^1D) + H_2O \longrightarrow 2\,OH \quad (B.7)$$
$$OH + O \longrightarrow H + O_2 \quad (B.8)$$
$$O_2 + H + M \longrightarrow HO_2 + M \quad (B.9)$$
$$HO_2 + O \longrightarrow OH + O_2 \quad (B.10)$$
$$OH + O_3 \longrightarrow HO_2 + O_2 \quad (B.11)$$
$$H + O_3 \longrightarrow OH + O_2 \quad (B.12)$$
$$OH + HO_2 \longrightarrow H_2O + O_2 \quad (B.13)$$
$$OH + OH \longrightarrow H_2O + O \quad (B.14)$$
$$OH + OH + M \longrightarrow H_2O_2 + M \quad (B.15)$$
$$H + HO_2 \longrightarrow OH + OH \quad (B.16)$$
$$H + HO_2 \longrightarrow H_2 + O_2 \quad (B.17)$$
$$H + HO_2 \longrightarrow H_2O + O \quad (B.18)$$
$$NO_2 + O \longrightarrow NO + O_2 \quad (B.19)$$
$$O_3 + NO \longrightarrow NO_2 + O_2 \quad (B.20)$$
$$NO_2 + O_3 \longrightarrow O_2 + NO_3 \quad (B.21)$$
$$HNO_3 + OH \longrightarrow H_2O + NO_3 \quad (B.22)$$
$$NO_2 + OH + M \longrightarrow HNO_3 + M \quad (B.23)$$
$$N_2O + O(^1D) \longrightarrow 2\,NO \quad (B.24)$$
$$N_2O + O(^1D) \longrightarrow N_2 + O_2 \quad (B.25)$$
$$HO_2 + HO_2 \longrightarrow H_2O_2 + O_2 \quad (B.26)$$
$$H_2O_2 + OH \longrightarrow H_2O + HO_2 \quad (B.27)$$
$$H_2O_2 + \text{rain} \longrightarrow \quad (B.28)$$
$$OH + CH_4 \longrightarrow CH_3 + H_2O \quad (B.29)$$
$$O(^1D) + CH_4 \longrightarrow CH_3 + OH \quad (B.30)$$
$$O(^1D) + CH_4 \longrightarrow HCHO + H_2 \quad (B.31)$$
$$O(^1D) + H_2 \longrightarrow OH + H \quad (B.32)$$
$$CO + OH \longrightarrow CO_2 + H \quad (B.33)$$
$$NO + HO_2 \longrightarrow NO_2 + OH \quad (B.34)$$
$$HO_2 + O_3 \longrightarrow OH + 2\,O_2 \quad (B.35)$$
$$HO_2 + NO_2 + M \longrightarrow HO_2NO_2 + M \quad (B.36)$$
$$HNO_3 + \text{rain} \longrightarrow \quad (B.37)$$
$$HO_2NO_2 + M \longrightarrow HO_2 + NO_2 + M \quad (B.38)$$
$$HO_2NO_2 + OH \longrightarrow H_2O + O_2 + NO_2 \quad (B.39)$$
$$HO_2NO_2 + \text{rain} \longrightarrow \quad (B.40)$$
$$CFCl_3 + O(^1D) \longrightarrow 2\,Cl + COFCl \quad (B.41)$$
$$CF_2Cl_2 + O(^1D) \longrightarrow 2\,Cl + COF_2 \quad (B.42)$$
$$Cl + O_3 \longrightarrow ClO + O_2 \quad (B.43)$$
$$ClO + O \longrightarrow Cl + O_2 \quad (B.44)$$
$$Cl + H_2O_2 \longrightarrow HCl + HO_2 \quad (B.45)$$
$$ClONO_2 + OH \longrightarrow HOCl + NO_3 \quad (B.46)$$

$$ClONO_2 + Cl \longrightarrow 2\,Cl + NO_3 \quad (B.47)$$
$$ClO + NO \longrightarrow Cl + NO_2 \quad (B.48)$$
$$CH_4 + Cl \longrightarrow CH_3 + HCl \quad (B.49)$$
$$H_2 + Cl \longrightarrow H + HCl \quad (B.50)$$
$$HO_2 + Cl \longrightarrow O_2 + HCl \quad (B.51)$$
$$HO_2 + Cl \longrightarrow OH + ClO \quad (B.52)$$
$$OH + HCl \longrightarrow H_2O + Cl \quad (B.53)$$
$$ClO + NO_2 + M \longrightarrow ClONO_2 + M \quad (B.54)$$
$$ClONO_2 + O \longrightarrow ClO + NO_3 \quad (B.55)$$
$$HOCl + Cl \longrightarrow HCl + ClO \quad (B.56)$$
$$HO_2 + ClO \longrightarrow HOCl + O_2 \quad (B.57)$$
$$HO_2 + ClO \longrightarrow HCl + O_3 \quad (B.58)$$
$$OH + HOCl \longrightarrow H_2O + ClO \quad (B.59)$$
$$O + HOCl \longrightarrow OH + ClO \quad (B.60)$$
$$ClO + ClO + M \longrightarrow Cl_2O_2 + M \quad (B.61)$$
$$ClO + ClO \longrightarrow Cl + Cl + O_2 \quad (B.62)$$
$$ClO + ClO \longrightarrow OClO + Cl \quad (B.63)$$
$$Cl_2O_2 + M \longrightarrow ClO + ClO + M \quad (B.64)$$
$$N + NO \longrightarrow N_2 + O \quad (B.65)$$
$$N + O_2 \longrightarrow NO + O \quad (B.66)$$
$$N + O_3 \longrightarrow NO + O_2 \quad (B.67)$$
$$OH + ClO \longrightarrow HO_2 + Cl \quad (B.68)$$
$$OH + ClO \longrightarrow HCl + O_2 \quad (B.69)$$
$$Cl_2O_2 + Cl \longrightarrow 3\,Cl + O_2 \quad (B.70)$$
$$CCl_4 + O(^1D) \longrightarrow 4\,Cl + R \quad (B.71)$$
$$CH_3CCl_3 + O(^1D) \longrightarrow 3\,Cl + R \quad (B.72)$$
$$CH_3CCl_3 + OH \longrightarrow 3\,Cl + R \quad (B.73)$$
$$CH_3Cl + O(^1D) \longrightarrow Cl + R \quad (B.74)$$
$$CH_3Cl + OH \longrightarrow Cl + R \quad (B.75)$$
$$CHF_2Cl + O(^1D) \longrightarrow Cl + R \quad (B.76)$$
$$CHF_2Cl + OH \longrightarrow Cl + R \quad (B.77)$$
$$C_2F_3Cl_3 + O(^1D) \longrightarrow 3\,Cl + R \quad (B.78)$$
$$NO_2 + NO_3 + M \longrightarrow N_2O_5 + M \quad (B.79)$$
$$N_2O_5 + M \longrightarrow NO_2 + NO_3 + M \quad (B.80)$$
$$NO_3 + NO \longrightarrow NO_2 + NO_2 \quad (B.81)$$
$$NO_3 + O \longrightarrow NO_2 + O_2 \quad (B.82)$$
$$CH_3 + O_2 + M \longrightarrow CH_3O_2 + M \quad (B.83)$$
$$CH_3O_2 + NO \longrightarrow CH_3O + NO_2 \quad (B.84)$$
$$CH_3O_2 + HO_2 \longrightarrow CH_3OOH + O_2 \quad (B.85)$$
$$CH_3O_2 + CH_3O_2 \longrightarrow 2\,CH_3O + O_2 \quad (B.86)$$
$$CH_3OOH + OH \longrightarrow CH_3O_2 + H_2O \quad (B.87)$$
$$CH_3OOH + OH \longrightarrow HCHO + OH + H_2O \quad (B.88)$$
$$CH_3O + O_2 \longrightarrow HCHO + HO_2 \quad (B.89)$$
$$HCHO + OH \longrightarrow CHO + H_2O \quad (B.90)$$
$$HCHO + O \longrightarrow CHO + OH \quad (B.91)$$
$$HCO + O_2 \longrightarrow CO + HO_2 \quad (B.92)$$
$$H_2 + OH \longrightarrow H_2O + H \quad (B.93)$$
$$HCHO + Cl \longrightarrow HCl + CHO \quad (B.94)$$
$$HCHO + \text{rain} \longrightarrow \quad (B.95)$$

$$CH_3Br + OH \longrightarrow Br + R \quad (B.96)$$
$$CClBrF_2 + O(^1D) \longrightarrow Br + Cl + COF_2 + R \quad (B.97)$$
$$CBrF_3 + O(^1D) \longrightarrow Br + COF_2 + HF + R \quad (B.98)$$
$$CH_3OOH + \text{rain} \longrightarrow \quad (B.99)$$
$$CH_3O_2 + ClO \longrightarrow Cl + CH_3O + O_2 \quad (B.100)$$
$$Br + O_3 \longrightarrow BrO + O_2 \quad (B.101)$$
$$BrO + O \longrightarrow Br + O_2 \quad (B.102)$$
$$BrO + NO \longrightarrow Br + NO_2 \quad (B.103)$$
$$BrO + OH \longrightarrow Br + HO_2 \quad (B.104)$$
$$BrO + ClO \longrightarrow Br + OClO \quad (B.105)$$
$$BrO + ClO \longrightarrow Br + Cl + O_2 \quad (B.106)$$
$$BrO + ClO \longrightarrow BrCl + O_2 \quad (B.107)$$
$$BrO + BrO \longrightarrow Br + Br + O_2 \quad (B.108)$$
$$BrO + NO_2 + M \longrightarrow BrONO_2 + M \quad (B.109)$$
$$BrO + HO_2 \longrightarrow HOBr + O_2 \quad (B.110)$$
$$BrO + HO_2 \longrightarrow HBr + O_3 \quad (B.111)$$
$$HOBr + O \longrightarrow BrO + OH \quad (B.112)$$
$$Br + HCHO \longrightarrow HBr + HCO \quad (B.113)$$
$$Br + HO_2 \longrightarrow HBr + O_2 \quad (B.114)$$
$$HBr + OH \longrightarrow Br + H_2O \quad (B.115)$$
$$HBr + O(^1D) \longrightarrow Br + OH \quad (B.116)$$
$$HBr + O \longrightarrow Br + OH \quad (B.117)$$
$$CH_3Br + O(^1D) \longrightarrow Br + R \quad (B.118)$$
$$BrONO_2 + O \longrightarrow BrO + NO_3 \quad (B.119)$$
$$CH_2Br_2 + O(^1D) \longrightarrow 2\,Br + R \quad (B.120)$$
$$CH_2Br_2 + OH \longrightarrow 2\,Br + R \quad (B.121)$$
$$CHBr_3 + O(^1D) \longrightarrow 3\,Br + R \quad (B.122)$$
$$CHBr_3 + OH \longrightarrow 3\,Br + R \quad (B.123)$$
$$COF_2 + O(^1D) \longrightarrow 2\,HF + R \quad (B.124)$$
$$COFCl + O(^1D) \longrightarrow HF + Cl + R \quad (B.125)$$

B.2. Heterogeneous Reactions

$$N_2O_5(g) + H_2O(s) \longrightarrow 2\,HNO_3(s) \quad (B.126)$$
$$ClONO_2(g) + H_2O(s) \longrightarrow HOCl(g) + HNO_3(s) \quad (B.127)$$
$$ClONO_2(g) + HCl(s) \longrightarrow 2\,Cl(g) + HNO_3(s) \quad (B.128)$$
$$N_2O_5(g) + HCl(s) \longrightarrow Cl(g) + NO_2(g) + HNO_3(s) \quad (B.129)$$
$$HOCl(g) + HCl(s) \longrightarrow 2\,Cl(g) + H_2O(s) \quad (B.130)$$
$$HOBr(g) + HBr(s) \longrightarrow 2\,Br(g) + H_2O(s) \quad (B.131)$$
$$HOBr(g) + HCl(s) \longrightarrow BrCl(g) + H_2O(s) \quad (B.132)$$
$$HOCl(g) + HBr(s) \longrightarrow BrCl(g) + H_2O(s) \quad (B.133)$$
$$BrONO_2(g) + HBr(s) \longrightarrow 2\,Br(g) + HNO_3(s) \quad (B.134)$$
$$BrONO_2(g) + HCl(s) \longrightarrow BrCl(g) + HNO_3(s) \quad (B.135)$$
$$ClONO_2(g) + HBr(s) \longrightarrow BrCl(g) + HNO_3(s) \quad (B.136)$$
$$BrONO_2(g) + H_2O(s) \longrightarrow HOBr(g) + HNO_3(s) \quad (B.137)$$
$$N_2O_5(g) + HBr(s) \longrightarrow Br(g) + NO_2(g) + HNO_3(s) \quad (B.138)$$

B.3. Photolysis Reactions

$$O_2 + h\nu \longrightarrow 2\,O \quad \text{(B.139)}$$
$$O_3 + h\nu \longrightarrow O_2 + O \quad \text{(B.140)}$$
$$O_3 + h\nu \longrightarrow O_2 + O(^1D) \quad \text{(B.141)}$$
$$NO + h\nu \longrightarrow N + O \quad \text{(B.142)}$$
$$NO_2 + h\nu \longrightarrow NO + O \quad \text{(B.143)}$$
$$NO_3 + h\nu \longrightarrow NO + O_2 \quad \text{(B.144)}$$
$$NO_3 + h\nu \longrightarrow NO_2 + O \quad \text{(B.145)}$$
$$HNO_3 + h\nu \longrightarrow NO_2 + OH \quad \text{(B.146)}$$
$$HO_2NO_2 + h\nu \longrightarrow NO_2 + HO_2 \quad \text{(B.147)}$$
$$N_2O + h\nu \longrightarrow N_2 + O(^1D) \quad \text{(B.148)}$$
$$N_2O_5 + h\nu \longrightarrow NO_2 + NO_3 \quad \text{(B.149)}$$
$$H_2O + h\nu \longrightarrow OH + H \quad \text{(B.150)}$$
$$HO_2 + h\nu \longrightarrow OH + O \quad \text{(B.151)}$$
$$H_2O_2 + h\nu \longrightarrow 2\,OH \quad \text{(B.152)}$$
$$ClONO_2 + h\nu \longrightarrow Cl + NO_3 \quad \text{(B.153)}$$
$$ClONO_2 + h\nu \longrightarrow ClO + NO_2 \quad \text{(B.154)}$$
$$CF_2Cl_2 + h\nu \longrightarrow 2\,Cl + 2\,F + R \quad \text{(B.155)}$$
$$CHF_2Cl + h\nu \longrightarrow Cl + 2\,F + R \quad \text{(B.156)}$$
$$CF_2CFCl_2 + h\nu \longrightarrow 2\,Cl + 2\,F + R \quad \text{(B.157)}$$
$$CH_3Cl + h\nu \longrightarrow CH_3 + Cl \quad \text{(B.158)}$$
$$CCl_4 + h\nu \longrightarrow 4\,Cl + R \quad \text{(B.159)}$$
$$HCl + h\nu \longrightarrow H + Cl \quad \text{(B.160)}$$
$$HOCl + h\nu \longrightarrow OH + Cl \quad \text{(B.161)}$$
$$OClO + h\nu \longrightarrow O + ClO \quad \text{(B.162)}$$
$$ClO + h\nu \longrightarrow O + Cl \quad \text{(B.163)}$$
$$Cl_2O_2 + h\nu \longrightarrow O_2 + 2\,Cl \quad \text{(B.164)}$$
$$BrO + h\nu \longrightarrow Br + O \quad \text{(B.165)}$$
$$HOBr + h\nu \longrightarrow Br + OH \quad \text{(B.166)}$$
$$HBr + h\nu \longrightarrow Br + H \quad \text{(B.167)}$$
$$BrONO_2 + h\nu \longrightarrow Br + NO_3 \quad \text{(B.168)}$$
$$BrCl + h\nu \longrightarrow Br + Cl \quad \text{(B.169)}$$
$$HCHO + h\nu \longrightarrow H + CHO \quad \text{(B.170)}$$
$$HCHO + h\nu \longrightarrow H_2 + CO \quad \text{(B.171)}$$
$$CH_3OOH + h\nu \longrightarrow CH_3O + OH \quad \text{(B.172)}$$
$$CH_3Br + h\nu \longrightarrow Br + CH_3 \quad \text{(B.173)}$$
$$CH_3CCl_3 + h\nu \longrightarrow 3\,Cl + R \quad \text{(B.174)}$$
$$CHBr_3 + h\nu \longrightarrow 3\,Br + R \quad \text{(B.175)}$$
$$CH_2Br_2 + h\nu \longrightarrow 2\,Br + R \quad \text{(B.176)}$$
$$CH_4 + h\nu \longrightarrow CH_3 + H \quad \text{(B.177)}$$
$$CClBrF_2 + h\nu \longrightarrow Br + Cl + 2\,F + R \quad \text{(B.178)}$$
$$CBrF_3 + h\nu \longrightarrow Br + 3\,F + R \quad \text{(B.179)}$$
$$COF_2 + h\nu \longrightarrow 2\,F + R \quad \text{(B.180)}$$
$$COFCl + h\nu \longrightarrow Cl + F + R \quad \text{(B.181)}$$

Appendix C.

Glossary and Abbreviations

Abbreviations

3-D Three-dimensional.

AoA Age of Air; refers to a passive tracer utilized to determine the mean age of the modeled atmosphere.

AVE Aura Validation Experiment; in this work data from the Pre-AVE and Cr-AVE campaign is used.

B3DCTM Bremen 3D CTM; CTM framework originally developed by Sinnhuber et al. (2003a).

BL (Planetary) Boundary Layer.

CAPE Convectively Available Potential Energy.

CCM Coupled Chemistry-Climate Model.

CFC ChloroFluoroCarbon.

CTM Chemistry Transport Model.

DJF December-January-February.

DU Dobson Unit; unit of measurement of total column ozone; corresponds to 2.69 $\times 10^{16}$ molec cm^{-2}.

ECMWF European Centre for Medium-Range Weather Forecasts.

ENSO El Niño Southern Oscillation.

FC*x* Denotes model run x with full chemistry setup, see appendix A, Table A.1.

GCM General Circulation Model.

HALOE HALogen Occultation Experiment, satellite-borne instrument.

ID*x* Denotes model run x with idealized setup, see appendix A, Table A.1.

ITCZ InterTropical Convergence Zone.

JJA June-July-August.

JPL Jet Propulsion Laboratory.

LNB Level of Neutral Buoyancy.

LPMA/DOAS Limb Profile Monitor of the Atmosphere/Differential Optical Absorption Spectroscopy; balloon-borne instrument.

LZRH Level of Zero clear sky Radiative Heating, located at around 360 K.

MAM March-April-May.

MBL Marine Boundary Layer.

NAT Nitric Acid Trihydrate.

NH Northern Hemisphere.

ODS Ozone Depleting Substances.

OSIRIS Optical Spectrograph and Infra-Red Imager System; satellite-borne instrument.

PGI Product Gas Injection, commonly refers to the injection of product gases into the stratosphere.

ppbv Part Per Billion by Volume; unit of volume mixing ratio.

ppmv Part Per Million by Volume; unit of volume mixing ratio.

pptv Part Per Trillion by Volume; unit of volume mixing ratio.
PSC Polar Stratospheric Cloud.
RH Relative Humidity with respect to ice.
SAOZ Systeme d'Analyse par Observations Zenithales; balloon-borne instrument.
SBUV Solar Backscatter UltraViolet, satellite-borne instrument.
SCIAMACHY Scanning Imaging Absorption Spectrometer for Atmospheric CHartographY; satellite-borne instrument.
SGI Source Gas Injection, commonly refers to the direct injection of source gases into the stratosphere.
SH Southern Hemisphere.
SHADOZ Southern Hemisphere ADditional OZonesondes, network of ozone sonde stations.
SLIMCAT In the context of this work this name denotes the chemistry scheme of the SLIMCAT CTM originally developed by Chipperfield et al. (1993).
SON September-October-November.
SST Sea Surface Temperature.
TO3 Total column ozone.
TOMS Total Ozone Mapping Spectrometer, satellite-borne instrument.
TT120 Test Tracer with 120 days lifetime; idealized CH_2Br_2 tracer.
TT20 Test Tracer with 20 days lifetime; idealized $CHBr_3$ tracer.
TTL Tropical Tropopause Layer.
UKMO United Kingdom Met Office.
UTC Coordinated Universal Time.
UTLS Upper Troposphere/Lower Stratosphere.
UV Ultra-Violet.
VMR Volume Mixing Ratio.
VSLS Very Short-Lived Substances; commonly refers to source gases whose average tropospheric lifetime is shorter than half a year.
WMO World Meteorological Organization.

Glossary

Artifact In this context artificial (unwanted) features in atmospheric models, for example in the trace gas distribution.
Brewer-Dobson Circulation Large-scale wave-driven circulation between low and high latitudes.
Cold Point Level that marks a local minimum in atmospheric temperature at the top of the tropopause, located at about 380 K.
Convective Updraft Refers to an upward directed flow of air driven by convection, typically accompanied by convective clouds.
Deep Convection Vigorous convective activity that is able to reach the upper troposphere and in rare cases the lower stratosphere.
Dehydration In this context refers to efficient removal of water vapor in the TTL.
Detrainment Refers to the flux of air out of a convective updraft.
El Niño/La Niña Recurrent anomaly of SST and convective activity predominantly located in the Western Pacific.
Entrainment Refers to the flux of air into a convective updraft.
ERA-Interim Data product based on model reanalyses provided by the ECMWF.
Heterogeneous Activation In this context refers to the transformation of halogen reservoir species into highly reactive radicals by reactions on aerosol or particle surfaces.

Isentropic Means "with constant potential temperature", e.g., an isentropic surface is a surface of constant potential temperature.

Maritime Continent Alias of the Southeast Asia region that comprises shallow seas and many islands.

Montreal Protocol Montreal Protocol on Substances That Deplete the Ozone Layer; international treaty to restrict production and usage of ozone depleting substances, signed in 1987.

Polar Vortex Large and persistent cyclone that forms over the poles in the corresponding winter season. Air within the vortex is relatively isolated from the surrounding mid latitudes.

Reservoir Species Commonly refers to halogen species which do not directly participate in ozone depletion.

Scavenging Refers to the removal of trace gases by rain or particle sedimentation.

Spin-Up In context of atmospheric modeling the time needed to minimize the impact of initialization artifacts.

Transport Efficiency In the context of this work refers to the efficiency of transport processes in a confined area, such as convection or advection, with respect to the injection of VSLS into the stratosphere.

Tropics In this study, the tropics are defined to be the region between 20°N to 20°S.

Symbols and Chemical Species

$\boldsymbol{A}$ Arrhenius frequency factor for bimolecular second-order reaction; unit: $\mathrm{cm^3 molec^{-1} s^{-1}}$.

$\boldsymbol{E/R}$ Activation energy coefficient; unit: $\mathrm{J mol^{-1}}$.

$\boldsymbol{W_s}$ Saturation mixing ratio of water vapor over ice.

$\bar{\boldsymbol{A}}$ Available particle surface area density; unit: $\mathrm{cm^2 cm^{-3}}$.

$\boldsymbol{\gamma}$ Heterogeneous uptake coefficient.

$[\boldsymbol{X}]_{\boldsymbol{c}}$ Detrainment mixing ratio of tracer X; unit: VMR.

$\boldsymbol{\theta}$ Potential temperature; vertical coordinate of the B3DCTM, unit: K.

$\boldsymbol{d_c}$ Detrainment rate; obtained from ECMWF ERA-Interim data set, denotes detrainment mass flux relative to the model grid box, unit: 1/s.

$\boldsymbol{k_g}$ Rate constant for bimolecular second-order reaction; unit: $\mathrm{cm^3 molec^{-1} s^{-1}}$.

$\boldsymbol{k_h}$ Rate constant for heterogeneous second-order reaction; unit: $\mathrm{cm^3 molec^{-1} s^{-1}}$.

$\boldsymbol{r}$ Correlation coefficient.

$\boldsymbol{r_e}$ Effective particle radius; unit: cm.

BrCl Bromine monochloride; bromine product gas, reservoir species.

$\mathbf{BrONO_2}$ Bromine nitrate; bromine product gas, reservoir species.

$\mathbf{BrO_x}$ Family of odd bromine species.

BrO Bromine monoxide; bromine product gas, reactive species, major constituent of stratospheric $\mathrm{Br_y}$.

$\mathbf{Br_y^{Long}}$ Inorganic bromine originated from long-lived source gases.

$\mathbf{Br_y^{VSLS}}$ Inorganic bromine originated from VSLS.

$\mathbf{Br_y^{ins}}$ Totally insoluble $\mathrm{Br_y}$ tracer in the idealized setup.

$\mathbf{Br_y^{sol}}$ Totally soluble $\mathrm{Br_y}$ tracer in the idealized setup.

$\mathbf{Br_y}$ Family of inorganic bromine product gases.

Br Atomic bromine; bromine product gas, reactive species.

$\mathbf{CBrF_3}$ Industrial name: Halon-1301; important long-lived bromine source gas.

$\mathbf{CClBrF_2}$ Industrial name: Halon-1211; important long-lived bromine source gas.

$\mathbf{CHBr_3}$ Bromoform; one of the major bromine VSLS.

$\mathbf{CH_2Br_2}$ Dibromomethane; one of the major bromine VSLS.

CH_3Br Methyl bromide; the most abundant long-lived bromine source gas.
Cl_y Family of inorganic chlorine product gases.
HBr Hydrogen bromide; bromine product gas, reservoir species, highly soluble on ice and in liquid water.
HOBr Hydrogen bromide; bromine product gas, reservoir species, highly soluble in liquid water.
HO_x Family of odd hydrogen species.
NO_x Family of odd nitrogen species.
O_3 Ozone.
O_x Family of odd oxygen species.

D. Bibliography

Aiuppa, A., Federico, C., Franco, A., Giudice, G., Gurrieri, S., Inguaggiato, S., Liuzzo, M., McGonigle, A. J. S., and Valenza, M.: Emission of bromine and iodine from Mount Etna volcano, Geochem. Geophy. Geosy., 6, doi:10.1029/2005GC000965, 2005.

Andrews, A. E., Boering, K. A., Daube, B. C., Wofsy, S. C., Hintsa, E. J., Weinstock, E. M., and Bui, T. P.: Empirical age spectra for the lower tropical stratosphere from in situ observations of CO_2: Implications for stratospheric transport, J. Geophys. Res.-Atmos., 104, 26 581–26 595, 1999.

Andrews, A. E., Boering, K. A., Daube, B. C., Wofsy, S. C., Loewenstein, M., Jost, H., Podolske, J. R., Webster, C. R., Herman, R. L., Scott, D. C., Flesch, G. J., Moyer, E. J., Elkins, J. W., Dutton, G. S., Hurst, D. F., Moore, F. L., Ray, E. A., Romashkin, P. A., and Strahan, S. E.: Mean ages of stratospheric air derived from in situ observations of CO_2, CH_4, and N_2O, J. Geophys. Res.-Atmos., 106, 32 295–32 314, 2001.

Andrews, D. G., Holton, J. R., and Leovy, C. B.: Middle atmosphere dynamics, Academic Press, 1987.

Aschmann, J., Sinnhuber, B.-M., Atlas, E. L., and Schauffler, S. M.: Modeling the transport of very short-lived substances into the tropical upper troposphere and lower stratosphere, Atmos. Chem. Phys., 9, 9237–9247, doi:10.5194/acp-9-9237-2009, 2009.

Aschmann, J., Sinnhuber, B.-M., Chipperfield, M. P., and Hossaini, R.: Impact of deep convection and dehydration on bromine loading in the upper troposphere and lower stratosphere, Atmos. Chem. Phys., 11, 2671–2687, doi:10.5194/acp-11-2671-2011, 2011.

Austin, J., Wilson, J., Li, F., and Vömel, H.: Evolution of water vapor concentrations and stratospheric age of air in coupled chemistry-climate model simulations, J. Atmos. Sci., 64, 905–921, doi:10.1175/JAS3866.1, 2007.

Balard, A.: Memoir on a peculiar Substance contained in Sea Water, Ann. Philos., 28, 381–387, 1826.

Barsugli, J. J. and Sardeshmukh, P. D.: Global atmospheric sensitivity to tropical SST anomalies throughout the Indo-Pacific basin, J. Climate, 15, 3427–3442, 2002.

Bates, D. R. and Nicolet, M.: Atmospheric hydrogen, Publ. Astron. Soc. Pac., 62, 106–110, 1950.

Berthet, G., Esler, J. G., and Haynes, P. H.: A Lagrangian perspective of the tropopause and the ventilation of the lowermost stratosphere, J. Geophys. Res.-Atmos., 112, doi:10.1029/2006JD008295, 2007.

Bobrowski, N., Hönninger, G., Galle, B., and Platt, U.: Detection of bromine monoxide in a volcanic plume, Nature, 423, 273–276, doi:10.1038/nature01638, 2003.

Boering, K. A., Wofsy, S. C., Daube, B. C., Schneider, H. R., Loewenstein, M., and Podolske, J. R.: Stratospheric mean ages and transport rates from observations of carbon dioxide and nitrous oxide, Science, 274, 1340–1343, 1996.

Böhm, H. P.: A General Equation for the Terminal Fall Speed of Solid Hydrometeors, J. Atmos. Sci., 46, 2419–2427, 1989.

Bönisch, H., Engel, A., Birner, T., Hoor, P., Tarasick, D. W., and Ray, E. A.: On the structural changes in the Brewer-Dobson circulation after 2000, Atmos. Chem. Phys., 11, 3937–3948, doi:10.5194/acp-11-3937-2011, 2011.

Bracher, A., Vountas, M., Dinter, T., Burrows, J. P., Röttgers, R., and Peeken, I.: Quantitative observation of cyanobacteria and diatoms from space using PhytoDOAS on SCIAMACHY data, Biogeosciences, 6, 751–764, 2009.

Brasseur, G. P. and Solomon, S.: Aeronomy of the Middle Atmosphere, Chemistry and Physics of the Stratosphere and Mesosphere, Springer, 3nd edition, 2005.

Brasseur, G. P., Orlando, J. J., and Tyndall, G. S.: Atmospheric Chemistry and Global Change, Oxford Univ. Press, 1999.

Brewer, A. W.: Evidence for a world circulation provided by the measurements of helium and water vapour distribution in the stratosphere, Q. J. Roy. Meteor. Soc., 75, 351–363, 1949.

Brioude, J., Portmann, R. W., Daniel, J. S., Cooper, O. R., Frost, G. J., Rosenlof, K. H., Granier, C., Ravishankara, A. R., Montzka, S. A., and Stohl, A.: Variations in ozone depletion potentials of very short-lived substances with season and emission region, Geophys. Res. Lett., 37, doi:10.1029/2010GL044856, 2010.

Burkholder, J. B., Wilson, R. R., Gierczak, T., Talukdar, R., McKeen, S. A., Orlando, J. J., Vaghjiani, G. L., and Ravishankara, A. R.: Atmospheric fate of CF_3Br, CF_2Br_2, CF_2ClBr, and CF_2BrCF_2Br, J. Geophys. Res.-Atmos., 96, 5025–5043, 1991.

Burkholder, J. B., Ravishankara, A. R., and Solomon, S.: UV visible and IR absorption cross-sections of $BrONO_2$, J. Geophys. Res.-Atmos., 100, 16 793–16 800, 1995.

Burrows, J. P., Weber, M., Buchwitz, M., Rozanov, V., Ladstätter-Weissenmayer, A., Richter, A., DeBeek, R., Hoogen, R., Bramstedt, K., Eichmann, K. U., and Eisinger, M.: The global ozone monitoring experiment (GOME): Mission concept and first scientific results, J. Atmos. Sci., 56, 151–175, 1999.

Butchart, N., Scaife, A. A., Bourqui, M., de Grandpre, J., Hare, S. H. E., Kettleborough, J., Langematz, U., Manzini, E., Sassi, F., Shibata, K., Shindell, D., and Sigmond, M.: Simulations of anthropogenic change in the strength of the Brewer-Dobson circulation, Clim. Dynam., 27, 727–741, doi:10.1007/s00382-006-0162-4, 2006.

Butler, J. H., King, D. B., Lobert, J. M., Montzka, S. A., Yvon-Lewis, S. A., Hall, B. D., Warwick, N. J., Mondeel, D. J., Aydin, M., and Elkins, J. W.: Oceanic distributions and emissions of short-lived halocarbons, Global Biogeochem. Cy., 21, doi:10.1029/2006GB002732, 2007.

Butler, J. H., Bell, T. G., Hall, B. D., Quack, B., Carpenter, L. J., and Williams, J.: Technical Note: Ensuring consistent, global measurements of very short-lived halocarbon gases in the ocean and atmosphere, Atmos. Chem. Phys., 10, 327–330, 2010.

Carlotti, M., Ade, P. A. R., Carli, B., Ciarpallini, P., Cortesi, U., Griffin, M. J., Lepri, G., Mencaraglia, F., Murray, A. G., Nolt, I. G., Park, J. H., and Radostitz, J. V.: Measurement of stratospheric HBr using high-resolution far-infrared spectroscopy, Geophys. Res. Lett., 22, 3207–3210, 1995.

Carpenter, L. J. and Liss, P. S.: On temperate sources of bromoform and other reactive organic bromine gases, J. Geophys. Res.-Atmos., 105, 20 539–20 547, 2000.

Carpenter, L. J., Jones, C. E., Dunk, R. M., Hornsby, K. E., and Woeltjen, J.: Air-sea fluxes of biogenic bromine from the tropical and North Atlantic Ocean, Atmos. Chem. Phys., 9, 1805–1816, 2009.

Carslaw, K. S., Clegg, S. L., and Brimblecombe, P.: A thermodynamic model of the system HCl-HNO_3-H_2SO_4-H_2O, including solubilities of HBr, from less-than-200 to 328 K, J. Phys. Chem.-US, 99, 11 557–11 574, 1995a.

Carslaw, K. S., Luo, B. P., and Peter, T.: An analytic-expression for the composition of aqueous HNO_3-H_2SO_4 stratospheric aerosols including gas-phase removal of HNO_3, Geophys. Res. Lett., 22, 1877–1880, 1995b.

Chapman, S.: On ozone and atomic oxygen in the upper atmosphere, Philos. Mag., 10, 369–383, 1930.

Charney, J. G., Fjørtoft, R., and von Neumann, J.: Numerical Integration of the Barotropic Vorticity Equation, Tellus, 2, 237–254, 1950.

Chiang, J. C. H. and Sobel, A. H.: Tropical tropospheric temperature variations caused by ENSO and their influence on the remote tropical climate, J. Climate, 15, 2616–2631, 2002.

Chipperfield, M., Cariolle, D., Simon, P., Ramaroson, R., and Lary, D. J.: A Three-Dimensional Modeling Study of Trace Species in the Arctic Lower Stratosphere During Winter 1989–1990, J. Geophys. Res.-Atmos., 98, 7199–7218, 1993.

Chipperfield, M. P.: Multiannual simulations with a three-dimensional chemical transport model, J. Geophys. Res.-Atmos., 104, 1781–1805, 1999.

Chipperfield, M. P.: New version of the TOMCAT/SLIMCAT off-line chemical transport model: Intercomparison of stratospheric tracer experiments, Q. J. Roy. Meteor. Soc., 132, 1179–1203, doi:10.1256/qj.05.51, 2006.

Chuang, H., Huang, X., and Minschwaner, K.: Interannual variations of tropical upper tropospheric humidity and tropical rainy-region SST: Comparisons between models, reanalyses, and observations, J. Geophys. Res.-Atmos., 115, doi:10.1029/2010JD014205, 2010.

Corti, T., Luo, B. P., Peter, T., Vömel, H., and Fu, Q.: Mean radiative energy balance and vertical mass fluxes in the equatorial upper troposphere and lower stratosphere, Geophys. Res. Lett., 32, doi:10.1029/2004GL021889, 2005.

Courant, R., Friedrichs, K., and Lewy, H.: Über die partiellen Differenzengleichungen der mathematischen Physik, Math. Ann., 100, 32–74, 1928.

Crowley, J. N., Ammann, M., Cox, R. A., Hynes, R. G., Jenkin, M. E., Mellouki, A., Rossi, M. J., Troe, J., and Wallington, T. J.: Evaluated kinetic and photochemical data for atmospheric chemistry: Volume V – heterogeneous reactions on solid substrates, Atmos. Chem. Phys., 10, 9059–9223, doi:10.5194/acp-10-9059-2010, 2010.

Crutzen, P. J.: Influence of nitrogen oxides on atmospheric ozone content, Q. J. Roy. Meteor. Soc., 96, 320–327, 1970.

Crutzen, P. J. and Arnold, F.: Nitric-acid cloud formation in the cold antarctic stratosphere - a major cause for the springtime ozone hole, Nature, 324, 651–655, 1986.

Crutzen, P. J., Isaksen, I. S. A., and MxAfee, J. R.: Impact of chloro-carbon industry on ozone-layer, J. Geophys. Res.-Oc. Atm., 83, 345–363, 1978.

Daniel, J. S. and Velders, G. J. M.: A Focus on Information and Options for Policymakers, Scientific assessment of ozone depletion: 2010, Global Ozone Research and Monitoring Project. Report No. 52, Chapter 5, World Meteorological Organization, Geneva, Switzerland, 2010.

Daniel, J. S., Solomon, S., Portmann, R. W., and Garcia, R. R.: Stratospheric ozone destruction: The importance of bromine relative to chlorine, J. Geophys. Res.-Atmos., 104, 23 871–23 880, 1999.

Dee, D. P., Uppala, S. M., Simmons, A. J., Berrisford, P., Poli, P., Kobayashi, S., Andrae, U., Balmaseda, M. A., Balsamo, G., Bauer, P., Bechtold, P., Beljaars, A. C. M., van de Berg, L., Bidlot, J., Bormann, N., Delsol, C., Dragani, R., Fuentes, M., Geer, A. J., Haimberger, L., Healy, S. B., Hersbach, H., Hólm, E. V., Isaksen, L., Kållberg, P., Köhler, M., Matricardi, M., McNally, A. P., Monge-Sanz, B. M., Morcrette, J.-J., Park, B.-K., Peubey, C., de Rosnay, P., Tavolato, C., Thépaut, J.-N., and Vitart, F.: The ERA-Interim reanalysis: configuration and performance of the data assimilation system, Q. J. Roy. Meteor. Soc., 137, 553–597, doi:10.1002/qj.828, 2011.

Dessens, O., Zeng, G., Warwick, N., and Pyle, J.: Short-lived bromine compounds in the lower stratosphere; impact of climate change on ozone, Atmos. Sci. Lett., 10, 201–206, doi:10.1002/asl.236, 2009.

Dessler, A. E.: The effect of deep, tropical convection on the tropical tropopause layer, J. Geophys. Res.-Atmos., 107, doi:10.1029/2001JD000511, 2002.

Dessler, A. E. and Sherwood, S. C.: Effect of convection on the summertime extratropical lower stratosphere, J. Geophys. Res.-Atmos., 109, doi:10.1029/2004JD005209, 2004.

Dobson, G. M. B.: Origin and distribution of the polyatomic molecules in the atmosphere, P. Roy. Soc. Lond. A Mat., 236, 187–193, 1956.

Dong, B., Gregory, J. M., and Sutton, R. T.: Understanding Land-Sea Warming Contrast in Response to Increasing Greenhouse Gases. Part I: Transient Adjustment, J. Climate, 22, 3079–3097, doi:10.1175/2009JCLI2652.1, 2009.

Dorf, M., Butz, A., Camy-Peyret, C., Chipperfield, M. P., Kritten, L., and Pfeilsticker, K.: Bromine in the tropical troposphere and stratosphere as derived from balloon-borne BrO observations, Atmos. Chem. Phys., 8, 7265–7271, 2008.

Dvortsov, V. L., Geller, M. A., Solomon, S., Schauffler, S. M., Atlas, E. L., and Blake, D. R.: Rethinking reactive halogen budgets in the midlatitude lower stratosphere, Geophys. Res. Lett., 26, 1699–1702, 1999.

ECMWF: IFS documentation CY36r1, URL `http://www.ecmwf.int/research/ifsdocs/CY36r1/index.html`, last access 9-May-2011, 2009.

Elkins, J. W., Fahey, D. W., Gilligan, J. M., Dutton, G. S., Baring, T. J., Volk, C. M., Dunn, R. E., Myers, R. C., Montzka, S. A., Wamsley, P. R., Hayden, A. H., Butler, J. H., Thompson, T. M., Swanson, T. H., Dlugokencky, E. J., Novelli, P. C., Hurst, D. F., Lobert, J. M., Ciciora, S. J., McLaughlin, R. J., Thompson, T. L., Winkler, R. H., Fraser, P. J., Steele, L. P., and Lucarelli, M. P.: Airborne gas chromatograph for in situ measurements of long-lived species in the upper troposphere and lower stratosphere, Geophys. Res. Lett., 23, 347–350, 1996.

Evensen, G.: Data Assimilation, The Ensemble Kalman Filter, Springer, 2nd edition, 2009.

Eyring, V., Harris, N. R. P., Rex, M., Shepherd, T. G., Fahey, D. W., Amanatidis, G. T., Austin, J., Chipperfield, M. P., Dameris, M., Forster, P. M. F., Gettelman, A., Graf, H. F., Nagashima, T., Newman, P. A., Pawson, S., Prather, M. J., Pyle, J. A., Salawitch, R. J., Santer, B. D., and Waugh, D. W.: A strategy for process-oriented validation of coupled chemistry-climate models, Bull. Am. Meteorol. Soc., 86, 1117–1133, doi:10.1175/BAMS-86-8-1117, 2005.

Eyring, V., Cionni, I., Bodeker, G. E., et al.: Multi-model assessment of stratospheric ozone return dates and ozone recovery in CCMVal-2 models, Atmos. Chem. Phys., 10, 9451–9472, doi:10.5194/acp-10-9451-2010, 2010.

Farman, J. C., Gardiner, B. G., and Shanklin, J. D.: Large losses of total ozone in antarctica reveal seasonal ClOX/NOX interaction, Nature, 315, 207–210, 1985.

Feng, W., Chipperfield, M. P., Davies, S., Sen, B., Toon, G., Blavier, J. F., Webster, C. R., Volk, C. M., Ulanovsky, A., Ravegnani, F., von der Gathen, P., Jost, H., Richard, E. C., and Claude, H.: Three-dimensional model study of the Arctic ozone loss in 2002/2003 and comparison with 1999/2000 and 2003/2004, Atmos. Chem. Phys., 5, 139–152, 2005.

Feng, W., Chipperfield, M. P., Dorf, M., Pfeilsticker, K., and Ricaud, P.: Mid-latitude ozone changes: studies with a 3-D CTM forced by ERA-40 analyses, Atmos. Chem. Phys., 7, 2357–2369, 2007.

Fitzenberger, R., Bosch, H., Camy-Peyret, C., Chipperfield, M. P., Harder, H., Platt, U., Sinnhuber, B.-M., Wagner, T., and Pfeilsticker, K.: First profile measurements of tropospheric BrO, Geophys. Res. Lett., 27, 2921–2924, 2000.

Folkins, I. and Martin, R. V.: The vertical structure of tropical convection and its impact on the budgets of water vapor and ozone, J. Atmos. Sci., 62, 1560–1573, 2005.

Folkins, I., Kelly, K. K., and Weinstock, E. M.: A simple explanation for the increase in relative humidity between 11 and 14 km in the tropics, J. Geophys. Res.-Atmos., 107, doi:10.1029/2002JD002185, 2002.

Fortuin, J. F. P. and Kelder, H.: An ozone climatology based on ozonesondes and satellite measurements, J. Geophys. Res., 103, 31 709–31 734, 1998.

Fueglistaler, S., Bonazzola, M., Haynes, P. H., and Peter, T.: Stratospheric water vapor predicted from the Lagrangian temperature history of air entering the stratosphere in the tropics, J. Geophys. Res.-Atmos., 110, doi:10.1029/2004JD005516, 2005.

Fueglistaler, S., Dessler, A. E., Dunkerton, T. J., Folkins, I., Fu, Q., and Mote, P. W.: Tropical Tropopause Layer, Rev. Geophys., 47, doi:10.1029/2008RG000267, 2009a.

Fueglistaler, S., Legras, B., Beljaars, A., Morcrette, J.-J., Simmons, A., Tompkins, A. M., and Uppala, S.: The diabatic heat budget of the upper troposphere and lower/mid stratosphere in ECMWF reanalyses, Q. J. Roy. Meteor. Soc., 135, 21–37, doi:10.1002/qj.361, 2009b.

Gettelman, A., Randel, W. J., Wu, F., and Massie, S. T.: Transport of water vapor in the tropical tropopause layer, Geophys. Res. Lett., 29, doi:10.1029/2001GL013818, 2002a.

Gettelman, A., Salby, M. L., and Sassi, F.: Distribution and influence of convection in the tropical tropopause region, J. Geophys. Res.-Atmos., 107, doi:10.1029/2001JD001048, 2002b.

Gettelman, A., Lauritzen, P. H., Park, M., and Kay, J. E.: Processes regulating short-lived species in the tropical tropopause layer, J. Geophys. Res.-Atmos., 114, doi:10.1029/2009JD011785, 2009.

Gilles, M. K., Turnipseed, A. A., Burkholder, J. B., Ravishankara, A. R., and Solomon, S.: Kinetics of the IO radical .2. Reaction of IO with BrO, J. Phys. Chem. A, 101, 5526–5534, 1997.

Gillotay, D., Simon, P. C., and Dierickx, L.: Temperature dependence of ultraviolet absorption cross-sections of brominated methanes and ethanes, Aeronomica Acta A 355, pp. 1–25, 1988.

Gillotay, D., Jenouvrier, A., Coquart, B., Merienne, M. F., and Simon, P. C.: Ultraviolet-absorption cross-sections of bromoform in the temperature-range 295-240K, Planet. Space Sci., 37, 1127–1140, 1989.

Grooß J.-U. and Russell, J. M. I.: Technical note: A stratospheric climatology for O_3, H_2O, CH_4, NO_x, HCl and HF derived from HALOE measurements, Atmos. Chem. Phys., 5, 2797–2807, doi:10.5194/acp-5-2797-2005, 2005.

Guilyardi, E., Braconnot, P., Jin, F.-F., Kim, S. T., Kolasinski, M., Li, T., and Musat, I.: Atmosphere Feedbacks during ENSO in a Coupled GCM with a Modified Atmospheric Convection Scheme, J. Climate, 22, 5698–5718, doi:10.1175/2009JCLI2815.1, 2009.

Hall, T. M., Waugh, D. W., Boering, K. A., and Plumb, R. A.: Evaluation of transport in stratospheric models, J. Geophys. Res.-Atmos., 104, 18 815–18 839, 1999.

Hanisco, T. F., Moyer, E. J., Weinstock, E. M., St. Clair, J. M., Sayres, D. S., Smith, J. B., Lockwood, R., Anderson, J. G., Dessler, A. E., Keutsch, F. N., Spackman, J. R., Read, W. G., and Bui, T. P.: Observations of deep convective influence on stratospheric water vapor and its isotopic composition, Geophys. Res. Lett., 34, doi:10.1029/2006GL027899, 2007.

Hanson, D. and Mauersberger, K.: Laboratory studies of the nitric-acid trihydrate - implications for the south polar stratosphere, Geophys. Res. Lett., 15, 855–858, 1988.

Harnisch, J., Borchers, R., Fabian, P., and Maiss, M.: Tropospheric trends for CF_4 and C_2F_6 since 1982 derived from SF_6 dated stratospheric air, Geophys. Res. Lett., 23, 1099–1102, 1996.

Hausmann, M. and Platt, U.: Spectroscopic measurement of bromine oxide and ozone in the high arctic during polar sunrise experiment 1992, J. Geophys. Res.-Atmos., 99, 25 399–25 413, 1994.

Hense, I. and Quack, B.: Modelling the vertical distribution of bromoform in the upper water column of the tropical Atlantic Ocean, Biogeosciences, 6, 535–544, 2009.

Heue, K.-P., Brenninkmeijer, C. A. M., Baker, A. K., Rauthe-Schoech, A., Walter, D., Wagner, T., Hörmann, C., Sihler, H., Dix, B., Frieß U., Platt, U., Martinsson, B. G., van Velthoven, P. F. J., Zahn, A., and Ebinghaus, R.: SO_2 and BrO observation in the plume of the Eyjafjallajökull volcano 2010: CARIBIC and GOME-2 retrievals, Atmos. Chem. Phys., 11, 2973–2989, doi:10.5194/acp-11-2973-2011, 2011.

Hollwedel, J., Wenig, M., Beirle, S., Kraus, S., Kuhl, S., Wilms-Grabe, W., Platt, U., and Wagner, T.: Year-to-year variations of spring time polar tropospheric BrO as seen by GOME, in: Trace constituents in the troposphere and lower stratosphere, edited by Burrows, J. P. and Thompson, A. M., vol. 34 of *Adv. Space Res.*, pp. 804–808, doi:10.1016/j.asr.2003.08.060, 2004.

Holton, J. R. and Gettelman, A.: Horizontal transport and the dehydration of the stratosphere, Geophys. Res. Lett., 28, 2799–2802, 2001.

Holton, J. R., Haynes, P. H., Mcintyre, M. E., Douglass, A. R., Rood, R. B., and Pfister, L.: Stratosphere-Troposphere Exchange, Rev. Geophys., 33, 403–439, 1995.

Höpfner, M., Orphal, J., von Clarmann, T., Stiller, G., and Fischer, H.: Stratospheric $BrONO_2$ observed by MIPAS, Atmos. Chem. Phys., 9, 1735–1746, 2009.

Hossaini, R., Chipperfield, M. P., Monge-Sanz, B. M., Richards, N. A. D., Atlas, E., and Blake, D. R.: Bromoform and dibromomethane in the tropics: a 3-D model study of chemistry and transport, Atmos. Chem. Phys., 10, 719–735, doi:10.5194/acp-10-719-2010, 2010.

Ingham, T., Bauer, D., Landgraf, J., and Crowley, J. N.: Ultraviolet-visible absorption cross sections of gaseous HOBr, J. Phys. Chem. A, 102, 3293–3298, 1998.

Jain, A. R., Das, S. S., Mandal, T. K., and Mitra, A. P.: Observations of extremely low tropopause temperature over the Indian tropical region during monsoon and postmonsoon months: Possible implications, J. Geophys. Res.-Atmos., 111, doi:10.1029/2005JD005850, 2006.

Jiang, J. H. et al.: Five year (2004–2009) observations of upper tropospheric water vapor and cloud ice from MLS and comparisons with GEOS-5 analyses, J. Geophys. Res.-Atmos., 115, doi:10.1029/2009JD013256, 2010.

Johnson, D. G., Traub, W. A., Chance, K. V., and Jucks, K. W.: Detection of HBr and upper limit for HOBr - bromine partitioning in the stratosphere, Geophys. Res. Lett., 22, 1373–1376, 1995.

Jorgensen, D. P. and LeMone, M. A.: Vertical velocity characteristics of oceanic convection, J. Atmos. Sci., 46, 621–640, 1989.

Kerkweg, A., Jöckel, P., Warwick, N., Gebhardt, S., Brenninkmeijer, C. A. M., and Lelieveld, J.: Consistent simulation of bromine chemistry from the marine boundary layer to the stratosphere - Part 2: Bromocarbons, Atmos. Chem. Phys., 8, 5919–5939, 2008.

Kiesewetter, G., Sinnhuber, B.-M., Vountas, M., Weber, M., and Burrows, J. P.: A long-term stratospheric ozone data set from assimilation of satellite observations: High-latitude ozone anomalies, J. Geophys. Res.-Atmos., 115, doi:10.1029/2009JD013362, 2010a.

Kiesewetter, G., Sinnhuber, B.-M., Weber, M., and Burrows, J. P.: Attribution of stratospheric ozone trends to chemistry and transport: a modelling study, Atmos. Chem. Phys., 10, 12 073–12 089, doi:10.5194/acp-10-12073-2010, 2010b.

Ko, M. K. W., Sze, N. D., Scott, C. J., and Weisenstein, D. K.: On the relation between stratospheric chlorine/bromine loading and short-lived tropospheric source gases, J. Geophys. Res.-Atmos., 102, 25 507–25 517, 1997.

Kobayashi, S., Matricardi, M., Dee, D., and Uppala, S.: Toward a consistent reanalysis of the upper stratosphere based on radiance measurements from SSU and AMSU-A, Q. J. Roy. Meteor. Soc., 135, 2086–2099, doi:10.1002/qj.514, 2009.

Kreher, K., Johnston, P. V., Wood, S. W., Nardi, B., and Platt, U.: Ground-based measurements of tropospheric and stratospheric BrO at Arrival Heights, Antarctica, Geophys. Res. Lett., 24, 3021–3024, 1997.

Krüger, K., Tegtmeier, S., and Rex, M.: Variability of residence time in the Tropical Tropopause Layer during Northern Hemisphere winter, Atmos. Chem. Phys., 9, 6717–6725, 2009.

Kumar, A., Yang, F. L., Goddard, L., and Schubert, S.: Differing trends in the tropical surface temperatures and precipitation over land and oceans, J. Climate, 17, 653–664, 2004.

Lary, D. J.: Gas phase atmospheric bromine photochemistry, J. Geophys. Res.-Atmos., 101, 1505–1516, 1996.

Lary, D. J. and Pyle, J. A.: Diffuse-radiation, twilight, and photochemistry 1., J. Atmos. Chem., 13, 373–392, 1991.

Laube, J. C., Engel, A., Bönisch, H., Moebius, T., Worton, D. R., Sturges, W. T., Grunow, K., and Schmidt, U.: Contribution of very short-lived organic substances to stratospheric chlorine and bromine in the tropics - a case study, Atmos. Chem. Phys., 8, 7325–7334, 2008.

Law, K. S. and Sturges, W. T.: Halogenated very short-lived substances, Scientific assessment of ozone depletion: 2006, Global Ozone Research and Monitoring Project. Report No. 50, Chapter 2, World Meteorological Organization, Geneva, Switzerland, 2007.

Li, F., Austin, J., and Wilson, J.: The strength of the Brewer-Dobson circulation in a changing climate: Coupled chemistry-climate model simulations, J. Climate, 21, 40–57, doi:10.1175/2007JCLI1663.1, 2008.

Liang, Q., Stolarski, R. S., Kawa, S. R., Nielsen, J. E., Douglass, A. R., Rodriguez, J. M., Blake, D. R., Atlas, E. L., and Ott, L. E.: Finding the missing stratospheric Br-y: a global modeling study of $CHBr_3$ and CH_2Br_2, Atmos. Chem. Phys., 10, 2269–2286, 2010.

Liu, C. T. and Zipser, E. J.: Global distribution of convection penetrating the tropical tropopause, J. Geophys. Res.-Atmos., 110, doi:10.1029/2005JD006063, 2005.

Lowe, D. and MacKenzie, A. R.: Polar stratospheric cloud microphysics and chemistry, J. Atmos. Sol.-Terr. Phy., 70, 13–40, doi:10.1016/j.jastp.2007.09.011, 2008.

Löwig, C.: Ueber Brombereitung und eine auffallende Zersetzung des Aethers durch Chlor, Mag. Pharma., 21, 31–36, 1828.

Lynch, P.: The origins of computer weather prediction and climate modeling, J. Comput. Phys., 227, 3431–3444, doi:10.1016/j.jcp.2007.02.034, 2008.

Maric, D., Burrows, J. P., and Moortgat, G. K.: A study of the UV-visible absorption-spectra of Br_2 and BrCl, J. Photoch. Photobio. A, 83, 179–192, 1994.

Marti, J. and Mauersberger, K.: A survey and new measurements of ice vapor-pressure at temperatures between 170 and 250 K, Geophys. Res. Lett., 20, 363–366, 1993.

McCormick, M. P., Steele, H. M., Hamill, P., Chu, W. P., and Swissler, T. J.: Polar stratospheric cloud sightings by SAM-II, J. Atm. Sci., 39, 1387–1397, 1982.

McCormick, M. P., Thomason, L. W., and Trepte, C. R.: Atmospheric effects of the Mt-Pinatubo Eruption, Nature, 373, 399–404, 1995.

McElroy, C. T., McLinden, C. A., and McConnell, J. C.: Evidence for bromine monoxide in the free troposphere during the Arctic polar sunrise, Nature, 397, 338–341, 1999.

McElroy, M. B., Salawitch, R. J., Wofsy, S. C., and Logan, J. A.: Reductions of antarctic ozone due to synergistic interactions of chlorine and bromine, Nature, 321, 759–762, 1986.

McLinden, C. A., Olsen, S. C., Hannegan, B., Wild, O., Prather, M. J., and Sundet, J.: Stratospheric ozone in 3-D models: A simple chemistry and the cross-tropopause flux, J. Geophys. Res.-Atmos., 105, 14 653–14 665, 2000.

McLinden, C. A., Haley, C. S., Lloyd, N. D., Hendrick, F., Rozanov, A., Sinnhuber, B.-M., Goutail, F., Degenstein, D. A., Llewellyn, E. J., Sioris, C. E., Van Roozendael, M., Pommereau, J.-P., Lotz, W., and Burrows, J. P.: Odin/OSIRIS observations of stratospheric BrO: Retrieval methodology, climatology, and inferred Br_y, J. Geophys. Res.-Atmos., 115, doi:10.1029/2009JD012488, 2010.

Meier, R. R., Anderson, D. E., and Nicolet, M.: Radiation-field in the troposphere and stratosphere from 240-1000 nm - 1. General-analysis, Planet. Space Sci., 30, 923–933, 1982.

Molina, L. T. and Molina, M. J.: Production of Cl_2O_2 from the self-reaction of the ClO radical, J. Phys. Chem., 91, 433–436, 1987.

Molina, M. J. and Rowland, F. S.: Stratospheric sink for chlorofluoromethanes - chlorine atomic-catalysed destruction of ozone, Nature, 249, 810–812, 1974.

Montzka, S. A. and Reimann, S.: Ozone-Depleting Substances (ODSs) and Related Chemicals, Scientific assessment of ozone depletion: 2010, Global Ozone Research and Monitoring Project. Report No. 52, Chapter 1, World Meteorological Organization, Geneva, Switzerland, 2010.

Mote, P. W., Rosenlof, K. H., Holton, J. R., Harwood, R. S., and Waters, J. W.: Seasonal-variations of water-vapor in the tropical lower stratosphere, Geophys. Res. Lett., 22, 1093–1096, 1995.

Nee, J. B., Suto, M., and Lee, L. C.: Quantitative spectroscopy study of HBr in the 105-235 nm region, J. Chem. Phys., 85, 4919–4924, 1986.

Nielsen, J. E. and Douglass, A. R.: Simulation of bromoform's contribution to stratospheric bromine, J. Geophys. Res.-Atmos., 106, 8089–8100, 2001.

NOAA: U.S. Standard Atmosphere, 1976, Tech. Rep. NOAA-S/T 76-1562, U.S. Government Printing Office, 1976.

Nolt, I. G., Ade, P. A. R., Alboni, F., Carli, B., Carlotti, M., Cortesi, U., Epifani, M., Griffin, M. J., Hamilton, P. A., Lee, C., Lepri, G., Mencaraglia, F., Murray, A. G., Park, J. H., Park, K., Raspollini, P., Ridolfi, M., and Vanek, M. D.: Stratospheric HBr concentration profile obtained from far-infrared emission spectroscopy, Geophys. Res. Lett., 24, 281–284, 1997.

Notholt, J., Luo, B. P., Fueglistaler, S., Weisenstein, D., Rex, M., Lawrence, M. G., Bingemer, H., Wohltmann, I., Corti, T., Warneke, T., von Kuhlmann, R., and Peter, T.: Influence of tropospheric SO_2 emissions on particle formation and the stratospheric humidity, Geophys. Res. Lett., 32, doi:10.1029/2004GL022159, 2005.

Oman, L., Waugh, D. W., Pawson, S., Stolarski, R. S., and Newman, P. A.: On the influence of anthropogenic forcings on changes in the stratospheric mean age, J. Geophys. Res.-Atmos., 114, doi:10.1029/2008JD010378, 2009.

Oppenheimer, C., Tsanev, V. I., Braban, C. F., Cox, R. A., Adams, J. W., Aiuppa, A., Bobrowski, N., Delmelle, P., Barclay, J., and McGonigle, A. J. S.: BrO formation in volcanic plumes, Geochim. Cosmochim. Ac., 70, 2935–2941, doi:10.1016/j.gca.2006.04.001, 2006.

Palmer, C. J. and Reason, C. J.: Relationships of surface bromoform concentrations with mixed layer depth and salinity in the tropical oceans, Global Biogeochem .Cy., 23, doi:10.1029/2008GB003338, 2009.

Pfeilsticker, K., Sturges, W. T., Bosch, H., Camy-Peyret, C., Chipperfield, M. P., Engel, A., Fitzenberger, R., Müller, M., Payan, S., and Sinnhuber, B.-M.: Lower stratospheric organic and inorganic bromine budget for the Arctic winter 1998/99, Geophys. Res. Lett., 27, 3305–3308, 2000.

Pisso, I., Haynes, P. H., and Law, K. S.: Emission location dependent ozone depletion potentials for very short-lived halogenated species, Atmos. Chem. Phys., 10, 12 025–12 036, doi:10.5194/acp-10-12025-2010, 2010.

Platt, U. and Hönninger, G.: The role of halogen species in the troposphere, Chemosphere, 52, 325–338, doi:10.1016/S0045-6535(03)00216-9, 2003.

Ploeger, F., Konopka, P., Günther, G., Grooß J.-U., and Müller, R.: Impact of the vertical velocity scheme on modeling transport in the tropical tropopause layer, J. Geophys. Res.-Atmos., 115, doi:10.1029/2009JD012023, 2010.

Poulet, G., Pirre, M., Maguin, F., Ramaroson, R., and Lebras, G.: Role of the BrO + HO_2 reaction in the stratospheric chemistry of bromine, Geophys. Res. Lett., 19, 2305–2308, 1992.

Prather, M. J.: Numerical advection by conservation of 2nd-order moments, J. Geophys. Res.-Atmos., 91, 6671–6681, 1986.

Pundt, I., Pommereau, J.-P., Chipperfield, M. P., Van Roozendael, M., and Goutail, F.: Climatology of the stratospheric BrO vertical distribution by balloon-borne UV-visible spectrometry, J. Geophys. Res.-Atmos., 107, doi:10.1029/2002JD002230, 2002.

Pyle, D. M. and Mather, T. A.: Halogens in igneous processes and their fluxes to the atmosphere and oceans from volcanic activity: A review, Chem. Geol., 263, 110–121, doi:10.1016/j.chemgeo.2008.11.013, 2009.

Pyle, J. A., Warwick, N., Yang, X., Young, P. J., and Zeng, G.: Climate/chemistry feedbacks and biogenic emissions, Philos. T. R. Soc. A, 365, 1727–1740, doi:10.1098/rsta.2007.2041, 2007.

Quack, B. and Wallace, D. W. R.: Air-sea flux of bromoform: Controls, rates, and implications, Global Biochem. Cy., 17, doi:10.1029/2002GB001890, 2003.

Quack, B., Atlas, E., Petrick, G., and Wallace, D. W. R.: Bromoform and dibromomethane above the Mauritanian upwelling: Atmospheric distributions and oceanic emissions, J. Geophys. Res.-Atmos., 112, doi:10.1029/2006JD007614, 2007a.

Quack, B., Peeken, I., Petrick, G., and Nachtigall, K.: Oceanic distribution and sources of bromoform and dibromomethane in the Mauritanian upwelling, J. Geophys. Res.-Oceans, 112, doi:10.1029/2006JC003803, 2007b.

Ramanathan, V. and Collins, W.: Thermodynamic regulation of ocean warming by cirrus clouds deduced from observations of the 1987 El Nino, Nature, 351, 27–32, 1991.

Ramaroson, R., Pirre, M., and Cariolle, D.: A box model for on-line computations of diurnal variations in a 1D model: Potential for application to multidimensional cases, Ann. Geophys., 10, 416–428, 1992.

Rasch, P. J., Mahowald, N. M., and Eaton, B. E.: Representations of transport, convection, and the hydrologic cycle in chemical transport models: Implications for the modeling of short-lived and soluble species, J. Geophys. Res.-Atmos., 102, 28 127–28 138, 1997.

Ray, E. A., Moore, F. L., Elkins, J. W., Dutton, G. S., Fahey, D. W., Vömel, H., Oltmans, S. J., and Rosenlof, K. H.: Transport into the Northern Hemisphere lowermost stratosphere revealed by in situ tracer measurements, J. Geophys. Res.-Atmos., 104, 26 565–26 580, 1999.

Rayner, N. A., Parker, D. E., Horton, E. B., Folland, C. K., Alexander, L. V., Rowell, D. P., Kent, E. C., and Kaplan, A.: Global analyses of sea surface temperature, sea ice, and night marine air temperature since the late nineteenth century, J. Geophys. Res.-Atmos., 108, doi:10.1029/2002JD002670, 2003.

Read, W. G., Schwartz, M. J., Lambert, A., Su, H., Livesey, N. J., Daffer, W. H., and Boone, C. D.: The roles of convection, extratropical mixing, and in-situ freeze-drying in the Tropical Tropopause Layer, Atmos. Chem. Phys., 8, 6051–6067, 2008.

Richardson, L. F.: Weather Prediction by Numerical Process, Cambridge University Press, Cambridge, 1922.

Richter, A., Wittrock, F., Eisinger, M., and Burrows, J. P.: GOME observations of tropospheric BrO in northern hemispheric spring and summer 1997, Geophys. Res. Lett., 25, 2683–2686, 1998.

Richter, A., Wittrock, F., Ladstätter-Weissenmayer, A., and Burrows, J. P.: GOME measurements of stratospheric and tropospheric BrO, in: Remote sensing of trace constituents in the lower stratosphere, troposphere and the Earth's surface: Global observations, air pollution and the atmospheric correction, edited by Burrows, J. P. and Takeucki, N., vol. 29 of *Adv. Space Res.*, pp. 1667–1672, 2002.

Rodriguez, J. M., Ko, M. K. W., Sze, N. D., Pierce, S. D., Anderson, J. G., Fahey, D. W., Kelly, K., Farmer, C. B., Toon, G. C., Coffey, M. T., Heidt, L. E., Mankin, W. G., Chan, K. R., Starr, W. L., Vedder, J. F., and McCormick, M. P.: Nitrogen and chlorine species in the spring antarctic stratosphere - comparison of models with airborne antarctic ozone experiment observations, J. Geophys. Res.-Atmos., 94, 16 683–16 703, 1989.

Romps, D. M. and Kuang, Z.: Do Undiluted Convective Plumes Exist in the Upper Tropical Troposphere?, J. Atmos. Sci., 67, 468–484, doi:10.1175/2009JAS3184.1, 2010.

Rozanov, A., Kühl, S., Doicu, A., McLinden, C., Pukite, J., Bovensmann, H., Burrows, J., Deutschmann, T., Dorf, M., Goutail, F., Grunow, K., Hendrick, F., von Hobe, M., Hrechanyy, S., Lichtenberg, G., Pfeilsticker, K., Pommereau, J. P., Van Roozendael, M., Stroh, F., and Wagner, T.: BrO vertical distributions from SCIAMACHY limb measurements: comparison of algorithms and retrieval results, Atmos. Measur. Tech. Discuss., 3, 5079–5178, doi:10.5194/amtd-3-5079-2010, 2010a.

Rozanov, A., Weigel, K., Bovensmann, H., Dhomse, S., Eichmann, K.-U., Kivi, R., Rozanov, V., Vömel, H., Weber, M., and Burrows, J. P.: Retrieval of water vapor vertical distributions in the upper troposphere and the lower stratosphere from SCIAMACHY limb measurements, Atmos. Measur. Tech. Discuss., 3, 4009–4057, doi:10.5194/amtd-3-4009-2010, 2010b.

Rozanov, A., Eichmann, K.-U., von Savigny, C., Bovensmann, H., Burrows, J. P., von Bargen, A., Doicu, A., Hilgers, S., Godin-Beekmann, S., Leblanc, T., and McDermid, I. S.: Comparison of the inversion algorithms applied to the ozone vertical profile retrieval from SCIAMACHY limb measurements, Atmos. Chem. Phys., 7, 4763–4779, 2007.

Salawitch, R. J., Weisenstein, D. K., Kovalenko, L. J., Sioris, C. E., Wennberg, P. O., Chance, K., Ko, M. K. W., and McLinden, C. A.: Sensitivity of ozone to bromine in the lower stratosphere, Geophys. Res. Lett., 32, doi:10.1029/2004GL021504, 2005.

Salawitch, R. J., Canty, T., Kurosu, T., Chance, K., Liang, Q., da Silva, A., Pawson, S., Nielsen, J. E., Rodriguez, J. M., Bhartia, P. K., Liu, X., Huey, L. G., Liao, J., Stickel, R. E., Tanner, D. J., Dibb, J. E., Simpson, W. R., Donohoue, D., Weinheimer, A., Flocke, F., Knapp, D., Montzka, D., Neuman, J. A., Nowak, J. B., Ryerson, T. B., Oltmans, S., Blake, D. R., Atlas, E. L., Kinnison, D. E., Tilmes, S., Pan, L. L., Hendrick, F.,

Van Roozendael, M., Kreher, K., Johnston, P. V., Gao, R. S., Johnson, B., Bui, T. P., Chen, G., Pierce, R. B., Crawford, J. H., and Jacob, D. J.: A new interpretation of total column BrO during Arctic spring, Geophys. Res. Lett., 37, doi:10.1029/2010GL043798, 2010.

Sander, S. P. et al.: Chemical kinetics and photochemical data fouse in atmospheric studies: Evaluation number 15, JPL Publ. 06-2, Jet Propul. Lab., Pasadena, CA, 2006.

Schoeberl, M. and Dessler, A.: Dehydration of the stratosphere, Atmos. Chem. Phys. Discuss., 11, 10 159–10 190, doi:10.5194/acpd-11-10159-2011, 2011.

Schofield, R., Fueglistaler, S., Wohltmann, I., and Rex, M.: Sensitivity of stratospheric Br_y to uncertainties in very short lived substance emissions and atmospheric transport, Atmos. Chem. Phys., 11, 1379–1392, doi:10.5194/acp-11-1379-2011, 2011.

Shepherd, T. G.: The middle atmosphere, J. Atmos. Sol.-Terr. Phy., 62, 1587–1601, 2000.

Shepherd, T. G.: Transport in the middle atmosphere, J. Meteorol. Soc. Jpn., 85B, 165–191, 2007.

Sherwood, S. C. and Dessler, A. E.: A model for transport across the tropical tropopause, J. Atmos. Sci., 58, 765–779, 2001.

Sherwood, S. C., Roca, R., Weckwerth, T. M., and Andronova, N. G.: Tropospheric water vapor, convection, and climate, Rev. Geophys., 48, doi:10.1029/2009RG000301, 2010.

Shine, K. P.: The middle atmosphere in the absence of dynamic heat fluxes, Q. J. Roy. Meteor. Soc., 113, 603–633, 1987.

Shiotani, M.: Annual, quasi-biennial, and El-Nino-Southern Oscillation (ENSO) time-scale variations in equatorial total ozone, J. Geophys. Res.-Atmos., 97, 7625–7633, 1992.

Shu, J., Tian, W., Austin, J., Chipperfield, M. P., Xie, F., and Wang, W.: Effects of sea surface temperature and greenhouse gas changes on the transport between the stratosphere and troposphere, J. Geophys. Res.-Atmos., 116, doi:10.1029/2010JD014520, 2011.

Simon, P. C., Gillotay, D., Vanlaethemmeuree, N., and Wisemberg, J.: Temperature-dependence of ultraviolet-absorption cross-sections of chlorofluoroethanes, Ann. Geophys.-Atm. Hydr., 6, 239–247, 1988.

Simpson, W. R., von Glasow, R., Riedel, K., Anderson, P., Ariya, P., Bottenheim, J., Burrows, J. P., Carpenter, L. J., Frieß U., Goodsite, M. E., Heard, D., Hutterli, M., Jacobi, H.-W., Kaleschke, L., Neff, B., Plane, J., Platt, U., Richter, A., Roscoe, H., Sander, R., Shepson, P., Sodeau, J., Steffen, A., Wagner, T., and Wolff, E.: Halogens and their role in polar boundary-layer ozone depletion, Atmos. Chem. Phys., 7, 4375–4418, 2007.

Sinnhuber, B.-M. and Folkins, I.: Estimating the contribution of bromoform to stratospheric bromine and its relation to dehydration in the tropical tropopause layer, Atmos. Chem. Phys., 6, 4755–4761, doi:10.5194/acp-6-4755-2006, 2006.

Sinnhuber, B.-M., Arlander, D. W., Bovensmann, H., Burrows, J. P., Chipperfield, M. P., Enell, C. F., Friess, U., Hendrick, F., Johnston, P. V., Jones, R. L., Kreher, K., Mohamed-Tahrin, N., Muller, R., Pfeilsticker, K., Platt, U., Pommereau, J.-P., Pundt, I., Richter,

A., South, A. M., Tornkvist, K. K., Van Roozendael, M., Wagner, T., and Wittrock, F.: Comparison of measurements and model calculations of stratospheric bromine monoxide, J. Geophys. Res.-Atmos., 107, doi:10.1029/2001JD000940, 2002.

Sinnhuber, B.-M., Weber, M., Amankwah, A., and Burrows, J. P.: Total ozone during the unusual Antarctic winter of 2002, Geophys. Res. Lett., 30, doi:10.1029/2002GL016798, 2003a.

Sinnhuber, B.-M., Rozanov, A., Sheode, N., Afe, O. T., Richter, A., Sinnhuber, M., Wittrock, F., Burrows, J. P., Stiller, G. P., von Clarmann, T., and Linden, A.: Global observations of stratospheric bromine monoxide from SCIAMACHY, Geophys. Res. Lett., 32, doi:10.1029/2005GL023839, 2005.

Sinnhuber, B.-M., Sheode, N., Sinnhuber, M., Chipperfield, M. P., and Feng, W.: The contribution of anthropogenic bromine emissions to past stratospheric ozone trends: a modelling study, Atmos. Chem. Phys., 9, 2863–2871, 2009.

Sinnhuber, M., Burrows, J. P., Chipperfield, M. P., Jackman, C. H., Kallenrode, M. B., Künzi, K. F., and Quack, M.: A model study of the impact of magnetic field structure on atmospheric composition during solar proton events, Geophys. Res. Lett., 30, doi: 10.1029/2003GL017265, 2003b.

Sioris, C. E., Kovalenko, L. J., McLinden, C. A., Salawitch, R. J., Van Roozendael, M., Goutail, F., Dorf, M., Pfeilsticker, K., Chance, K., von Savigny, C., Liu, X., Kurosu, T. P., Pommereau, J.-P., Boesch, H., and Frerick, J.: Latitudinal and vertical distribution of bromine monoxide in the lower stratosphere from Scanning Imaging Absorption Spectrometer for Atmospheric Chartography limb scattering measurements, J. Geophys. Res.-Atmos., 111, doi:10.1029/2005JD006479, 2006.

Solomon, S.: Stratospheric ozone depletion: A review of concepts and history, Rev. Geophys., 37, 275–316, 1999.

Solomon, S., Garcia, R. R., Rowland, F. S., and Wuebbles, D. J.: On the depletion of antarctic ozone, Nature, 321, 755–758, 1986.

Steele, H. M., Hamill, P., McCormick, M. P., and Swissler, T. J.: The formation of polar stratospheric clouds, J. Atm. Sci., 40, 2055–2067, 1983.

Stiller, G. P., von Clarmann, T., Hoepfner, M., Glatthor, N., Grabowski, U., Kellmann, S., Kleinert, A., Linden, A., Milz, M., Reddmann, T., Steck, T., Fischer, H., Funke, B., Lopez-Puertas, M., and Engel, A.: Global distribution of mean age of stratospheric air from MIPAS SF_6 measurements, Atmos. Chem. Phys., 8, 677–695, 2008.

Stolarski, R. S. and Cicerone, R. J.: Stratospheric chlorine - possible sink for ozone, Can. J. Chem., 52, 1610–1615, 1974.

Stolarski, R. S. and Frith, S. M.: Search for evidence of trend slow-down in the long-term TOMS/SBUV total ozone data record: the importance of instrument drift uncertainty, Atmos. Chem. Phys., 6, 4057–4065, 2006.

Sturges, W. T., Oram, D. E., Carpenter, L. J., Penkett, S. A., and Engel, A.: Bromoform as a source of stratospheric bromine, Geophys. Res. Lett., 27, 2081–2084, 2000.

Tallmadge, J. A., Butt, J. B., and Solomon, H. J.: Minerals from sea salt, Ind. Eng. Chem., 56, 44–65, 1964.

Theys, N., Van Roozendael, M., Dils, B., Hendrick, F., Hao, N., and De Maziere, M.: First satellite detection of volcanic bromine monoxide emission after the Kasatochi eruption, Geophys. Res. Lett., 36, doi:10.1029/2008GL036552, 2009.

Thompson, A. M., Witte, J. C., McPeters, R. D., Oltmans, S. J., Schmidlin, F. J., Logan, J. A., Fujiwara, M., Kirchhoff, V. W. J. H., Posny, F., Coetzee, G. J. R., Hoegger, B., Kawakami, S., Ogawa, T., Johnson, B. J., Vömel, H., and Labow, G.: Southern Hemisphere Additional Ozonesondes (SHADOZ) 1998-2000 tropical ozone climatology - 1. Comparison with Total Ozone Mapping Spectrometer (TOMS) and ground-based measurements, J. Geophys. Res.-Atmos., 108, doi:10.1029/2001JD000967, 2003.

Tiedtke, M.: A comprehensive mass flux scheme for cumulus parameterization in large-scale models, Mon. Weather Rev., 117, 1779–1800, 1989.

Toon, O. B., Hamill, P., Turco, R. P., and Pinto, J.: Condensation of HNO_3 and HCl in the winter polar stratospheres, Geophys. Res. Lett., 13, 1284–1287, 1986.

Tost, H., Lawrence, M. G., Brühl, C., Jöckel, P., GABRIEL Team, and SCOUT-O3-DARWIN ACTIVE Team: Uncertainties in atmospheric chemistry modelling due to convection parameterisations and subsequent scavenging, Atmos. Chem. Phys., 10, 1931–1951, 2010.

Tung, K. K., KO, M. K. W., Rodriguez, J. M., and Sze, N. D.: Are antarctic ozone variations a manifestation of dynamics or chemistry?, Nature, 322, 811–814, 1986.

Uppala, S. M., Kallberg, P. W., Simmons, A. J., Andrae, U., Bechtold, V. D., Fiorino, M., Gibson, J. K., Haseler, J., Hernandez, A., Kelly, G. A., Li, X., Onogi, K., Saarinen, S., Sokka, N., Allan, R. P., Andersson, E., Arpe, K., Balmaseda, M. A., Beljaars, A. C. M., Van De Berg, L., Bidlot, J., Bormann, N., Caires, S., Chevallier, F., Dethof, A., Dragosavac, M., Fisher, M., Fuentes, M., Hagemann, S., Holm, E., Hoskins, B. J., Isaksen, L., Janssen, P. A. E. M., Jenne, R., McNally, A. P., Mahfouf, J. F., Morcrette, J. J., Rayner, N. A., Saunders, R. W., Simon, P., Sterl, A., Trenberth, K. E., Untch, A., Vasiljevic, D., Viterbo, P., and Woollen, J.: The ERA-40 re-analysis, Q. J. Roy. Meteor. Soc., 131, 2961–3012, doi:10.1256/qj.04.176, 2005.

von Glasow, R., von Kuhlmann, R., Lawrence, M. G., Platt, U., and Crutzen, P. J.: Impact of reactive bromine chemistry in the troposphere, Atmos. Chem. Phys., 4, 2481–2497, 2004.

von Glasow, R., Bobrowski, N., and Kern, C.: The effects of volcanic eruptions on atmospheric chemistry, Chem. Geol., 263, 131–142, doi:10.1016/j.chemgeo.2008.08.020, 2009.

Vountas, M., Dinter, T., Bracher, A., Burrows, J. P., and Sierk, B.: Spectral studies of ocean water with space-borne sensor SCIAMACHY using differential optical absorption Spectroscopy (DOAS), Ocean Sci., 3, 429–440, 2007.

Wallace, J. M. and Hobbs, P. V.: Atmospheric Science, An introductory survey, Academic Press, 2nd edition, 2006.

Wamsley, P. R., Elkins, J. W., Fahey, D. W., Dutton, G. S., Volk, C. M., Myers, R. C., Montzka, S. A., Butler, J. H., Clarke, A. D., Fraser, P. J., Steele, L. P., Lucarelli, M. P., Atlas, E. L., Schauffler, S. M., Blake, D. R., Rowland, F. S., Sturges, W. T., Lee, J. M.,

Penkett, S. A., Engel, A., Stimpfle, R. M., Chan, K. R., Weisenstein, D. K., Ko, M. K. W., and Salawitch, R. J.: Distribution of halon-1211 in the upper troposphere and lower stratosphere and the 1994 total bromine budget, J. Geophys. Res.-Atmos., 103, 1513–1526, 1998.

Warwick, N. J., Pyle, J. A., Carver, G. D., Yang, X., Savage, N. H., O'Connor, F. M., and Cox, R. A.: Global modeling of biogenic bromocarbons, J. Geophys. Res.-Atmos., 111, doi:10.1029/2006JD007264, 2006.

Waugh, D. W. and Hall, T. M.: Age of stratospheric air: Theory, observations, and models, Rev. Geophys., 40, doi:10.1029/2000RG000101, 2002.

Wennberg, P.: Atmospheric chemistry - Bromine explosion, Nature, 397, 299–301, 1999.

Winkler, H., Sinnhuber, M., Notholt, J., Kallenrode, M.-B., Steinhilber, F., Vogt, J., Zieger, B., Glassmeier, K.-H., and Stadelmann, A.: Modeling impacts of geomagnetic field variations on middle atmospheric ozone responses to solar proton events on long timescales, J. Geophys. Res.-Atmos., 113, doi:10.1029/2007JD008574, 2008.

Wofsy, S. C., McElroy, M. B., and Yung, Y. L.: Chemistry of atmospheric bromine, Geophys. Res. Lett., 2, 215–218, 1975.

World Meteorological Organization: Scientific Assessment of Ozone Depletion: 1991, Global Ozone Research and Monitoring Project-Report No. 25, Geneva, Switzerland, 1991.

World Meteorological Organization: Scientific Assessment of Ozone Depletion: 2010, Global Ozone Research and Monitoring Project-Report No. 52, Geneva, Switzerland, 2010.

Wuebbles, D. J., Patten, K. O., Wang, D., Youn, D., Martínez-Avilés, M., and Francisco, J. S.: Three-dimensional model evaluation of the Ozone Depletion Potentials for n-propyl bromide, trichloroethylene and perchloroethylene, Atmos. Chem. Phys., 11, 2371–2380, doi:10.5194/acp-11-2371-2011, 2011.

Yang, X., Cox, R. A., Warwick, N. J., Pyle, J. A., Carver, G. D., O'Connor, F. M., and Savage, N. H.: Tropospheric bromine chemistry and its impacts on ozone: A model study, J. Geophys. Res.-Atmos., 110, doi:10.1029/2005JD006244, 2005.

Yokouchi, Y., Hasebe, F., Fujiwara, M., Takashima, H., Shiotani, M., Nishi, N., Kanaya, Y., Hashimoto, S., Fraser, P., Toom-Sauntry, D., Mukai, H., and Nojiri, Y.: Correlations and emission ratios among bromoform, dibromochloromethane, and dibromomethane in the atmosphere, J. Geophys. Res.-Atmos., 110, doi:10.1029/2005JD006303, 2005.

Yung, Y. L., Pinto, J. P., Watson, R. T., and Sander, S. P.: Atmospheric bromine and ozone perturbations in the lower stratosphere, J. Atm. Sci., 37, 339–353, 1980.

Acknowledgments

I would like to thank especially Prof. Dr. John P. Burrows for supervising my PhD work. In the past years, his experience and valuable advice guided me through this challenging time. I also will gladly remember our prolonged discussions about science, life and everything else, thank you for this opportunity! I would also like to thank Dr. Björn-Martin Sinnhuber who sparked my interest in atmospheric modeling. His groundbreaking ideas really brought forward my research. Without his great support and seemingly endless patience to answer my numerous questions I could not have finished this work. Special thanks goes to the former Magister Kazeminejad and Kiesewetter that gave me a vivid lesson in intercultural competence and significantly expanded my vocabulary.

I would also like to thank my other colleagues at the IUP for their support and the friendly working environment. Prof. Dr. Justus Notholt for reviewing this thesis. Prof. Dr. Klaus Pawelzik and PD Christian von Savigny for their participation in the examination board. Marco Vountas, Günther Lehnert and Peter Grupe for their excellent IT support. Lars Jeschke, Anke Werner and Petra Horn for paving the way for me through the shallows of academic bureaucracy. Martin Langowski and Gregor Kiesewetter for the great time in the office and their help. Holger Winkler, Nadine Wieters and Miriam Sinnhuber for their invaluable support with the model and chemistry scheme.

I acknowledge the Zentrale Forschungsförderung of the University of Bremen, the EU within the projects SCOUT-O3 and SHIVA and the DFG research unit SHARP for financial support. Furthermore I acknowledge the ECMWF for providing the ERA-Interim data through the special project DECDIO.

Curriculum Vitæ

Jan Aschmann was born on November 1, 1981 in Bremen, Germany. He studied Computer Sciences and Physics at the University of Bremen. After receiving his Diploma degree of Computer Sciences in 2008 he joined the Atmospheric Modeling Group at the Institute of Environmental Physics Bremen as research assistant, working on the atmospheric transport and chemistry of very short-lived bromine substances. He finished his PhD in October 2011.

Publications

Peer-Reviewed Articles

- Aschmann, J., Sinnhuber, B.-M., Chipperfield, M. P., and Hossaini, R.: Impact of deep convection and dehydration on bromine loading in the upper troposphere and lower stratosphere, Atmos. Chem. Phys., 11, 2671-2687, 2011.
- Aschmann, J., Sinnhuber, B.-M., Atlas, E. L., and Schauffler, S. M.: Modeling the transport of very short-lived substances into the tropical upper troposphere and lower stratosphere, Atmos. Chem. Phys., 9, 9237-9247, 2009.

Conference Contributions

- Aschmann, J., Sinnhuber, B.-M., Impact of deep convection and dehydration on stratospheric bromine loading, WCRP Open Science Conference, Denver, USA, October 2011.
- Gebhardt, C., Aschmann, J., Hommel, R., Rozanov, A., Weber, M., Burrows, J. P., BrO - SHARP related results from SCIAMACHY, 2nd Annual SHARP Meeting, Karlsruhe, Germany, May 2011.
- Aschmann, J., Sinnhuber, B.-M., Transport of very short-lived substances into the tropical upper troposphere and lower stratosphere: A modeling study, EGU General Assembly, Vienna, Austria, May 2010.
- Sinnhuber, B.-M., Aschmann, J., Modeling the transport of VSLS and the trend of stratospheric bromine, 1st Annual SHARP Meeting, Bremen, Germany, May 2010.
- Aschmann, J., Sinnhuber, B.-M., Modeling the transport of very short-lived substances into the tropical upper troposphere and lower stratosphere, SCOUT-O3 Final Meeting, Schliersee, Germany, June 2009.